Dissertation

Paleoenvironmental and sedimentary systems within the land-ocean interface reconstructed by biomarker analysis of Miocene sediments from Brunei and Hokkaido, Japan

（ブルネイおよび北海道の中新統堆積岩のバイオマーカー分析による陸-海インターフェイスにおける古環境および堆積システムの復元）

Muhammad Adam Bin Ismail

Department of Natural History Sciences, Faculty of Science, Hokkaido University

September 2024

Table of contents

Acknowledgements

I would like to thank the Ministry of Education, Culture, Sports, Science and Technology (Monbusho) Japan for funding my studies and my stay in Japan from 2019 to 2024. I would also like to thank my parents for supporting me throughout my studies even though we are in totally separate countries.

I would also like to show appreciation to Dr. Sawada Ken for supporting me academically throughout my studies. I would like to thank Dr. Nakamura Hideto for in-depth discussion on biomarkers. I would also like to thank the members of 5G for helping me with research, fieldwork and lab stuff.

Special thanks also goes to…

Dr. Amajida Roslim from Universiti Brunei Darussalam, Dr. Laszlo Kocsis from University of Lausanne, and Dr. Mike Simmons from University of Aberdeen (and Halliburton) for help with fieldwork, foraminiferal analysis and discussions on Brunei's stratigraphy;

Dr. Satoshi Furota and Dr. Osamu Takano from AIST-Geological Survey of Japan for discussion on Japan's Kawabata Formation and Bibai Formations' flood deposits;

Dr. Carlos Zavala from GCS Argentina for help with understanding lofting plumes and for being the first person to cite my first paper;

Dusan Radisalvjevic and Marco Bertacchini for going with me to do fieldwork in Bibai.

Abstract

Lipid biomarkers are created by specific marine and terrestrial organisms and are capable of being preserved in the geological record throughout time. They are useful in reconstructing environmental systems as their source organisms respond to changes in the environments such as aridity and precipitation, salinity, temperature and etc. While most studies on paleoenvironmental reconstruction use calcareous fossils such as foraminiferas or diatoms, their preservation can be negatively affected by diagenesis. Lipid biomarkers have been shown to be well preserved even when microfossils are poorly preserved, giving them an advantageous but underused method in environmental reconstruction. In this Doctoral Dissertation, I use lipid biomarkers to reconstruct environmental and sedimentary systems in the land-ocean interface of Brunei and Hokkaido, Japan. Specifically, I reconstruct how sedimentary processes may create large carbon sinks in sandstones, the changes in hinterland vegetation due to tectono-sedimentary changes during stable climates, and the changes in terrestrial and marine carbon production during global cooling and evolving East Asian Monsoon.

In chapter 1, the effects of sedimentary processes on terrigenous carbon preservation within sandstones were investigated. OM-rich sediments deposited by sandy floods such as crevasse splay (floodplain) and deep-sea hyperpycnites were collected from the Bibai Formation (exposed in Bibai) and the Kawabata Formation (exposed in Yubari), respectively, with the former representing early-stage floods while the latter represents later stage floods. OM-rich sediments deposited by tidal reworking were collected from the Belait Formation exposed in Meragang Beach of Brunei. Using pr/ph (pristane/phytane) and C_{27} sterane ratios, terrigenous and marine OM input and transformations from source to sink were analysed. It was found that early-stage floods have high amounts of OM_{terr} but no $OM_{mar.}$ However, as floods flow seawards, some OM is lost due to escape from the flow due to density reversal of less-dense plant deposits compared to seawater. Marine OM is also incorporated into later-stage sandy flows as sea-floor sediments are eroded and incorporated into the sandy flow, with mud-clast being a contributing factor towards their detection and preservation in sandy-deposits. Analysis of hyperpycnal flows also shows more woody material in denser deposits with more leafy material in less-dense deposits, further suggesting that OM distribution is due to density differences between the OM and the flow. Lastly, in tidal-reworked sediments, two OM-rich facies were identified, which are rippled sandstones with wavy bedding (a type of mud-drape) and trough cross-stratified sandstones. Rippled sandstones have high amounts of TOC%, leaf wax-derived *n*-alkanes, and diatom-derived highly branched isoprenoids (HBI) when compared to OM-poor sandstones. As tides flow, ripples are created, but the flow energy is too high to enable settling

of OM. However, before the tide reverses, there is a period of slack/stagnant water that is calm enough to allow OM to be deposited along with mud on the ripples – creating a wavy bed rich in OM. For the trough cross-stratified sandstones, which are created by strong unidirectional water currents, OM is often found on the lee-side of strata. It is believed that small eddies formed in front of the lee-side of ripples trapped OM on the lee-side of the rippled. These studies suggests that sandstones can become large and important carbon sinks depending on their respective sedimentary processes, in addition to mudstones.

In chapter 2, the effects of uplifting and expansion of low-land environments on vegetation patterns during stable climates were investigated. Samples were collected from shallow-water Belait Formation outcrops (about 12 Ma) exposed in Meragang Beach and deeper offshore Miri Formation outcrops (about 10 Ma) exposed in Batong of Brunei, North Borneo. These were deposited during a period of continuous uplifting and lowland-expansion with stable climates as shown from $\delta^{18}O$ and mg/ca (magnesium/calcium) paleotemperature reconstructions from the South China Sea. Cadalene, an angiosperm biomarker commonly found in *Dipterocarpacaea* plants, are more abundant in younger and distal offshore outcrops. This is contradictory to modern analogues where terrestrial OM is less abundant in distal marine settings than in proximal settings, showing that facies change was not a control in their distribution over longer geological timescales. Since younger outcrops were deposited during a period with a larger low-land hinterland area, it is probable that the increased accommodation space allowed the growth of more cadalene-rich *Dipterocarpaea* plants. Diterpenoids, which are found in conifers, are also in higher abundances in younger outcrops. Since temperatures were stable from 12 to 10 Ma, cooling climates cannot be attributed to their expansion. However, as we see in modern day vegetational patterns of Borneo, conifers are abundant in mountains with high elevations. Thus, it is interpreted that their expansion is related to higher mountain tops created due to continuous uplifting of the Bornean hinterland.

In chapter 3, the effects of increased aridity/reduced precipitation caused by global cooling and strengthening East Asian Winter Monsoon on the Japanese Island and Sea between 15 and 9 Ma was investigated. Samples were taken from mudstones of the Kawabata Formation exposed along the Soumokumaisawa and Higashiyama rivers in Yubari, Japan. Leaf wax *n*-alkanes show a slight decrease in younger sediments while gymnosperm-derived diterpenoids show an increase relative to angiosperms. These suggest reduced river discharge and cooling-driven vegetation changes respectively. This in in contrast to a study done by Wang et al., (2003, *Rev. Paleobot. Palynol*.) where pollens in South Japan show an increase in angiosperms, suggesting a warming climate. Thus,

it is probable that cooling affected North Japan first as the Subpolar Front migrated southwards. The Average Chain Length (ACL), Carbon Preference Index (CPI), Aquatic Macrophyte Index (P_{aq}) and long-chain *n*-alkanes ratios do not show significant variation throughout the studied interval, suggesting that aridity may have been weak. This is also in contrast with a study done by Peng et al. (2016, *Quater. Int.*) where an increase in the above proxies showed two drying intervals between 14.5 – 12.5 Ma and 10 – 4 Ma. These suggest that aridification was stronger in Central Asia than in the Japanese Islands. C_{27} sterane ratios and HBI concentrations also shows an increase in younger sediments. A plot of MTTCI (chroman index) against pr/ph ratios shows a shift from semi-saline freshwater conditions to normal marine-like conditions during deposition of samples with high marine OM. Additionally, HBI shows a good correlation with gammacerane concentrations (R = 0.55) and a pr/ph (R = -0.66), showing that diatoms grow when bottom waters are saline and/or anoxic/dysoxic respectively. These changes in primary productivity could be due to periodic intrusion and upwelling of nutrient-rich Oxygen Minimum Zone (OMZ) waters. A shift from calcareous to silicate-rich environment of the North Pacific during the Miocene could also be a cause. These results show aridification affects the Japanese Islands lesser than Central Asia, while primary productivity in the Japan Sea is controlled mainly by upwelling of deep waters.

In conclusion, lipid biomarkers were used to reconstruct the changes in the land-ocean interface. We found that sedimentary processes can cause large OM_{terr} deposition and preservation in sandstones, creating a new, unconventional carbon sink. We also found that vegetation change in the hinterland is not only related to climate change, but also local tectono-sedimentary changes. Lastly, we found that global cooling would change riverine OM_{terr} delivery and vegetation in North Japan earlier than South Japan, while the physico-chemical properties of Japan Sea and diatom-primary productivity are mainly controlled by oceanographic processes.

General introduction

The Earth's biosphere, atmosphere, hydrosphere and lithosphere are often studied as separate entities. However, in reality, all of these subsystems all act together and influence each other through complex and intricate mechanisms that can change the environment over long geological timescales. For example, a shrinking paratethys ocean due to tectono-sedimentary activity can reduce the amount of water evaporated to the atmosphere. This in turn reduces the amount of water transported by westerly winds to Central and East Asia while the partial uplifting of the Himalayan Tibetan Plateau can redirect wind flow (see Tada et al., 2016 and references therein). Furthermore, this uplifting, which also caused carbon drawdown through increased silicate weathering and organic carbon burial, also caused global cooling, which caused the ITCZ to migrate from an estimated latitude of 25°N to its current mean location on the equator, bringing along heavy amounts of rainfall (Armstrong & Allen, 2011). It is very clear that Earth is a complex system contain linear and non-linear elements that can affects its inhabitants. However, these complex mechanisms are still poorly understood.

All these changes in the Earth's subsystems affects organic matter production, which is a crucial element to human civilization. For example, changing physico-chemical properties of the oceans due to climate change can affect marine ecosystems, food-web dynamics and migratory patterns of aquatic life. In addition to the above subsystems, these changes in physico-chemical properties are also brought about by the complex linkage between the land and the ocean. One such element is the transport of sediments from continents to the ocean, which is heavily discussed in this thesis. In chapter 1, we challenge the idea that only mudstones or muddy depocenters can preserve organic carbon (Mayer, 1994). It has always been thought that sandy sediments cannot preserve sediments. However, scientists have recently discovered that gravity flows and sediment reworked by tides or bottom currents can enhance organic carbon preservation in sandstones. Additionally, it has also always been thought that anoxia is also a key factor in OC preservation (Demaison & Moore, 1980; Walters, 2006). But, this will also be challenged in this thesis, as we discuss that even in oxic and sand dominated environments, high amounts of OM can be preserved.

Another new approach to studying environmental change will also be introduced in chapter 2 of this thesis. Here, we discuss how changing paleovegetation and the delivery of terrestrial OM to the marine environment is not simply related to only climatic changes, as most geochemical proxies only factor in one element of change rather than considering an interplay of other subsystems. In this

chapter, we will challenge the notion that only global cooling or warming brings about vegetational composition changes. Here, we discuss how uplifting and an expansion of low-lands by tectono-sedimentary processes can affect vegetational patterns that can be mistakenly interpreted as being caused by climatic changes.

Lastly, in chapter 3, we will discuss the importance of how a changing climate can affect the ecosystem. Here we will discuss how atmospheric and oceanographic systems such as East Asian Monsoons and fluctuating inflow of nutrient-rich water bodies can affect the composition of primary producers in the marine and terrestrial environments. We will show in this chapter that even during global or large-scale/regional climatic changes, not all areas will react similarly.

Chapter 1

Reconstruction of enhanced organic matter preservation in sandstones by flooding events and tidal reworking by biomarker analysis of Japan and Brunei sediments

1.1. Introduction

In marine sediments, the global burial flux of organic carbon is estimated to be about 0.1 to 0.2 gigatons per year, less than the 0.4 gigatons of dissolved and particulate organic carbon delivered by rivers (Berner, 1989; Hedges et al., 1997; Hedges & Keil, 1995). Conversely, seaward increases in carbon isotopes ($\delta^{13}C$) from shallow coasts to offshore areas reveal a decrease in terrigenous organic carbon and an increase in algal-derived organic carbon during transport from river mouths to the ocean (Hedges et al., 1997; Xing et al., 2011). This discrepancy between river-transported organic carbon and marine burial fluxes suggests that the burial mechanism of terrigenous organic matter is poorly constrained, or that terrigenous organic matter is remineralized faster than previously thought (Selvaraj et al., 2015). In addition, mudstones are commonly believed to be the key to organic carbon preservation in marine environments because they prevent degradation (Mayer, 1994). Yet, some studies have shown that marine sands in turbidites or submarine fans can preserve vast amounts of organic carbon such as woody debris (Hage et al., 2020). Since the preservation of terrigenous organic matter (OM) in marine sands is often overlooked, more understanding of the transport and burial of terrigenous OM in marine sediments is needed to better understand the global carbon cycle.

While studies on the transport of sediments from rivers to shallow, deltaic systems are numerous (Clift & Jonell, 2021; Manh et al., 2014; Staub et al., 2000; Z. Yang et al., 2011) in recent years, hyperpycnal flows which are defined as a type of turbidity flow originating from the terrestrial environment with sediment densities higher than surrounding water, has been seen to show the ability to transport, deposit and preserve vast amounts of terrigenous sediments to the marine environment from continents as extrabasinal turbidites (Lihong et al., 2020; Mulder et al., 2003; H. Wang et al., 2010; Zavala & Arcuri, 2016). These hyperpycnal flows not only transport sediments and freshwater, but also terrigenous OM such as woody fragments, plant leaves and chemical compounds known as biomarkers which can be used to infer the source of sediments and OM (Dadson et al., 2005; Furota et al., 2021; Pierdomenico et al., 2019; Zavala et al., 2012)(Dadson, et al., 2005; Zavala et al., 2012; Pierdomenico et al., 2019; Furota et al., 2021). On the other hand, intrabasinal turbidites (Bouma-type turbidites), commonly defined as deposits with sediments originating from within the marine basin by the collapse of slope sediments due to slope instability, commonly have relatively poor preservation potential of OM due to resuspension of sediments which allows the further degradation of any existing OM (Zavala & Arcuri, 2016). An example of a recent hyperpycnal flow can be seen in the deep-sea sediments of Taiwan, where a cyclone-induced hyperpycnal flow traveled from the terrestrial environment to the deep sea. The bulk $\delta^{13}C$ and C/N

analyses of the hyperpycnite samples from that study suggested that the OM was terrigenous sourced, as they were similar in composition with landslide sediments in the area (Selvaraj et al., 2015). Analysis of heat and salinity also suggests a presence of freshwater within the hyperpycnite, contrasting that of the surrounding water (Kao et al., 2010).

Even though rivers act as conduits transporting freshwater, particulate and dissolved OM to the oceans (McKee et al., 2004), only about 5% of sediment delivered by rivers reaches the deep sea (Meade, 1996). Thus, the discovery of hyperpycnal flow deposits with interbedded plant fragments in the deep sea provides a good opportunity to study sediment transport mechanisms along with terrestrial OM deposition and preservation in deep-sea settings, helping us understand more about terrigenous carbon burial in deep marine environments. While published records of turbidite deposition with preservation of terrestrial OM such as pollen and plant debris are comparatively numerous (Quattrocchio et al., 2018; Slater et al., 2017; Yoshida et al., 2009), detailed studies of freshwater, terrigenous OM transport and the distribution and OM preservation potential of these turbidite deposits in deep-sea settings are relatively scarce. A previous study by Furota et al. (2021) elucidated the transport of terrigenous OM to the deep sea by hyperpycnal sustained turbidity flows, but detailed studies on plant fragment segmentation by density differences within different facies and the entrainment of marine OM during flow were not conducted. Considering that hyperpycnal flow deposits may act as unconventional carbon sinks or even source rocks, such detailed studies are necessary to identify regions of higher OM preservation.

Another mechanism that appears to be able to pack in OM into sandstones are tides. Gong et al. (2016) has shown that tides and contour flows can rework turbidites and create sedimentary structures such as mud-drapes, double mud layers and cross-beds that contain OM. Another study has shown that rhythmic cross-beds created by neap and spring tides can also create sandstones that can preserve OM (Chen et al., 2015). However in both these studies, OM was only noted to exist within tidal-reworked sandstones, but no in-depth studies on carbon contents or typing of OM have been performed. Similar to the above, it is possible that OM preservation in tidal reworked sandstones may also be an unconventional and understudied carbon sink. Their OM preservation potential should be further studied as they may play an important role in carbon drawdown mechanisms

Thus, the objectives of this study are: (1) to assess both the transport, distribution and preservation of sediments and terrigenous OM by analyzing sedimentological characteristics and biomarker profiles

within different facies of sandy extrabasinal turbidite deposits and comparing them to floodplain deposits, and (2) to assess terrigenous OM preservation mechanisms of tidal-reworked sandstones.

1.2. Geological setting and study area

1.2.1. Kawabata Formation – Chidorigataki Outcrop

The Kawabata Formation, distributed in south-central Hokkaido, Japan (Fig. 1.1), consists of sandy and muddy gravity flow deposits formed in the Ishikari-Teshio Belt deposited along the western side of the Hidaka collision zone during the middle to late Miocene (Kawakami et al., 2004). This unit has been subdivided by into two members: the Amagiri Sandstone and Mudstone Lower Member and the Higashiyama Sandstone and Conglomerate Upper Member (Fig. 1.2). The Amagiri Sandstone and Mudstone Member is characterized as a basinal turbidite system consisting of mudstone dominated mudstone-sandstone interbeds, and the Higashiyama Sandstone and Conglomerate Member is characterized by sandstone dominated alternations and thick conglomerate layers deposited by slope-apron turbidite system (Kawakami et al., 2002). There are five key beds of acidic tuff (K1 - K5 tuffs), and the age of the K5 tuff in the Higashiyama Member shows an age of 13.2 ± 0.9 Ma by fission-track dating (Kawakami et al., 2002). It was estimated that the Kawabata Formation was deposited below 1000 m water depth by the presence of the benthic foraminifera *Uvigerina proboscidea* that is associated with the lower middle bathyal marine zone (Tsubakihara, 1990). Due to burying and isostatic uplift of the hinterland orogen, the basin shallowed, and this shallowing caused the change in sedimentary systems from the basinal environment of the Amagiri Member to the slope-apron environment of the Higashiyama Member (Kawakami et al., 2004; Kawakami, 2013).

The outcrop of interest from the Miocene Kawabata Formation is the Chidorigataki Falls outcrop. The Chidorigataki Falls is located in Takinoue Park, Yubari, Hokkaido and represents the lowermost part of the Higashiyama Member (Fig. 1.2B). It is composed of conglomerate beds, pebbly sandstone beds, sand–mud alternations, the K5 tuff bed, and some plant fragment-concentrated sandstone beds (Furota et al., 2021). This outcrop contains both the common intrabasinal (Bouma-type) turbidites as well as extrabasinal hyperpycnites, the former exhibiting classic fining-up sequences with sedimentary structures changing from upper-flow regime structures at the base to lower flow regime structures on top while the latter shows intrasequence erosional contacts and an abundance of

terrestrial plant fragments, both diagnostic features of extrabasinal turbidites (Mulder et al., 2003; Zavala et al., 2011) (Fig 1.3). Coarsening followed by fining of the sediments seen in classical hyperpycnites reported by Mulder et al. (2005) was not seen.

1.2.1. Bibai Formation – Bibai River Outcrop

The Ishikari Group was deposited in from middle to late Eocene (46 – 37 Ma) as confirmed by fission track dating. The Ishikari Group has a total thickness of about 3000m containing sandstones, mudstones and coal seems that were deposited in non-marine to littoral environments, specifically of braided-fluvial, meandering fluvial, lacustrine and bay-estuarine systems. It is part of the Sorachi-Ezo belt that extends from north to south of central Hokkaido. Prior to the Early Eocene, the paleo-Okhotsk plate subducted westwards underneath the eastern margin of the Eurasian plate. Subsequently, in the middle Eocene, an arc system on the eastern plate collided and obducted onto the western Eurasian plate, causing the Sorachi-Ezo Belt to be converted to a foreland setting in front of the collision zone. The Ishikari Group is divided into nine lithostratigraphic formations which begins the Noborikawa Fm., followed by the Horokabetsu, Yubari, Wakanabe, Bibai, Akabira, Ikushunbetsu, Hiragishi, and Ashibetsu Formations (Takano & Waseda, 2003).

In this study, flood-plain sediments are necessary to be used as an analogue for early stages of flood or hyperpycnal flow formation. Flood-plain sediments are abundant and easily accessible at the Bibai River that belongs to the Bibai Formation (Fig 1.4). 25 metres of an outcrop interval was logged and silty to sandy plant-fragment rich sediments were found, along with a coal seam and muddy coals.

1.2.3. Belait Formation – Meragang Beach Outcrop

Uplifting of the Bornean hinterland (known as the Crocker-Rajang mountain belt) began in the Late Paleogene-Neogene due to the collision of the South China Sea part of the Eurasian plate with the Sundaland plate (Hutchison et al., 2000). This uplifting coupled with a general sea-level fall during the Neogene onwards caused erosion of hinterland sediments and the development of a rapidly prograding clastic depositional system. The Meragang Beach outcrop, is part of the Belait Formation.

The Belait Formation is characterised as a sandy shallow water proximal system deposited in a tide- and wave-dominated environment (Lambiase et al., 2003). A more detailed explanation on Brunei's lithostratigraphy is given in chapter 2.

In this study, sediments exhibiting tide-created sedimentary structures that are rich in OM such as rippled wavy-bedded sandstones and trough cross-stratified sandstones are necessary to study how tidal activity packs in OM into sandstones. Such sediments are exposed in Meragang Beach which is part of the lower Belait Formation (Fig 1.5).

1.3. Materials and methods

1.3.1. Samples and facies identification

To study plant fragment distribution in sandy sediments of hyperpycnites, it is necessary to find a layer exhibiting two types of facies deposited by the same event but with different sediment concentrations (the amount of sediment particles relative to fluid within flow). Only one layer containing two different facies was found in the Chidorigataki Falls and is shown between interval 14 cm and 48 cm (Fig. 1.3). 27 sediment samples from sandy hyperpycnite-mudstone and sandy intrabasinal turbidite-mudstone couplets in the three turbidite sequences (sites A, B, and C) of the Chidorigataki Falls section were collected. To study organic geochemical analysis of early-stage flood or hyperpycnal flow formation, 14 PF-concentrated silts and sands were collected from flood-plain deposits of the Bibai outcrop. To analyse how tides affect OM preservation in sandstones. OM-absent layers and OM-abundant layers such as rippled wavy-bedded sandstones and trough cross-bedded sandstones were collected.

All samples from all locations (n=56) were then filed with a penknife to remove weathered surfaces and were then crushed to powder in a mortar before performing solvent extraction for biomarker analysis.

Facies of the turbidites found in the Chidorigataki Falls section were identified based on Zavala et al. (2011) and (Bouma, 1964). Considering sedimentary structures and plant fragment orientation such as dispersed (randomly) or laminated (subhorizontal), sandstones with plant fragment-dispersed, plant fragment-laminated and plant fragment-laminated with horizontal lamination corresponding to dense S1, less dense S1 and S2 facies respectively were identified and are collectively known as

plant fragment-concentrated sandstones. Coarse and structureless basal sandstones were identified as T_a sandstones, while siltstone and mudstones were classified as Bouma $T_{e.}$ or lofting deposits.

Facies of the Bibai River interval were identified based on Okano and Waseda (2003). In the study interval, four facies were found. The channel sandstone facies is characterized by coarse-sized grains with cross-stratification with some ripples. The flood-plain sandstones and silts are characterized by alternating beds of very fine sands or silts with current-ripple cross-lamination and abundant plant-fragments. The coal and coaly mudstones are characterized by high coal abundance.

Facies of the Meragang Beach outcrop were identified based on (Breckenridge et al., 2019; Collins et al., 2018). Four facies were found and were all of medium-coarse sands. Horizontal-laminated and structureless sandstones were mostly absent in OM, except for one structureless sandstone at the base of the outcrop.

1.3.2. Transmitted light and fluorescent light microscopy

30µm-thick thin sections of plant fragment-concentrated sandstones attached to a glass slide with epoxy were made for the observation of plant fragments within the sample. A transmitted light microscope and an Olympus BX41 reflected light fluorescent microscope with an Olympus ULH100HG mercury lamp and a DM4000 dichroic mirror containing 330-385nm excitation filter and a 420nm long pass barrier filter was used. Based on previously published studies (i.e. Tyson, 1995; Batten, 1996; Sawada et al. 2012), woody material would have no fluorescence, resin would have strong orange fluorescence, and cuticles would have strong yellow to white fluorescence. However, thermal maturity, oxidation and degradation may reduce or eliminate any fluorescence exhibited by these materials.

1.3.3. Total organic carbon content (TOC%)

A portion of each powdered sediment sample was acidified with 1 M HCl and allowed to stand for half a day to remove carbonates. Carbonate-free samples were then vacuum-dried and analyzed for TOC content using a J-Science Micro Corder JM10 instrument at the Center for Instrumental Analysis of Hokkaido University.

1.3.4. Biomarker analysis

Extraction and separation of lipids were performed as reported in Sawada (2006). Briefly, extractable organic molecules of the sediment samples were extracted with methanol (MeOH) and dichloromethane (DCM) (1/1, v/v) with ultrasonification. The extracted lipids were then evaporated and redissolved in hexane before being passed through a 95% activated silica gel column to be divided into 4 fractions - the aliphatic hydrocarbon (F1), aromatic hydrocarbon (F2), ketone-ester (F3) and polar lipid (F4) fractions. Afterwards, an internal standard, tetracosane-d_{50} was added to each fraction.

For F1 and F2, reduced copper was added to the solution to remove any sulfur. Afterwards, the above fractions were evaporated in a rotary evaporator and then redissolved in hexane before being passed through a gas chromatograph coupled with a mass spectrometer (GC-MS). In this study, the Agilent Technologies 7890B GC System (with DB-5HT fused silica column) coupled to an Agilent Technologies 5977A Mass Spectrometer (electron voltage of 70 eV, initial temperature of 50°C held at 4 mins, then ramped up to 310°C at 4°C/min and held at 20 min, scan range: *m/z* 50 – *m/z* 650 in 1.3s) was used.

1.4. Results and interpretation

1.4.1. Sedimentary facies of the Kawabata and Bibai Formations

A total of 5 sedimentary facies were recognized in the three studied sites of the Chidorigataki Falls section, including sandy layers rich in plant fragments. Site C is 20 m horizontally apart from site B. Site B is 15 m horizontally apart from site A. All sites are 145 cm thick. The plant fragment-dispersed sandstone unit in site B tapers out before it reaches both sites, suggesting that this may be a fringe zone of an inner lobe. Site C also contains a plant fragment-dispersed unit in the middle of an intrabasinal turbidite (Fig. 1.3).

As for the Bibai Formation, 3 sedimentary facies were recognized based on the description provided by Okano and Waseda (2003) (Fig. 1.4). In general, PF-absent coarse sandstones are interpreted to be channel deposits, while PF-rich rippled fine-grained sandstones are interpreted to be crevasse-splay deposits. Coals and coaly muds were also found and are interpreted to have been formed in back marshes. A detailed description on the sedimentary facies of the Chidorigataki Falls and Bibai outcrops is provided in table 1.1.

1.4.2. Sedimentary facies of the Belait Formation

A total of 4 sedimentary facies were found in the Belait Formation shallow water succession (Fig. 1.5.). Most sedimentary structures found are indicative of rapid unidirectional flow or indicative of reversing currents such as tides. They are interpreted to have been deposited in the upper-shoreface of a shallow water clastic system dominated by tidal reworking. A detailed description of the sedimentary facies found are described in table 1.2.

1.4.3. Plant fragments seen within sediments

Figure 1.6 shows large plant fragments seen within the plant fragment-concentrated sandstone layers and mudstones of the Kawabata Formation. Plant fragment-laminated layers show horizontal/sub-horizontal orientation of plant fragments while plant fragment-dispersed layers show smaller plant fragments dispersed at random throughout the sandstone. Mudstones found above plant fragment-concentrated sandstones contain some flat plant fragments. Figure 1.7 shows various types of terrestrial OM under transmitted light and fluorescent light microscopy of the plant fragment-concentrated sandstones of the study. Plant fragment-concentrated sandstones contain abundant plant fragments such as woody material, leaf cuticles and resin. Woody fragments are large, opaque in both transmitted and fluorescent light, angular, of varying sizes and with some containing resinous substances within them. Leaf cuticles appear brown in transmitted light and weak yellow under fluorescent light. They are elongated and appear with opaque, non-fluorescent leaf tissues. Resins appear orange in transmitted light and pale-yellow in fluorescent light with smooth liquid-like edges. Plant fragments (or tissues) are thin, elongated and opaque in both transmitted and fluorescent light. However, since no internal structures or diagnostic features can be seen within these plant fragments, the type of plant tissue cannot be identified specifically.

1.4.4. TOC% and biomarker data of Chidorigataki Falls and Bibai River section.

TOC% data for the Chidorigataki Falls and Bibai River sections are shown in table 1.3 while representative mass fragmentograms of the apolar fractions (F1) of the Chidorigataki Falls section are shown in figure 1.8.

For the Bibaigawa section, TOC% ranges 1.73% to 60.53% in coals and coaly muds, 0.17% to 4.92% in plant fragment-concentrated sandstones and mudstones, and 0.45% in the silt layer. For the Chidorigataki Falls section, TOC% is highest in plant fragment-concentrated sandstones with values ranging from 0.55% to 15.03%. Mudstones show moderate TOC% values, ranging from 0.34% to 0.54%. T_a sandstones have the lowest TOC% values, ranging from 0.10% to 0.29%.

Using *m/z* 57, pristane/phytane (Pr/Ph), *n*-alkanes as well as the indices P_{aq} and CPI were quantified (Fig 1.9 & 1.10).

Total *n*-alkane concentrations (μg/g-sed) are used to give an idea on how much *n*-alkanes are in a gram of sediment. In the Bibai River section, *n*-alkane concentrations range between 6.26 to 490.22 in coaly sediments, and range between 1.26 to 55.57 in PFC-sandstones, PFC-mudstones and silts. In Chidorigataki Falls, *n*-alkane concentrations are highest in plant fragment-concentrated sandstones, ranging from 2.86 to 12.8. Mudstones have lower concentrations at 2.31 to 5.77, while T_a sandstones have the lowest concentrations from 0.05 to 0.13.

The aquatic macrophyte *n*-alkane proxy, P_{aq}, is deduced by the relative amounts of C_{23} and C_{25} *n*-alkanes compared to C_{29} and C_{31} *n*-alkanes (Ficken et al., 2000). In the Bibai River section, Paq ranges between 0.45 to 0.71. In the Chidorigataki Falls section, the P_{aq} is highest in plant fragment-concentrated sandstones with values ranging from 0.49 to 0.89. T_a sandstones have lower values at 0.39 to 0.80. Mudstones have the lowest values at 0.33 to 0.56.

Pr/Ph is used as a redox indicator as well as a non-specific terrigenous OM indicator. Phytol, derived from the epicuticular leaf waxes of land plants and phytoplankton, degrades to produce more pristane (Pr) than phytane (Ph) under oxic conditions, while under anoxic conditions it produces more phytane than pristane (Didyk et al., 1978a). It has been interpreted that Pr/Ph ratios greater than 1.5 indicate oxic environments. In addition, the Pr/Ph values > 3 indicates high input of terrigenous OM (Powell, 1988). In the Bibai River section, pr/ph values are high, ranging from 12.85 to 6.16. In the Chidorigataki Falls section, the Pr/Ph ratios are highest in plant fragment-concentrated sandstones, ranging from 2.88 to 5.86, and mudstones and T_a sandstones range from 1.62 to 2.80

Long chain *n*-alkanes with odd carbon numbers (C_{25} to C_{33}) are derived from epicuticular leaf waxes and are quite stable in the fossil record for tens of millions of years due to being straight-chain hydrocarbons with no functional groups (Eglinton & Logan, 1991). Hence, they are used to determine leaf wax concentrations in the sediments (Peters et al., 2005)(Peters et al., 1991). The

carbon preference index (CPI) is used to determine the ratio of odd-chain, epicuticular leaf wax derived *n*-alkanes from land plants to even-chain *n*-alkanes from marine sources but should be used with caution as degradation or thermal alteration can convert odd-numbered *n*-alkanes to even-numbered *n*-alkanes (Bray & Evans, 1961; X. Chen et al., 2021; Eglinton & Hamilton, 1963a). In the Bibai River section, Long-chain *n*-alkane concentrations (μg/g-TOC) range between 303.00 and 2010.8. In the Chidorigataki Fall section, long chain *n*-alkane concentrations are lowest in T_a sandstones, ranging from 0.11 to 0.37 (μg/g-TOC). Plant fragment-concentrated sandstones have moderate *n*-alkane concentrations per TOC, from 0.16 to 5.21. Mudstones have the highest *n*-alkane concentrations per TOC at 2.46 to 6.43. CPI values are low in T_a sandstones, with values ranging from 1.37 to 1.91. Moderate values are seen in plant fragment-concentrated sandstones, at values between 1.46 to 2.18. Highest values are seen in mudstones ranging from 1.93 to 2.32 (Fig. 11).

Using *m/z* 217 and the molecular ions M+ 372, 386, and 400 for C_{27}, C_{28} and C_{29} regular steranes respectively, steranes were identified and quantified. The C_{27} and C_{28} regular steranes are steroids derived from phytoplankton and zooplankton while C_{29} steroids are generally derived from higher plants (Volkman, 1986). Higher C_{27} ratios indicate higher input of marine OM. No C_{27} or C_{28} steranes were detected in the Bibai River section. In the Chidorigataki Falls section, the C_{27} regular sterane ratios are lowest in plant fragment-concentrated sandstones, ranging from 0.03 to 0.26. Mudstones and T_a sandstones have C_{27} sterane ratios between 0.35 to 0.52.

Highly branched isoprenoid (HBI) alkane with a C_{25} carbon number is an isoprenoid derived from certain species of diatoms (J. Damsté et al., 2004). HBI/*n*-C_{21} ratios are lowest in plant fragment-concentrated sandstones, ranging from 0.01 to 0.36. Mudstones and T_a sandstones have similar HBI/*n*-C_{21} ratios ranging from 0.30 to 0.64. Total HBI is measured as the sum of C_{25} HBI *n*-alkane and HBI thiophene and is used to estimate diatom abundances. The HBI thiophenes were identified using the base peak *m/z* 293 and *m/z* 265 with an M+ ion of 378. Similar to the above, no marine-derived OM or diatoms were discovered in the Bibai River section. In the Chidorigataki Falls section, total HBI concentrations are highest in mudstones, ranging from 0.151 to 0.339 (μg/g-TOC). Plant fragment-concentrated sandstones have the lowest concentrations, between 0.001 to 0.023, suggesting low diatom input. T_a sandstones have values between 0.009 to 0.021.

1.4.5. TOC% and biomarker data of Meragang Beach sandstones.

Biomarker data for the Meragang Beach outcrop is shown in figure 1.12 and table 1.4. For the Meragang Beach sands, trough cross-stratified sandstones with PFs have the highest TOC% values, at 10.78 to 4.89. The wavy-bedded rippled sandstones have lesser values, ranging from 0.89% to 1.61%. Other PF-absent sandstones (structureless sandstones, horizontal laminated sandstones and stratified sandstones without PFs) have lower values at 0.09 to 0.27%, with an anomaly of 0.76%.

Wavy bedded - rippled sandstones have high total *n*-alkane concentrations (μg/g-sed) of 3.58 to 5.11, while trough cross-stratified sandstones have lower values at 3.94 to 4.60. PF-absent sands have the lowest values, ranging between 0 to 3.76. Pr/Ph values are highest in wavy-bedded rippled and trough-cross laminated sands, with values ranging from 3.67 to 4.19. PF-absent sandstones did not have detectable amounts of pr/ph, except for 3 layers that values between 1.2 to 2.33. Long-chain *n*-alkane concentrations (μg/g-TOC) are highest in rippled sandstones, at values between 197.9 to 322.4, and are generally lower in trough cross-stratified sandstones, with values ranging from 36.9 to 59.0. PF-absent sandstones mostly have no *n*-alkane biomarkers, or have values ranging from 14.7 to 230. Sterane are low in all samples, ranging between 0.15 to 0.25. HBIs were found only in wavy-bedded sandstones, with total HBIs (μg/g-TOC) ranging from 0.19 to 0.03.

1.5. Discussion

1.5.1. Terrigenous OM characterization and distribution in flood-plain and sandy extrabasinal turbidites

Hyperpycnal flows are formed when sediment concentration of floods exceeds that of the marine environment. The increase of sediments due to flooding events can happen gradually under regular storm conditions or suddenly such as by natural “dam-breaking” flood events (Mulder et al., 2003). Selvaraj et al (2015) collected river water and deep-sea hyperpycnite samples when typhoon Marakot and Parma created flooding in Taiwan. Isotopic analysis showed that river water and hyperpynites had similar terrigenous organic matter source. They further elucidated that deep-sea sediments had more marine-derived nitrogen and shallow water diatoms, suggesting a change in flow compositions from rivers to the deep sea. However, they used bulk analysis made no reference to sedimentological properties of the flow.

In ancient outcrops, river channels are usually sandy sediments absent in OM. However, flood-plain deposits that are deposited by channel overflow during floods can preserve OM from flood-events. Thus, in this study, flood-plain deposits are used as an analogue for hyperpycnal flows before they enter the marine environment and undergo flow transformations.

Using Pr/Ph ratios, C_{27} sterane ratios, long chain *n*-alkane concentrations per TOC, and P_{aq}, terrestrial organic matter distributions within the flood-plain deposits and extrabasinal turbidites were elucidated. In the flood-plain sediments, pr/ph ratios are very high (> 10) with no detectable amounts of algal steranes, showing very high oxicity and terrigenous OM contents. In the Chidorigataki Falls section, pr/ph values are still high but lower than that of flood-plains. These results show a loss of terrigenous OM during flow from continents to deep-sea. In the Chidorigataki Falls section, Pr/Ph ratios are higher in the plant fragment-concentrated layers indicating higher terrigenous OM contents as opposed to marine mudstones. Higher Pr/Ph values (> 3) are seen in plant fragment-laminated layers while lower values are seen in the plant fragment-dispersed layer, indicating enrichment of plant fragments in less dense flows of hyperpycnal turbidity currents that develops by flow transformation when the flow wanes. The low C_{27} regular sterane ratios (< 0.2) of the plant fragment-concentrated layers indicate that these layers not only have a high abundance of terrestrial OM, but also indicates less mixing with ambient waters, as the marine mudstones in this study have higher C_{27} regular sterane ratios (> 0.38). Less mixing of extrabasinal turbidity flows with marine waters are caused when quasi-steady hyperpycnal flows develop sediment densities higher than ambient waters, causing no mixing with ambient waters as they travel like a ‘wedge’ between the sea floor and water column (Fig. 1.13) (Mulder et al., 2005; Zavala and Arcuri; 2016). This wedge-like transport and no mixing with marine waters may have also facilitated the preservation of OM and plant fragments seen in these sandy hyperpycnal deposits (TOC% 0.60 – 15.03), as rapid transport and direct deposition of OM from the terrestrial environment to the deep sea by hyperpycnal flows reduces time spent in zones facilitating microbial degradation of OM, protecting it from degradation (Ibach, 1982). In addition, the deposition of mudstones directly on top of the sandy layer by vertical settling of hemipelagic deposits acts as a seal to reduce the transfer of water into the sandy layers, preventing further oxidation of OM (Hartnett et al., 1998). The outer layers of plant fragments seen in this study may have also prevented the degradation of biomarkers residing within the plant fragments. The oxic character seen in plant fragment-concentrated layers may have been due to freshwater interstitial waters in sandy hyperpycnal flows, as discovered by Kao et al (2010).

The presence of such freshwater within the sandy layers of extrabasinal turbidites would cause more pristane (Pr) to be produced than phytane (Ph).

Long-chain *n*-alkane concentrations after being normalized by TOC% aid in characterizing leafy to non-leaf plant fragments, as waxes of leaf cuticles produce higher amounts of long chain *n*-alkanes compared to woody fragments. In the Bibaigawa outcrop, n-alkanes show a very large range, with higher values indicating high leaf-wax accumulations and lower values with high TOC% indicating more woody material accumulations. In the Chidorigataki Falls section, lower values are seen but fractionation is also evident between PF-sandstones and mudstones, with the former having lower leafy/more woody contents while the latter has more leafy/lower woody contents. In the Chidorigataki Falls section, plant fragment-laminated sandstone layers have lower long chain *n*-alkane concentrations (< 3 μg/g-TOC) compared to plant fragment-dispersed layers. The low long chain *n*-alkane concentration coupled with higher TOC% with more visible woody fragments, while the opposite is seen in the plant fragment-dispersed sandstone, suggests that woody fragments are likely to enrich less-dense parts of sandy flows rather than denser sandy flows. The high long chain *n*-alkane concentration seen in plant fragment-dispersed sandstones of Site B resembles that of mudstones also in site B, reflecting that erosion and incorporation of seafloor sediments incorporated leafy material previously deposited by hemipelagic deposition on the seabed, supported by the slightly higher values of marine biomarkers of this layer compared to plant fragment-laminated layers.

P_{aq} is an index reflecting the contribution of *n*-alkanes derived from aquatic macrophytes. In the Bibaigawa section, P_{aq} shows moderate values, suggesting a mixture of aquatic and non-aquatic plants. However, in the Chidorigataki Falls sections, the high values of P_{aq} in the plant fragment-containing sandstones suggests that large amounts of OM were derived from aquatic plants while the lower values in mudstones suggest lower contribution of aquatic plants (Fig. 9A). These results indicates that hemipelagic deposits with OM delivered by normal river discharge do not carry much aquatic plant remains, while large flood events capable of delivering sand to the deep sea may entrain and transport relatively more aquatic plants from wetland areas such as marshes and swamps.

1.5.2. Marine OM incorporation in sandy turbidite systems

Using C_{27} regular sterane ratios, along with diatomaceous biomarker indices such as HBI/*n*-C_{21} and total HBI (μg/g-TOC), marine input into both floodplain and extrabasinal turbidite systems was elucidated. In the Chidorigataki Falls section, plant fragment-concentrated layers contained low regular sterane ratios (< 0.21) than T_e mudstones (> 0.38) deposited directly above them. The low C_{27} regular sterane ratios and HBI indices of the plant fragment-concentrated sandstones are due to sediments sourced from the terrigenous environment with no mixing with ambient waters, although some marine OM has been incorporated into the flow due to erosion and incorporation of sea-floor sediments.

1.5.3. Organic matter variations from early stage floods to later stage floods

Based on the above, we can see a trend in the transformation of floods during transport from its early stages in continents (as represented by floodplain deposits) to the later stage in the deep sea (as represented by hyperpycnites). In early stages before entering the sea, terrigenous OM is high with no marine OM, however upon entering the marine realm, some terrigenous OM is lost due to lofting while some remains in the sandy part of floods. Some marine OM is eroded and entrained in the sandy flow, but much more marine OM is introduced to lofting plume deposits that come from hemipelagic-pelagic deposition (Fig 1.14).

1.5.4. Incorporation of terrigenous and marine OM in sandstones by tidal processes

The Meragang Beach sandstones showed significant differences between the OM-containing facies (wavy-bedded rippled sandstones and trough cross-stratified sandstones) and OM-absent facies (structureless sandstones and horizontal laminated sandstones). In general, the OM-absent facies were deposited rapidly by sandy flows that were too fast to develop ripples, which is believed to be the reason why OM cannot be deposited. However, an exception is seen in the first structureless sandstone layer which contained OM. This layer contained woody fragments randomly oriented within the layer and is believed to be developed by frictional freezing of dense sandy flows similar to that of Lowe sequences. Similar to turbidity currents, the detection of algal steranes in this layer also suggests that these high-density flows eroded and incorporated marine sediments during flow. As for

OM-containing wavy-bedded rippled sandstones and trough cross-stratified sandstones, results show high amounts of terrigenous OM in both facies, although only the former contained algal sediments. Both these facies are created by migrating ripples. In wavy-bedded rippled sandstones, the formation of mud-drapes deposited on ripples that creates the wavy-bedding suggests bidirectional currents where muddy layers are deposited on ripples during slack/stagnant waters (Daidu et al., 2013). In this study, OM was also found within such inter-sandstone muddy intercalations. These sediments contained high amounts of leaf-waxes and TOC% higher than OM-absent sandstones but lower than trough cross-stratified sandstones. Additionally, these muddy intercalations also contained HBI. These show that slack/stagnant waters that occur before the reversal of tidal currents allows fine-grained material and OM to be deposited and even preserved within sandy sediments. In trough cross-stratified sandstones, the formation of eddies in front of the lee-side of ripples allows plant-fragments to be trapped within migrating ripples (Shanley et al., 1992). Similar to sandy hyperpycnal deposits, leafy material was less abundant as seen by low leaf wax *n*-alkane values, but visible woody fragments and large TOC% (up to 10%) was observed. These results further support previous findings that woody material occupy denser areas whereas leafy material occupy less dense (usually muddy) areas.

1.5.5. Implications for transport and deposition of terrigenous OM

As hyperpycnal flows are rarely observed in nature because they occur during catastrophic events such as earthquakes or cyclones, the discovery of hyperpycnal flow deposits in outcrops provides a good opportunity for studying how terrestrial derived material, in particular terrestrial OM, are transferred to the deep-sea. As mentioned in the introduction, global burial fluxes of OM in marine environments do not match that of riverine-derived OM. Additionally, sandstones are generally thought to have poor preservation potential of sedimentary OM compared to mudstones, because OM cannot efficiently attach to the surface of non-clay minerals (Bianchi et al., 2018). In this study, the preservation of high amounts of OM in sandstones challenges the general idea that sandstones hardly preserve OM. This may have been caused by two factors: (1) direct deposition of hyperpycnal flows without mixing with ambient waters and the deposition of a mudstone seal prevented microbial oxidation; (2) large OM such as woody fragments may have preserved OM within them; (3) tidal activity that creates muddy layers within rippled sandstones that aid in preservation or rapid flows and deposition that can create OM-rich trough cross-laminated sandstones.

Based on the results of this study, sandstones deposited by extrabasinal turbidites via hyperpycnal flows and tidal-reworking of sediments can preserve OM regardless of the quartzite mineralogy as it is also dependent on sedimentary processes where terrigenous organic matter tends to concentrate in deposits created by less dense flows, such as plant fragment laminated layers rather than dispersed layers, or T_b and T_d layers of intrabasinal turbidites. As such, we show here that sandstones can also sequester high amounts of terrestrial organic carbon and become important carbon storage sinks. Thus, dirty rivers that can deliver sediments via hyperpycnal flows, such as the Huanghe River in China, or the Tsengwen and Choshui in Taiwan (H. Wang et al., 2010), can act as important conduits for the transfer and sequestering of OM within sandy deposits to the ocean. Since studies on OM preservation within sandstones deposited by hyperpycnal flows are scarce, these findings suggests that more dirty rivers with the potential to develop hyperpycnal flows should also be studied for their potential to preserve OM in sandstones. Furthermore, the discovery of OM-rich sandstones in the coastal environments challenge the idea that offshore muds are the only lithology that preserves sandstones. As a result, it is possible that the amount of OM estimated to be preserved in oceans may have been underestimated and that carbon sequestration in oceans with respect to the global carbon cycle may be inaccurate.

Apart from the transfer of OM to the oceans, the ability of hyperpycnal flows to deliver terrestrial OM to the deep-sea also suggests that they are also able to deliver anthropogenic pollutants to the deep-marine realms, as also reported by Pierdomenico et al. (2022). Thus, such studies on hyperpycnal flow pathways from river mouths to deposition zones may also aid in remediation or preventative methods to reduce pollutant delivery to the oceans.

Lastly, this study also highlights the use of biomarkers as an alternative yet not widely used method to aid in sedimentological interpretations. While calcareous microfossils may indicate marine input into sedimentary systems, the absence of fossils makes such quantifications difficult. In this study, biomarkers were used to quantify not only marine input but also terrestrial input. Hence, biomarkers may act as alternative tools to the more widespread use of isotope indices such as C/N ratios or $\delta^{13}C$.

1.6. Summary

Using sedimentology and biomarker analysis, OM deposition in relation to sedimentary processes was elucidated. Plant fragment-concentrated sandstones of the Chidorigataki Falls section were deposited by hyperpycnal extrabasinal turbidites originating from the terrestrial environment and flowed directly to the deep-sea without mixing with ambient water by wedge-like quasi-steady hyperpycnal flow. As such, higher terrigenous OM input was determined by high Pr/Ph values and high TOC%. High OM preservation seen in high TOC% values is due to rapid deposition and the presence of a mudstone seal. High TOC% coupled with low leaf-wax derived *n*-alkanes per TOC suggests abundance of plant tissues other than leaf-cuticles in sandy sediments. Terrigenous biomarker proxies also reveal higher terrigenous OM and woody material in sandy deposits deposited by less dense flows, such as the plant fragment-laminated sandstones. Mudstones deposited by lofting and normal hemipelagic deposition also contain high leaf *n*-alkanes per OC due to the escape of less-dense OM from the sandy part of the flow and into the plume. This could be due to differences in the flow densities that deposited each facies where woody plant fragments were largely deposited in less dense flows by weaker traction and small suspension fallout rather than in denser flows by strong traction fallout. Similar to that of the Chidorigataki Falls section, higher Pr/Ph and TOC% were present in layers with visible plant fragments, whereas T_a sandstones and T_e siltstones contained higher marine biomarkers due to erosion and incorporation of sea-floor sediments. The presence of mud clasts in T_a sandstones may also aid in preservation of OM within sandy sediments. Within shallower environments, bidirectional tides or rapid unidirectional currents can help preserve OM in woody intercalations within sandy sediments or by rapid deposition and burial in lee-side of ripples. The discovery of large organic matter accumulations in sandy sediments suggests that sandstones should not be overlooked over mudstones in considering carbon burial fluxes in the marine environment.

1.7. Figures

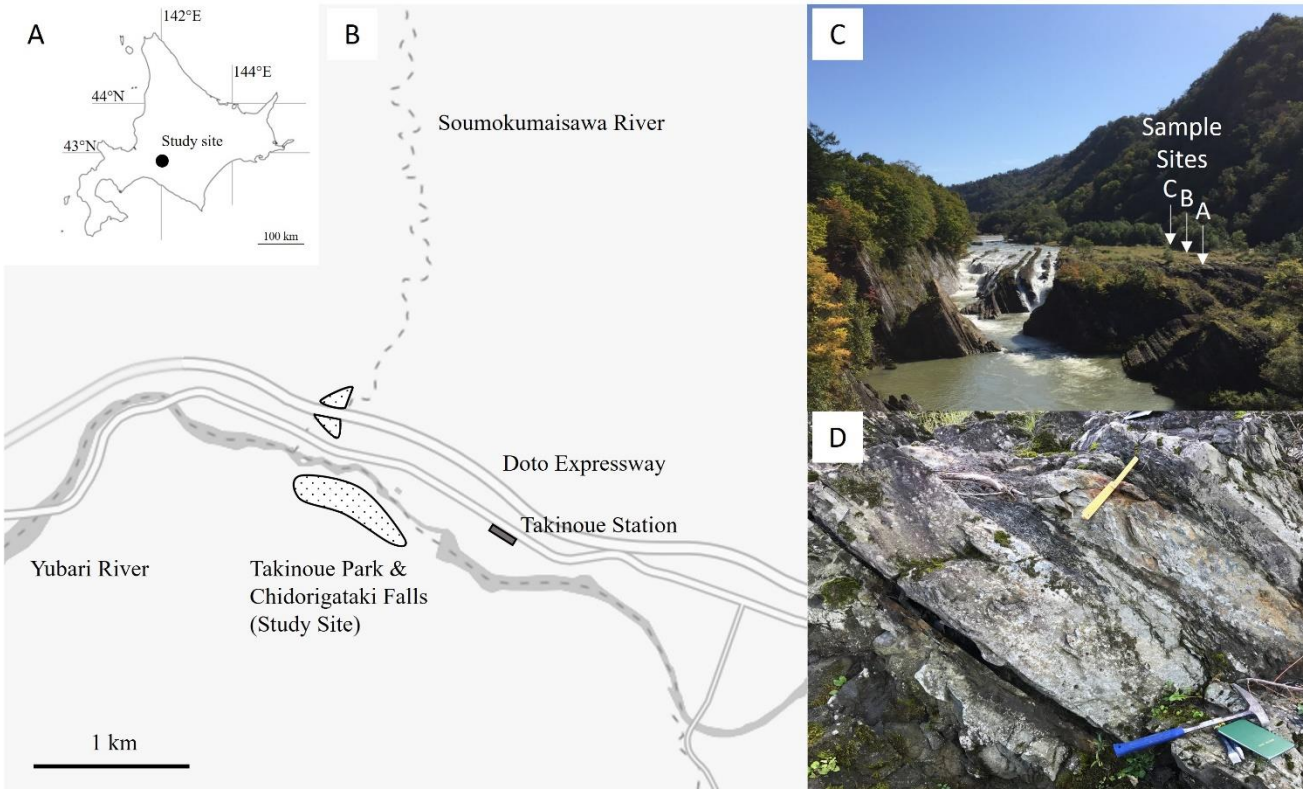

Figure 1.1. (A) Study site location shown on a map of Hokkaido, Japan. (B) Specific study site of the Chidorigataki Falls section in Takinoue Park and the Soumokumaisawa River Section, Yubari, Hokkaido. (C) The Chidorigataki Falls section with sample site labels. (D) The Chidorigataki Falls section.

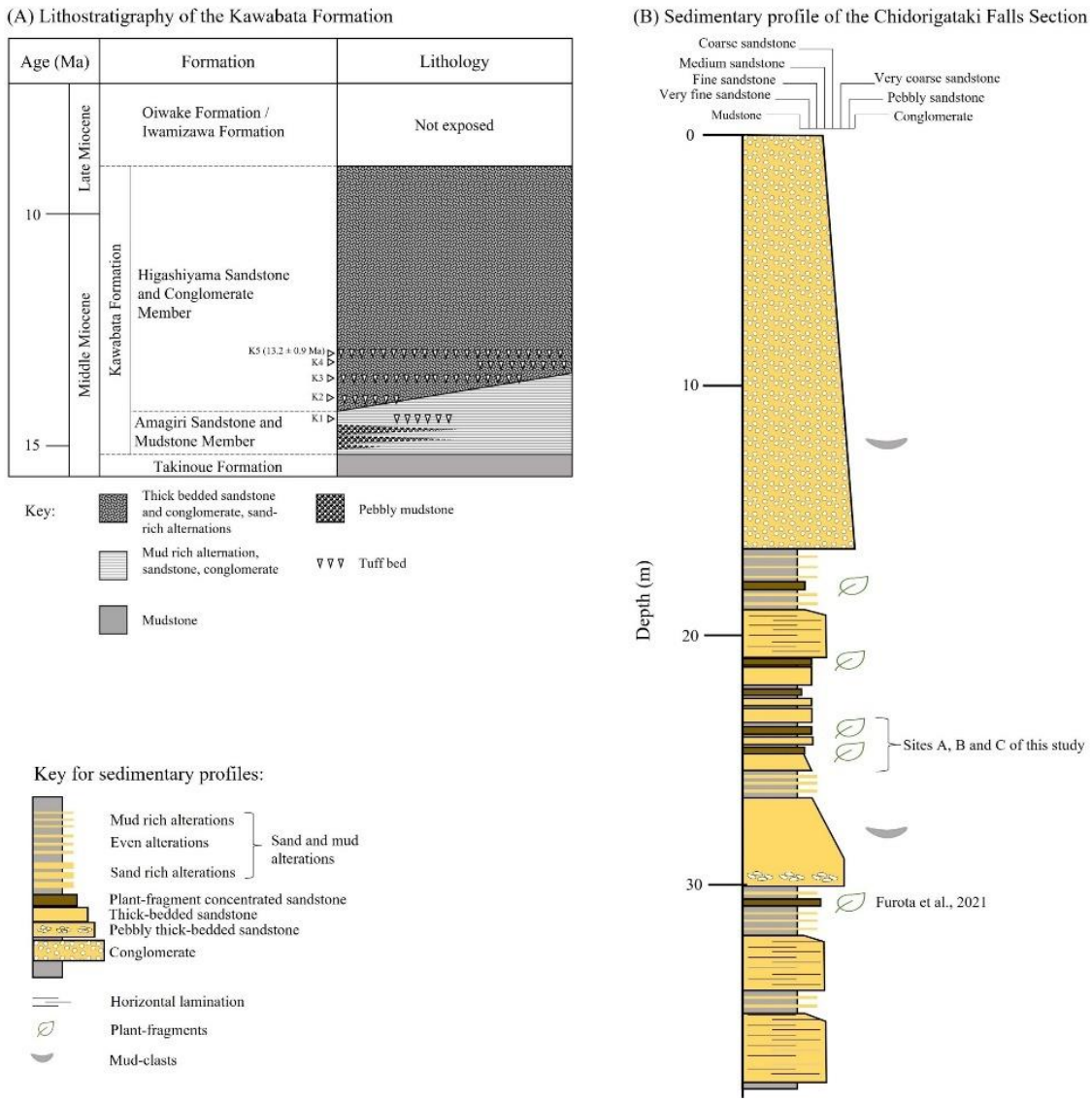

Figure 1.2. (A) Lithostratigraphic chart showing the Higashiyama Sandstone and Conglomerate member and the Amagiri Sandstone and Conglomerate member of the Kawabata Formation (adapted and modified from Kawakami et al., 2002). (B) Sedimentary profile of the Chidorigataki Falls section (adapted from Furota et al., 2021).

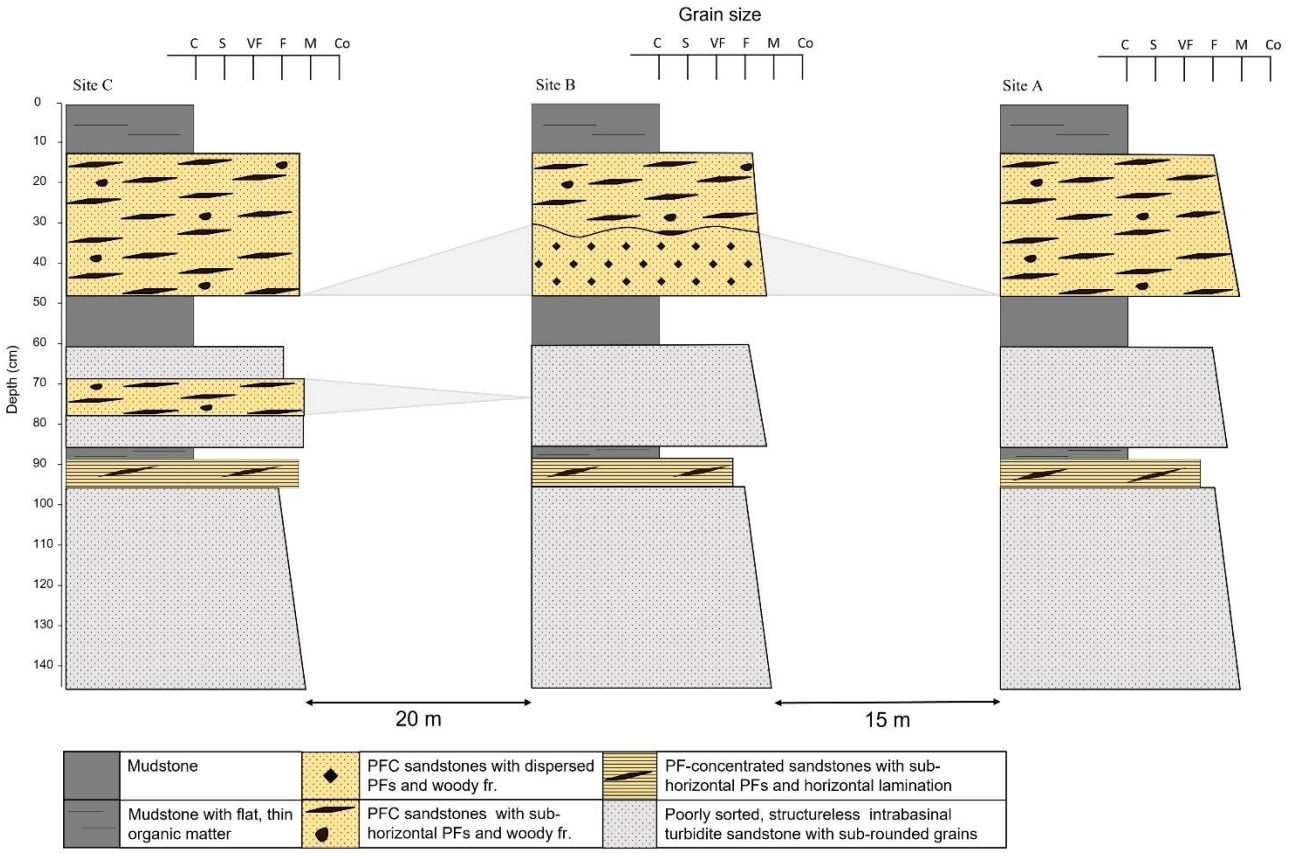

Figure 1.3. Sedimentary profiles of sample sites A, B and C. Site A is 15 metres apart from Site B. Site B is 20 metres apart from site C. Only site B contains a plant fragment-dispersed sandstone which disappears before it reaches site C and A. Site C contains a plant fragment-laminated sandstone with horizontal lamination in the middle of a T_a sandstone that is not visible in site B and A. PFC: Plant fragment-concentrated.

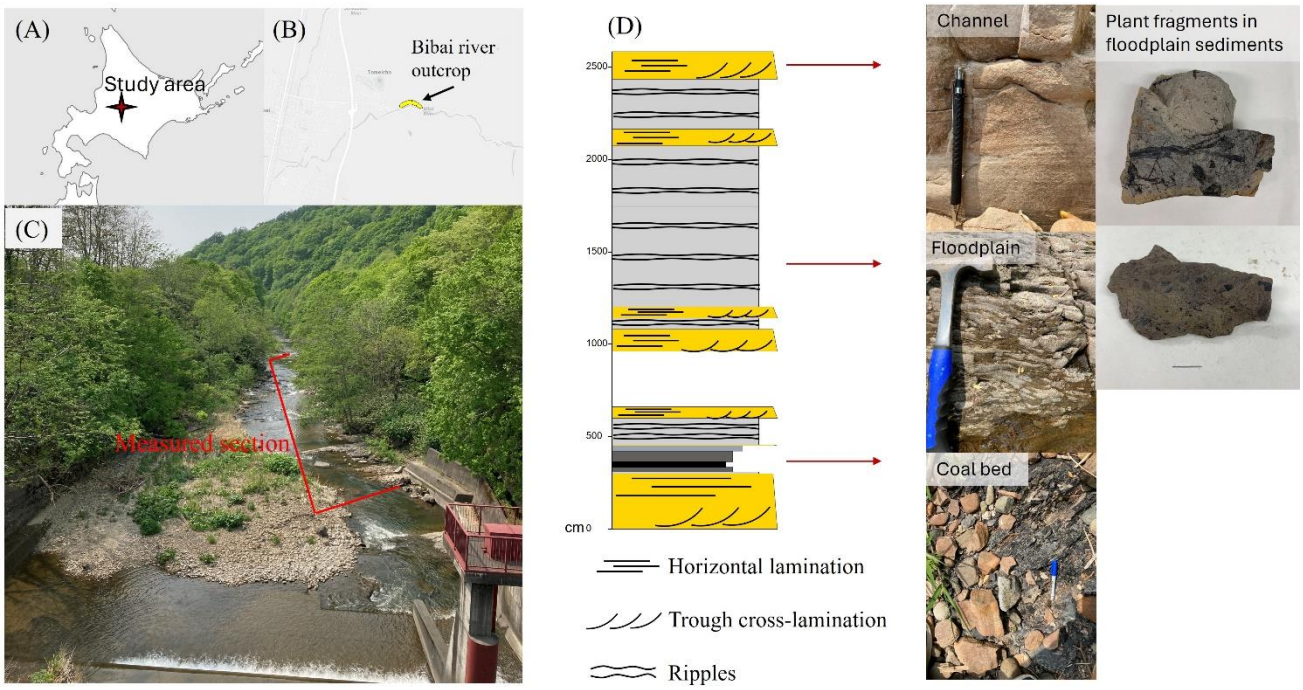

Figure 1.4. (A) Study area shown on Hokkaido's map. (B) Route map showing the location of the Bibai River outcrop. (C) Bibai River outcrop. (D) Sedimentary profile of the Bibai River outcrop.

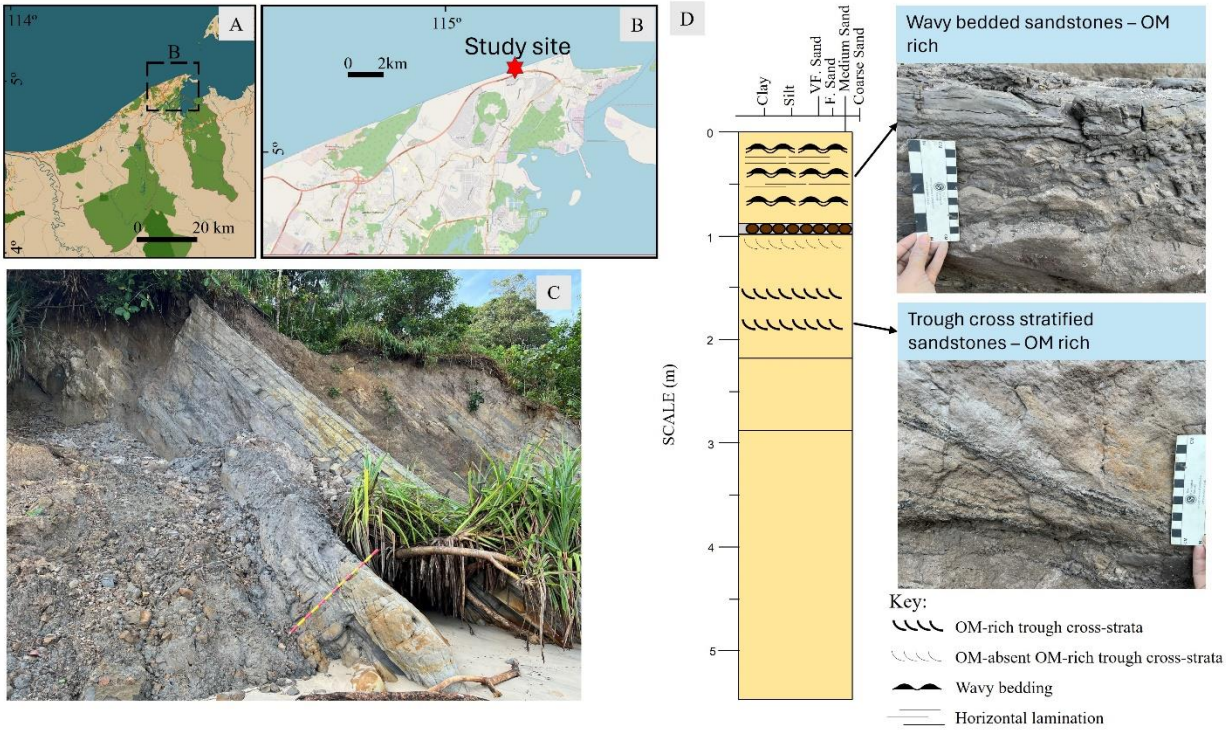

Figure 1.5. (A) Map of Brunei Darussalam. (B) Route map showing the location of Meragang Beach outcrop – study site. (C) Meragang Beach outcrop. (D) Sedimentary profile of the Meragang Beach outcrop.

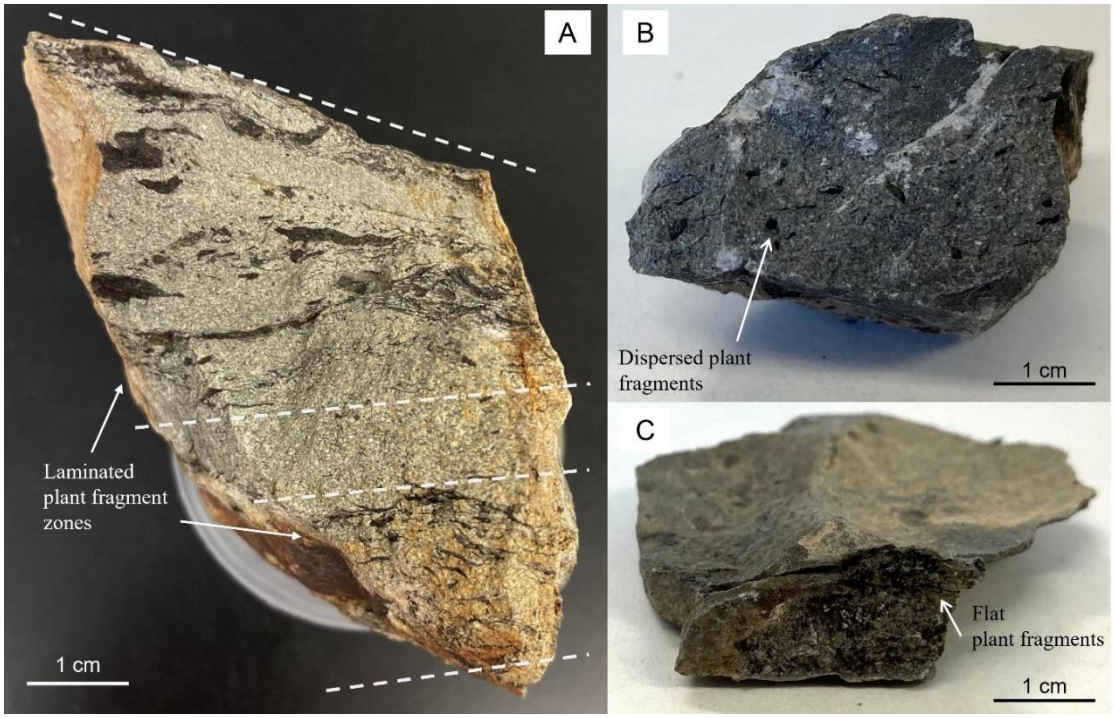

Figure 1.6. Different types of plant fragment distribution within sediments. (A) Plant fragment-laminated sandstones showing laminar, sub-horizontal plant fragment distribution. (B) Plant fragment -dispersed sandstones showing scattered arrangement of plant fragment, and (C) mudstone with thin, flat plant fragment.

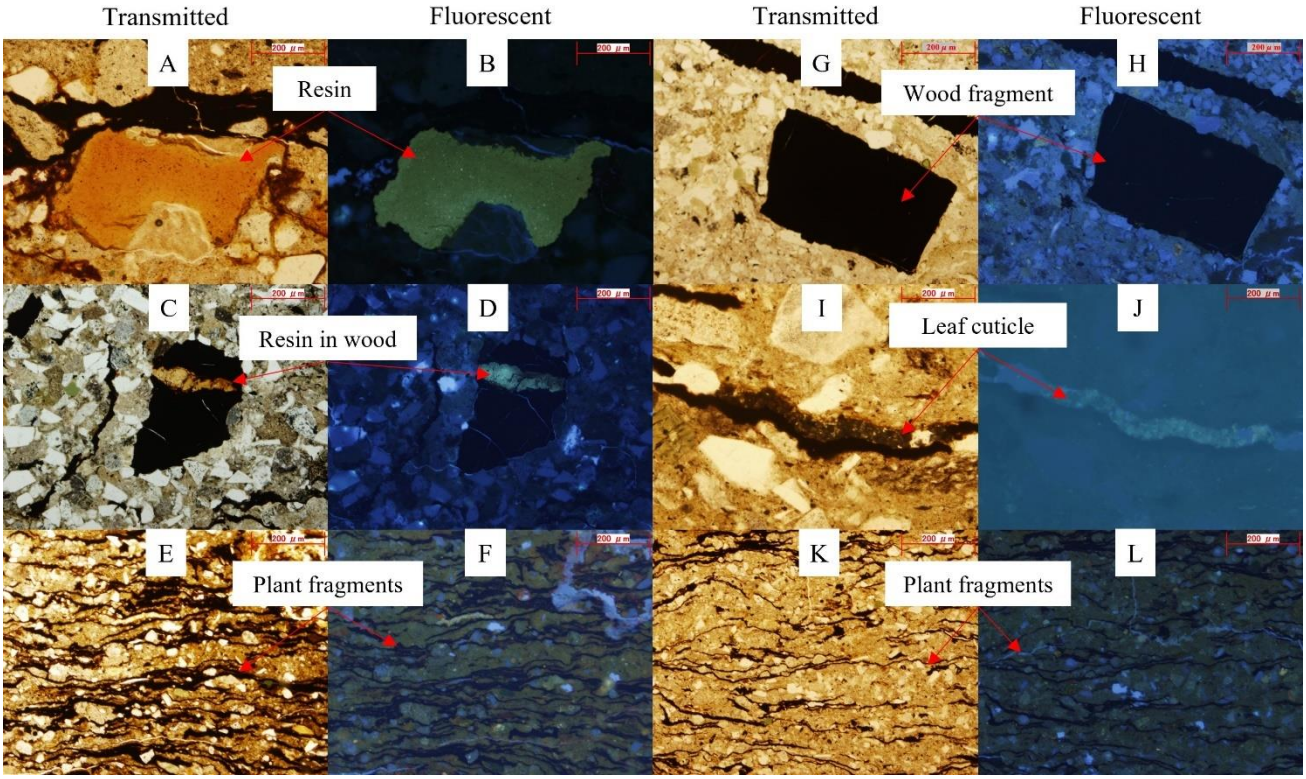

Figure 1.7. View of plant fragment - concentrated sandstones from the Chidorigataki Falls outcrop under transmitted light and fluorescent light microscopes. Wood fragments and plant fragments are dark with no fluorescence. Leaf cuticles show light fluorescence while resin shows strong fluorescence.

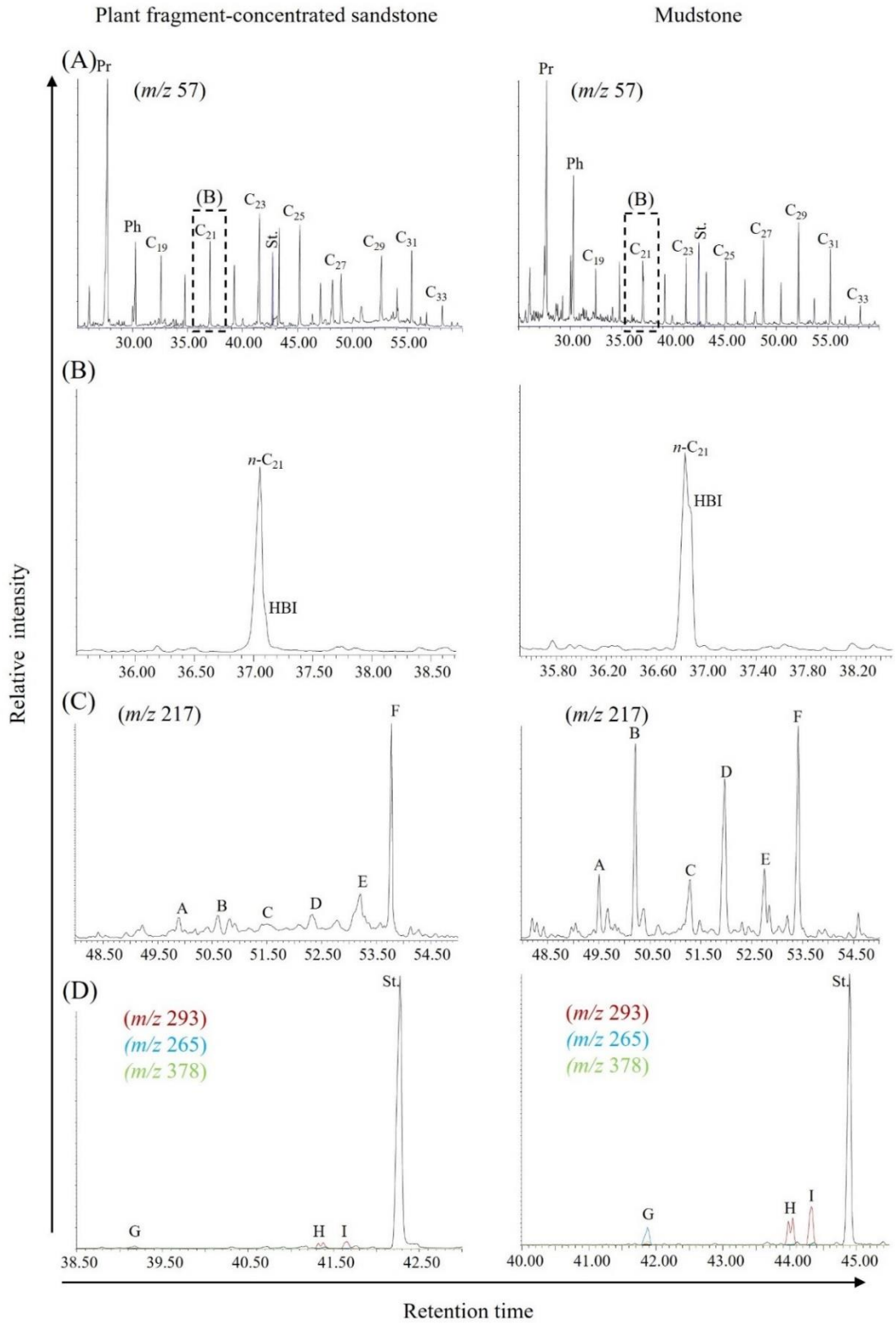

Figure 1.8. Mass fragmentograms of alkanes, HBI n-alkane C_{25}, regular steranes and HBI thiophene of plant fragment-concentrated sandstones (left) and mudstones (right) of the Chidorigataki Falls section sediments. Ph: prystane, Ph: phytane, St.: internal standard, A: C_{27} 5β(H),20R, B: C_{27} 5α(H),20R, C: C_{28} 5β(H),20R, 5: C_{28} 5α(H),20R, E: C_{29} 5β(H),20R, F: C_{29} C_{27} 5α(H),20R, HBI: higher branched isoprenoid, G: HBI thiophene (m/z 293), H and I: HBI thiophene isomers (m/z 265).

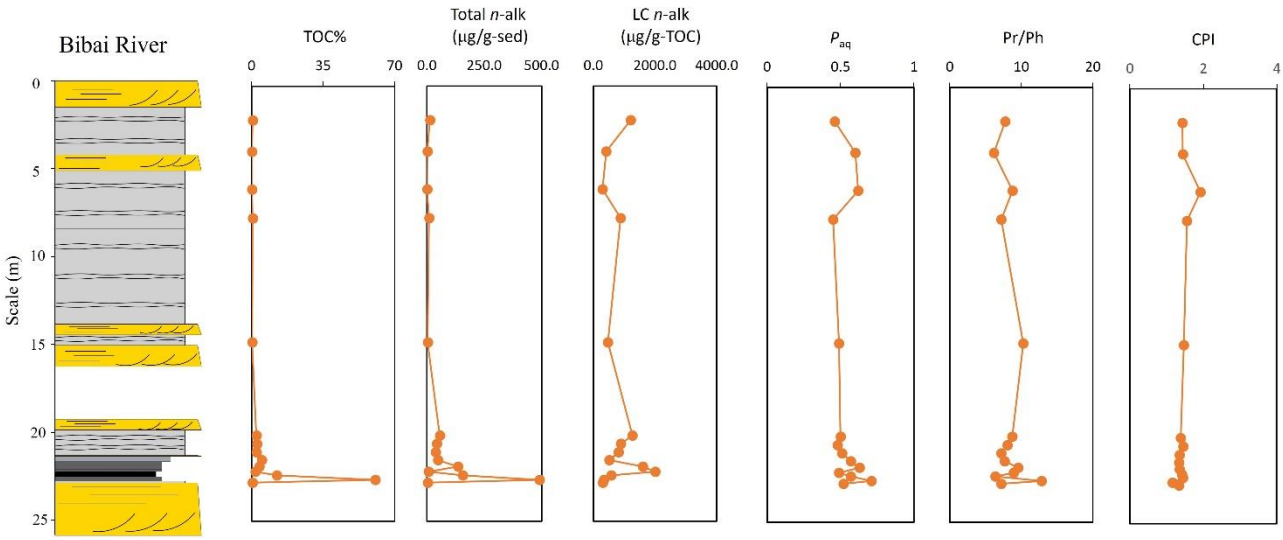

Figure 1.9. TOC% and biomarker data of the Bibai River section.

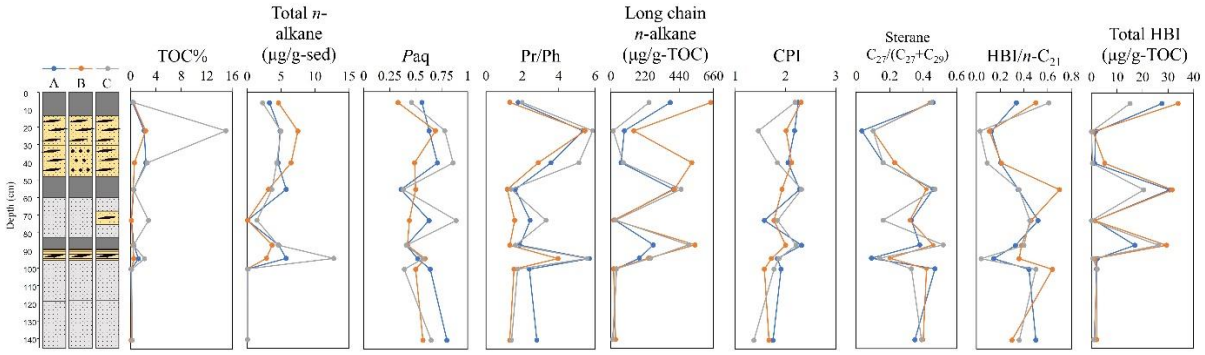

Figure 1.10. Biomarker data of the Chidorigataki Falls section.

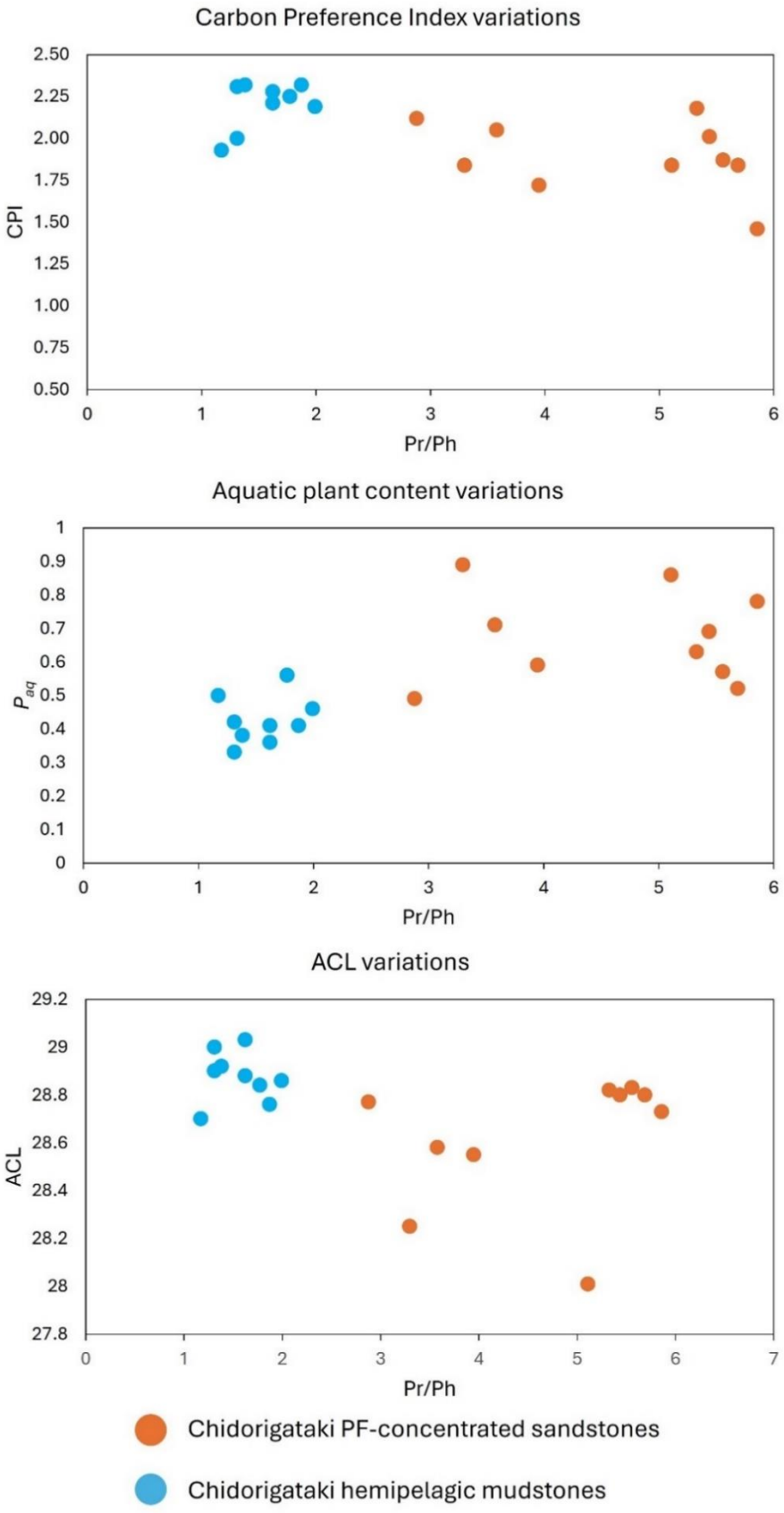

Figure 1.11. Variation in CPI, Paq and ACL of the Chidorigataki Falls section.

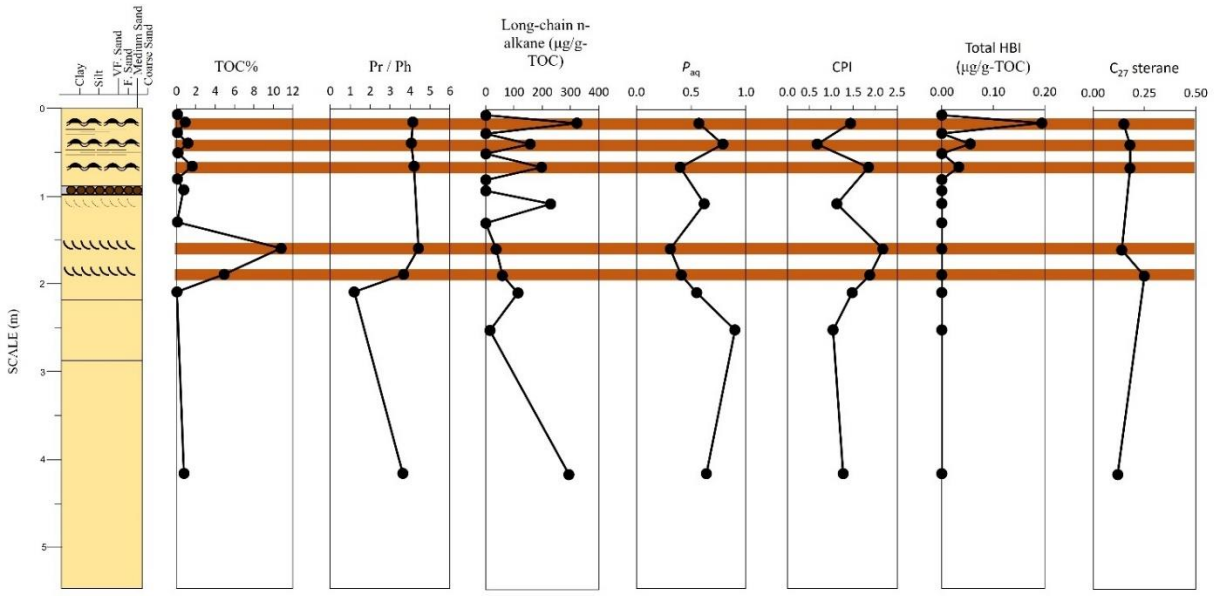

Figure 1.12. TOC% and biomarkers of Meragang Beach outcrop.

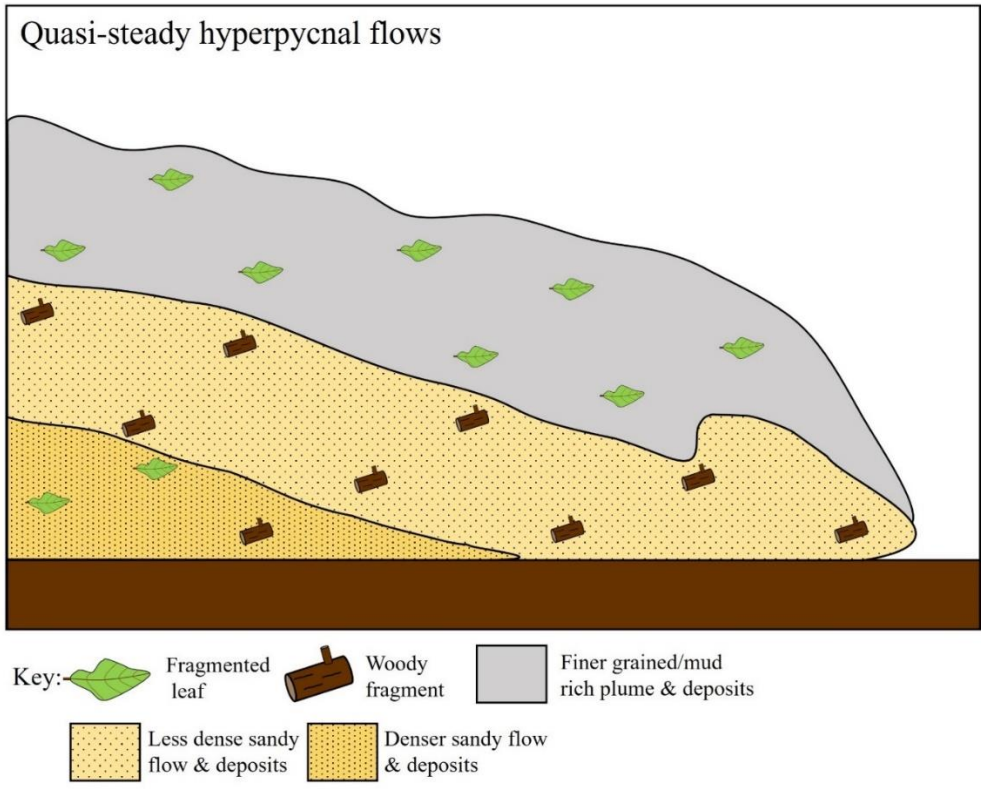

Figure 1.13. Quasi-steady hyperpycnal flows showing density fractionation of organic material within different types of flow.

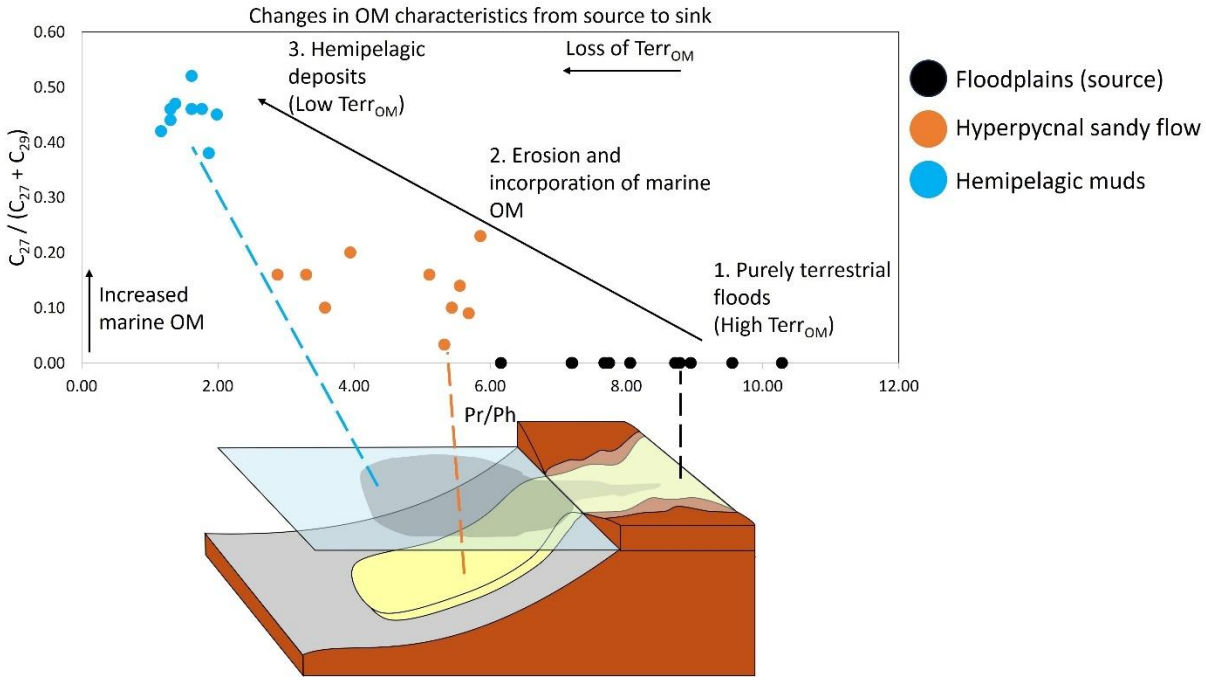

Figure 1.14. Changes in terrestrial and marine OM characteristics from source (early stage floods deposited as floodplain or crevasse splay sediments) to sink (hyperpycnal flood-flows that flowed to the deep sea).

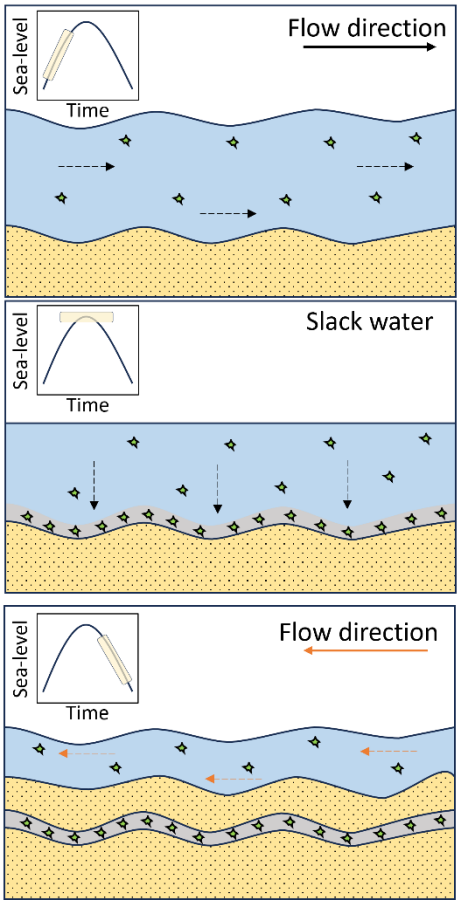

Figure 1.15. Deposition of wavy-bedded rippled sandstones and the introduction of muddy layers and OM in sandy bodies by tidal activity (Daidu et al., 2013).

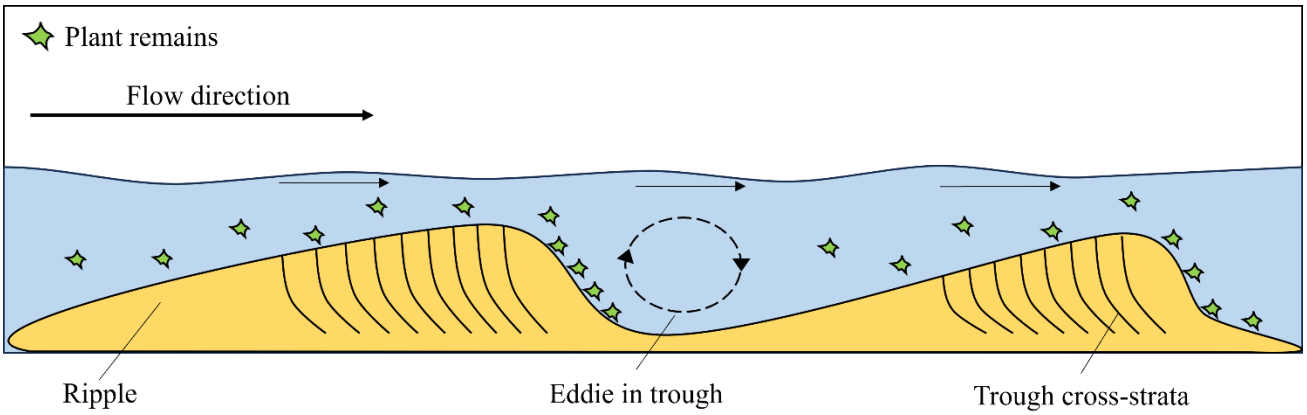

Figure 1.16. Deposition of OM-rich trough cross-stratified rippled sandstones by unidirectional currents (Shanley et al., 1992).

1.8. Tables

Table 1. Sedimentary facies and interpretation of sediments found in the Bibai River outcrop and Chidorigataki Falls outcrop

Facies	Main sedimentary features	Interpretation
T_e mudstone	3 cm to 12.5 cm thick Sharp basal contact Present above plant fragment-concentrated sandstone as well as plant fragment-poor intrabasinal sandstones May contain thin layers of very fine sand Flat plant fragments less than 1 mm thick present	Lofting plume deposits when above a plant fragment-concentrated sandstone (Zavala and Arcuri, 2016) or normal hemipelagic deposits when above plant fragment-poor sandstone Bouma T_e (Bouma, 1962)
Plant fragment-laminated sandstone (Plant fragment-concentrated sandstone with subhorizontal plant fragment distribution)	19 cm to 35 cm thick Well sorted, upper fine to lower fine-grained sandstone Structureless Sharp basal contact but has an erosive basal contact when above a plant fragment-dispersed layer Subhorizontal plant and woody fragments Plant and woody fragments greater than 2mm thick	Hyperpycnite deposited by gradual deposition Deposited at a more distal location than plant fragment-dispersed sandstone Facies corresponds to Zavala S1(Zavala and Arcuri, 2016)
Plant fragment-dispersed sandstone (Plant fragment-concentrated sandstone with dispersed plant fragment distribution)	16 cm thick Well sorted, upper fine-grained sandstone Sharp basal contact Upper boundary cut into by PF-laminated sandstone Forms the base of a fining upwards sequence with overlying plant fragment-laminated sandstone Structureless Dispersed plant and woody fragments Woody and leaf fragments are angular and greater than 2 mm in diameter	Hyperpycnite deposited by rapid deposition (Kneller and Branney, 1995) Deposited at a more proximal location thanplant fragment-laminated sandstor Facies corresponds to Zavala S1 (Zavala and Arcuri, 2016)
Plant fragment-laminated sandstone with horizontal lamination (Plant fragment concentrated sandstone with subhorizontal plant fragment distribution)	3 cm thick Well sorted, very fine to fine grained-sandstone Sharp basal contact Horizontal lamination present Subhorizontal plant fragments greater than 2mm thick	Hyperpycnite deposited by gradual deposition (Zavala and Arcuri, 2016) Deposited at a more distal location than plant fragment-laminated sandstone Facies corresponds to Zavala S2 (Zavala and Arcuri, 2016)
T_a sandstone	25 cm to 50 cm thick Poorly sorted medium to fine-grained sands but may also show general fining upwards sequence Structureless No visible plant or woody fragments Layer at site C (cum. thickness 60 cm to 85 cm incised by plant fragment-laminated sandstone)	Intrabasinal turbidite formed by deposition of slope sediments Facies corresponds to Bouma T_a (Bouma, 1962)
Rippled plant-fragment-lamindated sandstones and silstone	60 cm to 270 cm thcik Well sorted, silt to fine grained sandstone Sharp but undulating basal contact Ripples on surface Abundant in plant fragments dispersed at random orientation Plant fragments larger than that seen in the above turbidite PF-concentrated sandstones Appears as multiple layers stacked on each other	Crevasse splay deposits (Takano and Waseda, 2003).
Coals and coaly mudstones	12 cm to 45 cm thick Dark dull grey to shiny black in colour	Formed in backmarsh environment (Takano and Waseda, 2003).
Large cross-stratified sandstones	4.4 cm to 300 cm thick Coarse-grained well sorted sandstones Planar cross-lamination present Horizontal lamination present Erosive features within the layers No plant fragments	Channelizing events followed by sedimentation Lateral accretion evident by cross stratification Point bar deposits (Takano and Waseda, 2003).

Table1. 2. Sedimentary facies and interpretation of sediments found in the Meragang Beach outcrop.

Facies	Description	Biogenic structures	Interpretation
Structureless coarse sandstones	Unstratified, large coarse-grained sandstones Poorly sorted but mainly consists of coarse-grained sands Occasionally contains visible plant fragments Sharp upper and lower boundaries	None	Rapid deposition of high-density flows that prevented efficeint sorting sorting (Magalhaes et al., 2015)
Trough cross-stratified sandstones	Well sorted medium-coarse grained sands Curved, unidirectional lee-side with abundant plant-material and mud-drapes and occasionally mud-clasts Sharp upper and lower boundaries	Skolithos Ophiomorpha Chonichnus Paleophycus	Migration of S-shape dunes at relatively high-speeds (Miall, 1996). Deposition by tidal currents above fairweather wave-base and/or storm flows (Collins et al., 2018)
Horizontal laminated sandstones	Well sorted fine or medium-coarse grained sands Laminations are parallel to bedding plane No organic material Sharp upper and lower boundaries		Deposition of plane bed around the upper flow regime in a shallow environment (Alexander and Fielding, 1997)
Wavy / ripple-cross laminated sandstones and occasional siltstones	Well sorted coarse sands or silts Ripples are either symmetrical or asymmetrical Ripples may have thin muddy layers deposited on surface - forming wavy lamination May have thick muddly layers deposited on surface - forming lenticular beds When exposed on the bedding plane, they are often sinuos		Assymetric ripples show a tidally influenced environment in lower flow regimes (Collinson et al., Symmetric ripples Wavy and lenticular beds suggests mud-deposition on top of ripples during slack tides (Martin, 2000).

Table 1.3. Biomarker data of the Bibai River outcrop and the Chidorigataki Falls outcrop.

Sample depth (cm)	Lithology	TOC%	Total *n* -alkane (μg/g-sed)	*P* aq	Pr/Ph	Long chain n-alkane (μg/g-TOC)	Carbon Preference Index (CPI)	Sterane $C_{27}/(C_{27}+C_{29})$	HBI/*n* -C_{21}	Total HBI (μg/g-TOC)
Chi. Site A										
6	T_e mudstone	0.34	3.31	0.56	1.77	382.5	2.25	0.46	0.34	27.62
22	PFC sandstone	2.16	4.87	0.63	5.33	87.0	2.18	0.03	0.13	1.66
40	PFC sandstone	2.45	4.58	0.71	3.58	66.2	2.05	0.16	0.20	1.28
55	T_e mudstone	0.52	5.77	0.36	1.62	402.4	2.28	0.46	0.35	30.54
72.5	T_a sandstone	0.15	0.05	0.63	2.43	25.1	1.58	0.33	0.52	1.39
86.5	T_e mudstone	0.54	4.66	0.41	1.87	273.3	2.32	0.38	0.33	17.06
94	PFC-sandstone	1.27	5.76	0.52	5.69	183.4	1.84	0.09	0.14	2.33
100	T_a sandstone	0.1	0.13	0.64	2.38	35.9	1.91	0.47	0.44	2.05
140	T_a sandstone	0.15	0.06	0.8	2.80	14.0	1.75	0.35	0.50	1.27
Chi. Site B										
6	T_e mudstone	0.48	4.64	0.33	1.31	643.3	2.31	0.44	0.50	33.90
22	PFC sandstone	2.39	7.51	0.69	5.44	147.5	2.01	0.10	0.11	0.65
40	PFC sandstone	0.61	6.48	0.49	2.88	520.8	2.12	0.23	0.21	5.20
55	T_e mudstone	0.45	3.18	0.5	1.17	409.9	1.93	0.42	0.70	31.64
72.5	T_a sandstone	0.16	0.05	0.44	1.58	19.4	1.77	0.32	0.46	1.29
86.5	Te mudstone	0.39	3.69	0.42	1.31	541.8	2.00	0.46	0.38	29.38
94	PFC-sandstone	0.55	2.86	0.59	3.95	242.8	1.72	0.20	0.36	1.43
100	T_a sandstone	0.15	0.05	0.5	1.54	17.3	1.58	0.42	0.64	2.12
140	T_a sandstone	0.14	0.08	0.57	1.31	29.9	1.67	0.40	0.30	2.11
Chi. Site C										
6	T_e mudstone	0.47	2.31	0.46	1.99	245.7	2.19	0.45	0.61	15.13
22	PFC sandstone	15.03	5.00	0.78	5.86	15.6	1.46	0.10	0.03	0.07
40	PFC sandstone	2.66	4.37	0.86	5.11	79.6	1.84	0.16	0.09	0.45
55	T_e mudstone	0.46	3.66	0.38	1.38	452.2	2.32	0.47	0.36	20.50
72.5	PFC sandstone	2.86	1.47	0.89	3.30	30.1	1.84	0.16	0.45	0.02
86.5	T_e mudstone	0.5	4.59	0.41	1.62	500.2	2.21	0.52	0.40	26.36
94	PFC-sandstone	2.22	12.80	0.57	5.56	255.3	1.87	0.14	0.04	0.52
100	T_a sandstone	0.18	0.09	0.39	1.74	37.0	1.77	0.33	0.50	2.28
140	T_a sandstone	0.29	0.07	0.65	1.41	10.8	1.37	0.39	0.36	0.99
Bibaigawa										
2.0	PFC sandstone	0.60	12.85	0.46	7.75	1211.7	1.43	n.d	n.d	n.d
3.8	PFC sandstone	0.17	1.96	0.60	6.16	417.2	1.44	n.d	n.d	n.d
5.9	PFC sandstone	0.17	1.26	0.62	8.79	303.0	1.92	n.d	n.d	n.d
7.6	PFC sandstone	0.60	9.65	0.45	7.20	882.8	1.55	n.d	n.d	n.d
14.7	PFC sandstone	0.26	2.92	0.49	10.29	476.0	1.47	n.d	n.d	n.d
20.1	PFC sandstone	2.37	55.57	0.50	8.72	1273.0	1.38	n.d	n.d	n.d
20.6	PFC sandstone	2.59	42.64	0.48	8.06	893.1	1.45	n.d	n.d	n.d
21.0	PFC sandstone	2.38	37.39	0.51	7.21	823.1	1.35	n.d	n.d	n.d
21.5	PFC Mudstone	4.92	47.58	0.57	7.68	523.9	1.34	n.d	n.d	n.d
21.9	Coaly mud	3.76	134.14	0.63	9.56	1608.1	1.35	n.d	n.d	n.d
22.1	Coaly mud	1.73	6.26	0.49	8.95	2010.8	1.41	n.d	n.d	n.d
22.4	Coal	12.25	155.83	0.57	6.38	586.3	1.44	n.d	n.d	n.d
22.6	Coaly mud	60.53	490.22	0.71	12.85	349.3	1.16	n.d	n.d	n.d
22.8	Silt	0.45	3.03	0.52	7.20	310.9	1.34	n.d	n.d	n.d

Table 1.4. Biomarker data of the Meragang Beach outcrop.

Depth (cm)	Lithology	TOC%	Total *n* -alkane (µg/g-sed)	*P* aq	Pr/Ph	Long chain *n* -alkane (µg/g-TOC)	Carbon Preference Index (CPI)	Sterane $C_{27}/(C_{27}+C_{29})$	HBI/*n* -C_{21}	Total HBI (µg/g-TOC)
6.5	Structureless SS	0.09	n.d	n.d	n.d	n.d	n.d	n.d	n.d	n.d
15.5	Rippled SS with W.L	0.89	5.11	0.57	4.14	322.4	1.44	0.15	n.d	0.19
27.5	Structureless SS	0.08	n.d	n.d	n.d	n.d	n.d	n.d	n.d	n.d
39.5	Rippled SS with W.L	1.16	3.58	0.79	4.06	157.3	0.68	0.18	n.d	0.06
50.5	Structureless SS	0.12	n.d	n.d	n.d	n.d	n.d	n.d	n.d	n.d
66	Rippled SS with W.L	1.61	4.81	0.4	4.19	197.9	1.85	0.18	n.d	0.03
80.5	Horizontal laminated SS	0.09	n.d	n.d	n.d	n.d	n.d	n.d	n.d	n.d
93	Mud clasts from channel scour	0.73	n.d	n.d	n.d	n.d	n.d	n.d	n.d	n.d
108	Trough cross-stratified SS (no PF)	0.03	0.12	0.62	2.33	230.0	1.13	n.d	n.d	n.d
130	Structureless SS	0.07	n.d	n.d	n.d	n.d	n.d	n.d	n.d	n.d
160	Trough cross-stratified SS with PF	10.78	4.60	0.31	4.42	36.9	2.18	0.14	n.d	n.d
190	Trough cross-stratified SS with PF	4.89	3.94	0.41	3.67	59.0	1.88	0.25	n.d	n.d
210	Structureless SS	0.04	0.06	0.55	1.2	114.0	1.48	n.d	n.d	n.d
253	Structureless SS	0.27	0.08	0.9	0	14.7	1.04	n.d	n.d	n.d
418	Structureless SS	0.76	3.75	0.64	3.63	294.4	1.27	0.12	n.d	n.d

Chapter 2

Paleoenvironmental reconstruction of shallow marine environments with respect to facies changes and uplifting hinterland by biomarker analysis of shallow water sediments of Brunei, North Borneo

2.1. Introduction

In the global oceans, the coastal margin is the major hot spot for burial of much organic carbon, with river deltas and non-deltaic shelf regions burying an estimated 184 Tg/C total per year. The open ocean buries only a small amount, at around 6 Tg/C per year (Burdige, 2005). These organic materials mainly constitutes a mixture of algal debris, plant material, petrogenic carbon as well as and diagenetically altered material such as resuspended sedimentary organic carbon and aged soil carbon (Blair & Aller, 2012). The organic material are also susceptible to hydrodynamic sorting and reside across a range of particle sizes and density, leading to clear seaward trends where lowest organic carbon levels are often associated with nearshore sands, while the hotspots are often associated with muddy depocenters (Cui et al., 2016; Wakeham et al., 2009).

The amount and type of OM transported to the oceans however is not constant throughout geological time. Changes in climate can change the strength of riverine discharge and the delivery of OM to the ocean. Additionally, changes in precipitation levels and temperature can also affect type of vegetation growing in the hinterlands. Van Aarssen et al. (2000) used plant-specific lipid biomarkers to develop the Higher Plant Parameter (HPP) proxy, which measures the ratio of retene to cadalene. Theoretically, high amounts of retene suggests warm/hot paleoclimates, whereas high amounts of cadalene indicate arid climates. This reasoning has been used to reconstruct the paleoclimate of Jurassic as well as Miocene Earth (Zakrzewski & Kosakowski, 2021). HPP has also been used as a paleovegetation indicator (Fleck et al., 2002)

The South China Sea, similar to the global trends, underwent the same climatic cooling events brought about by the Cenozoic Cooling, such as the Antarctic Glaciation (~34 Ma), the Mid Miocene Climatic Optimum (~15 Ma) and the Northern Hemisphere Glaciation (~2.5 Ma), as seen by $\delta^{18}O$ of ODP 1146 drill core sediments (Raymo & Ruddiman, 1992; P. Wang et al., 2003). At the same time (since the Oligocene), the South China Sea, which is part of the Eurasian Plate, spread and collided with the Sundaland Plate (Hutchison et al., 2000). The compressional tectonic forces caused uplifting of the Bornean hinterland which caused large amounts of sediments to be deposited seawards, causing progradational shallow water systems to develop and the growth of the Bornean land mass. A study done by Morley & Back (2008) shows an increase of erosion rates with increasing elevation, and the seawards growths of Borneo's shorelines from the Early Miocene to Recent.

Analysis of pollens of the Bornean hinterland, surprisingly shows opposite results to global trends. Global cooling is thought to have brought about global aridification, however, a study on pollens by

Morley (1998) suggests that Borneo Island switched from being arid in the Oligocene to becoming ever-wet in the Miocene onwards. The mechanisms for such an increase in precipitation remains poorly understood.

The Miocene sediments of Borneo Island are well exposed and were deposited during some periods of stable climate, making it an excellent location to study changes in the hinterland vegetation during periods of tectonic uplifting and growing land mass without the effects of climate change. Thus, the objective of this research is to study how hinterland vegetation is affects by tectonic uplifting and to compare with the effects of facies change throughout geological time.

2.2.2. Geological setting and study area

Uplifting of the Bornean hinterland (known as the Crocker-Rajang mountain belt) began in the Late Paleogene-Neogene due to the collision of the South China Sea part of the Eurasian plate with the Sundaland plate. This uplifting coupled with a general sea-level fall during the Neogene onwards caused erosion of hinterland sediments and the development of a rapidly prograding clastic depositional system (Hutchison et al., 2000). The Setap Shale Formation, characterised as a deep-sea basinal system rich in planktonic forams, dinoflagellate tests and pollens, is dated to be of the Early Miocene age due to the presence of the mangrove pollen *Florschuetzia trilobata* (Simmons et al., 1999). Due to the presence of a progradational clastic system, the basinal system shallowed, causing the deposition of shallower sedimentary systems such as the proximal Belait Formation and the distal Miri Formation (Fig. 2.1)(Sandal, 1996).

The Belait Formation is characterised as a sandy shallow water proximal system deposited in a tide- and wave-dominated environment with little to no microfossils usable for age determination. Two methods have been used to estimate the age of the Belait Formation. One involves correlation of Belait Formation sediments where they are intertwined with the Setap Shale and Miri Fm., as the lower part of the Belait Fm. was deposited at the same time with the former, while the upper part of the Belait Fm. was deposited at the same time with the latter. This gives an estimate that the deposition of the Belait Formation began in the Early to lower Middle Miocene and continued to the end of the late Miocene (Liechti et al., 1960). Since the Miri Formation overlays the Setap Shale and does not intertwine with the Setap Shale, it is determined to be younger than the lower Belait Formation. The second and most recent method for dating Brunei's sediments was done by (Kocsis

et al., 2022) using strontium isotopes of bivalve, shark teeth and oyster shells. As such, we can determine that the upper part of the lower Belait Fm. began its deposition at around 12.1 Ma.

The Miri Fm. is commonly characterized as the clay rich, distal part of the progradational system that was deposited at the same time as the upper Belait Fm. It contains abundant foraminifera, molluscs, pollen and spores as well as fish remains and leaf imprints. Recent work done by Laszlo et al (2022) points most known and remaining outcrops of the Miri Fm. to have been deposited from 10.3 Ma and younger. To date, there has been no published records of the discovery of diatom fossils in sediments exposed in Brunei Darussalam.

Two sites were chosen for this study. The first is the Meragang Beach outcrop which is part of the proximal and sandy lower Belait Fm. and exposes a sand-rich upper and mud-rich lower shoreface sedimentary facies. It is 44 m thick. No fossils have been found in both this and previous studies that allows us to determine its exact age. However, it is located roughly along the same horizon and syncline flank as the Subok (Sub) outcrop dated by Laszlo et al to be of 12.1 Ma. The second outcrop is the Batong outcrop which belongs to the distal and muddy Miri Fm. and is largely offshore claystone with few thin sand beds (Fig 2.1, 2.2). It is 5 m thick. The benthic forams found in this study are not age-specific. However, it is located in close proximity with the Lion King (LiK) and Tanjung Nangka (JT1) outcrops dated by Laszlo et al to be of 10.3 Ma. As such, for this study, it is estimated that the Meragang Beach outcrop and Batong outcrop are around 12.1 and 10.3 Ma respectively.

2.3. Methodology

2.3.1. Fieldwork and sample collection

9 mudstone samples were taken from the Batong outcrop while a total of 20 mudstone samples were taken from upper (sand rich) and lower (mud rich) shoreface zones of the Meragang Beach outcrop. All samples (n=29) were analysed for TOC% and lipid biomarker contents, while only one sample was analysed for foraminifera analysis.

For foraminifera analysis, 1000g worth of mudstones were taken from each calcareous layer of the Batong outcrop.

2.3.2. Foraminifera extraction

1000g worth of mudstones were crushed and treated with 30% Hydrogen Peroxide with a 4:1 ratio of Hydrogen Peroxide to water to dissolve organic matter. Samples were then dried, weighed, and washed over a 2 mm, 1 mm, 0.6 mm, 0.25 mm, 0.125 mm, 0.063 mm sieve and then dried again. All dried residues were then merged, split using a microsplitter and examined under a stereomicroscope. To standardise the data sets, foraminifera contents in 5g of sediments from each of the two calcareous layers were identified.

2.3.3. TOC% measurement

3 mols of hydrochloric acid was added to crushed mudstone samples and were allowed to stand for six hours to dissolve any carbonates present. After samples were dried on a hotplate overnight, the samples were sent to the Hokkaido University Global Facility Centre – Shionogi Drug Centre for TOC% measurement. Analysis was done using a J-Science Micro Corder JM10.

2.3.4. Biomarkers

Methanol (MeOH) and dichloromethane (DCM) were used to extract lipids from the powdered samples. Due to the varying polarities of organic compounds, MeOH, MeOH/DCM (1/1) and then DCM were used to extract all lipids. Afterwards, the MeOH – DCM organic solvent mixture was evaporated using a rotary evaporator before being redissolved in hexane.
The hexane extract was then separated into 4 fractions based on their polarityusing organic solvents below:

1. Hexane – to extract aliphatic compounds
2. Hexane / toluene (3/1) – to extract aromatic compounds
3. Hexane / ethyl acetate (9/1) – to extract ketones
4. Methanol / ethyl acetate (1/1) – to extract alcohols and acids

Tetracosane ($C_{24}D_{50}$) was then added to each fraction to aid in compound identification and quantification. Reduced copper bars were added to fractions 1 and 2 to remove any sulfur. Afterwards, the above fractions were then evaporated in a rotary evaporator and then redissolved in hexane before being passed through a gas chromatograph coupled with a mass spectrometer

(GC/MS). In this study, only fractions 1 and 2 were used for biomarker analysis as fractions 3 and 4 had low concentration of biomarkers.

GC/MS was used to identify and quantify organic compounds according to their mass spectra and retention time. In this study, the Agilent Technologies 7890B GC System (with DB-5HT fused silica column) coupled to an Agilent Technologies 5977A Mass Spectrometer (electron voltage of 70 eV, initial temperature of 50°C held a 4 mins, then ramped up to 310°C at 4°C/min and held at 20 min, scan range: *m/z* 50 – *m/z* 650 in 1.3s) was used. Biomarkers were then identified and quantified using the M+ ion, base peak, other characteristic ions as well as other literatures.

2.4. Results

2.4.1. Sedimentary facies

In the Meragang Beach Outcrop, two coarsening upward parasequences were found and contained a total of seven facies and are detailed in table 2.1. Each parasequence begins with a mud-rich lower shoreface zone and ends with a silty to medium-coarse sandy upper shoreface zone. The lower shoreface zone is muddy and contains fine sandstones with hummocky-swaley cross-stratification that is indicative of distal shallow water environments deep enough to be below the fair-weather waves base. The upper shoreface zone contains mostly tabular, stratified beds with plenty of sedimentary structures indicative (but not limited to) of tidal processes such as trough and planar cross-stratification, asymmetric ripples and wavy to lenticular bedding. Some symmetric ripples commonly attributed to wave reworking is also present but minor. These characteristic are indicative of deposition above the fair-weather wave base. Bioturbation is present throughout the outcrop, with most being vertical bioturbation (ophiomorpha, skolithos and conichnus) and minor horizontal bioturbation (Fig 2.2).

The Batong outcrop is largely offshore zone mudstones with few thin and structureless fine-grained sandstone beds that are interpreted to be deposited by vertical settling of fine-grained sediments in calmer waters. Two muddy layers were rich in carbonate shell fragments and bivalve moulds. Both layers were also rich in foraminifera (Fig 2.2)

2.4.2. Foraminifera

A total of 2677 foraminifera tests belonging to 17 taxas were found and identified: 7 tests from the 0.6 mm filter; 2648 tests from the 0.125 mm filter; 16 tests from the 0.063 mm filter. The three most

abundant taxas are the *Textularia agglutinans* (1206 tests), *Ammonia umbonata* (233 tests), *Ammobaculites agglutinans* (190 tests). Other remaining taxas were found at abundances of less than 45 tests each. Species identified are shown in figure 2.3.

2.4.3. TOC%

TOC% is generally higher in shoreface zones, ranging from 0.29 to 1.43, and lower in offshore zones, ranging from 0.37 to 0.69.

2.4.4. Biomarkers

Chromatograms of the biomarkers detected are shown in figure 2.4 and 2.5 with identification of aliphatic triterpenoids and hopanoids and aromatic triterpenoids shown in tables 2.2 and 2.3. TOC% and terrigenous biomarker trends are shown in figure 2.6.

Long chain *n*-alkanes (C_{25} to C_{33}) are derived from epicuticular leaf waxes and are quite stable in the fossil record for tens of millions of years due to being straight-chain hydrocarbons with no functional groups (Eglinton and Logan, 1991). Hence, they are used to determine leaf wax concentrations in the sediments (Peters et al., 1991). Total *n*-alkanes (μg/gsed) are generally higher in shoreface zones, ranging between 0.75 to 7.17, and lower in offshore zones, ranging from 0.80 to 2.99. Long chain *n*-alkanes (μg/gTOC) follow the same trend, with higher values in the shoreface zones between 74.1 and 535.7, and lower values in the offshore zone at 111.6 to 319.0.

The aquatic macrophyte *n*-alkane proxy, P_{aq}, is deduced by the relative amounts of C_{23} and C_{25} *n*-alkanes compared to C_{29} and C_{31} *n*-alkanes (Ficken et al., 2000). The carbon preference index (CPI) is used to determine the ratio of odd-chain, epicuticular leaf wax derived *n*-alkanes from land plants to even-chain *n*-alkanes from marine sources but should be used with caution as degradation or thermal alteration can convert odd-numbered *n*-alkanes to even-numbered *n*-alkanes (Bray and Evans, 1961; Eglinton and Hamilton, 1963; Chen et al., 2021). The average chain length (ACL) is used to estimate the proportion of woody OM to grassy OM, with the former producing high amounts of C_{27} and C_{29} *n*-alkanes and the latter producing C_{31} *n*-alkanes. Formulae for P_{aq}, ACL and CPI are shown below.

$P_{aq} = (C_{23} + C_{25}) / (C_{23} + C_{25} + C_{29} + C_{31})$

$ACL = (27 \times [C_{27}] + 29 \times [C_{29}] + 31 \times [C_{31}]) / ([C_{27}] + [C_{29}] + [C_{31}])$

$CPI = 1/2\{(C_{23} + C_{23} + C_{27} + C_{29} + C_{31}) / (C_{22} + C_{24} + C_{26} + C_{28} + C_{30}) + (C_{25} + C_{27} + C_{29} + C_{31}) / (C_{24} + C_{26} + C_{28} + C_{30} + C_{32})\}$

The aquatic plant index (P_{aq}), Average Chain Length (ACL) and Carbon Preference Index (CPI) show similar ranges throughout both shoreface and offshore zones, at 0.37 to 0.83, 28.0 to 29.3 and 1.10 to 1.91 respectively.

The pristane to phytane ratio (Pr/Ph) is used as a redox indicator as well as a non-specific terrigenous OM indicator. Phytol, derived from the epicuticular leaf waxes of land plants and phytoplankton, degrades to produce more pristane than phytane under oxic conditions, while under anoxic conditions it produces more phytane than pristane (Didyk et al., 1978b). It has been interpreted that Pr/Ph ratios greater than 1.5 indicate oxic environments. In addition, the Pr/Ph values > 3 indicates high input of terrigenous OM (Powell, 1988). Pristane/phytane (pr/ph) ratios show higher values in shoreface zones, at 2.11 to 4.90, and lower values in offshore zones at 1.22 to 1.64.

Perylene is thought to be derived from perylene quinones, which is abundant in the black pigments of plants, wood-degrading fungi, insects and crinoids (Jiang et al., 2000). Triterpenoids with oleanane-, lupane-, and ursane-skeletons are derived from β-amyrin, a compound abundant in angiosperms and their concentrations can be used to infer angiosperm input (Stout, 1992). They include aliphatic triterpenoids as well as aromatic triterpenoids. Aliphatic triterpenoids were identified based on m/z 191 for saturated compounds and m/z 218 for unsaturated triterpenes (Fig 2.5, table 2.2). Aromatic triterpenoids were numerous and were identified based on their respective base peak and M+ ion (Fig 2.5, table 2.3). Perylene and triterpenoid concentrations (μg/gTOC) are generally higher in shoreface zones, ranging from 0.2 to 106.8 and 26.7 to 198.7 respectively, and lower in offshore zones, ranging from 4.5 to 25.9 and 51.6 to 88.6 respectively.

Diterpenoids are derived from gymnosperms such as conifers (Otto & Wilde, 2001). Diterpenoid concentrations (μg/gTOC) generally show an increasing trend from the youngest layer shoreface layer to the oldest offshore layer, with concentrations ranging from 0.03 to 1.60. Cadalene is a sesquiterpenoid derived from angiosperms (Bastow et al., 1997). It also shows a similar trend to diterpenoids, with lower concentrations (μg/gTOC) in shoreface zones at 0.5 to 10.6, and higher concentrations in offshore zones at 14.2 to 38.7. Hopane $C_{31}S/(S+R)$ ratios, which is used as a

maturity indicator, do not show any differences between both zones, with a range between 0.35 and 0.54.

Marine derived biomarkers were also detected and their biomarker trends are shown in figure 2.7. Using *m/z* 217 and the molecular ions M+ 372, 386, and 400 for C_{27}, C_{28} and C_{29} regular steranes respectively, steranes were identified and quantified. The C_{27} and C_{28} regular steranes are steroids derived from phytoplankton and zooplankton respectively while C_{29} steroids are generally derived from higher plants (Volkman, 1986). $C_{27}/(C_{27} + C_{29})$ sterane ratios show similar trends in both zones, at values between 0.110 to 0.359. However, analysis of the abundance of C_{27}, C_{28} and C_{29} steranes show an increase in C_{29} sterane ratios in older horizons of both zones, showing a tendency for higher plants to dominate older sediments especially in the offshore zones. C_{27} sterane % remains constant, while C_{28} sterane % falls in older horizons (Fig 2.8A).

Highly branched isoprenoid (HBI) alkane with a C_{25} carbon number is an isoprenoid derived from certain species of diatoms and is identified with base peak m/z 57 and M+ 238 (Sinninghe Damsté et al., 2004). The HBI thiophenes were identified using the base peak *m/z* 293 and *m/z* 265 with an M+ ion of 378. Dinosteranes are identified using m/z 231 and M+ 414 and are derived from dinoflagellates. Dinosterane and HBI concentrations differ between lower and upper shoreface zones. Lower shoreface zones generally have more HBI than dinosteranes, at concentrations (μg/gTOC) between 0.024 to 0.517 and 0.003 to 0.235 respectively. Upper shoreface zones generally have less HBI but more dinosteranes, at concentrations (μg/gTOC) of 0.049 to 0.211 and 0.064 and 0.169 to 0.169 respectively. Offshore zones have even higher concentrations (μg/gTOC) of HBI than shoreface zones, at values of 1.04 to 3.73, while dinosterane concentrations (μg/gTOC) are similar to shoreface zones, at values between 0.047 to 0.144.

Gammacerane, is derived from tetrahymanol, which is produced by bacterivorous ciliates living in stratified water columns (Harvey & Mcmanus, 1991). Thus, they can be used as a stratification index (Sinninghe Damste et al., 1995). Total hopanes and gammacerane concentrations (μg/gTOC) do not show significant trends between both zones, at concentrations between 4.90 to 18.1 and 0.25 to 1.84 respectively. However, gammacerane index (ratio of gammacerane to C_{30} hopanes shows that shoreface zones have lower values at 0.075 to 1.02, while higher values are seen in offshore zones at 0.173 to 0.338 (Fig 2.8B). Data of all biomarkers are shown in table 2.4.

2.5. Discussion

2.5.1. Terrigenous OM transport – facies vs vegetation change

Terrigenous OM input into the sea was quantified using the concentration of long-chain *n*-alkanes and perylene, which are derived from leaf-waxes and fungi respectively. Both proxies have higher amounts in shoreface zones rather than offshore zones. Pr/Ph ratios, which are used as an oxicity and a terrigenous input indicator, shows similar trends. These results suggests that most terrigenous OM and freshwater are concentrated in the shallower areas rather than offshore zones, which are concordant with modern day trends including the active Baram Delta to the west of the study area. P_{aq}, which as an aquatic macrophyte index, is used to measure the amount of submerged aquatic plants in an area and has been used to determine the relative expanse of wetlands in the hinterland (Ficken et al., 2000; Seki et al., 2009). Both areas have similarly high values of P_{aq}, with most values being greater than 0.4 and as high as 0.83. Previous studies have shown that coals formed in peatlands or mires are widespread in Southeast Asia (Esterle & Ferm, 1994; Page et al., 2010). Furthermore, studies have shown that Upper Eocene and Middle Miocene coals of Southeast Borneo has relatively lower amounts of P_{aq} (< 0.3)(Fikri et al., 2022). The higher amounts of aquatic plants in North Bornean sediments of this study may suggest wetter conditions in the northern part of Borneo during the Miocene. However, due to the lack of long-time scale studies in the region, the exact cause of these wetter conditions is unknown.

ACL has been used as a proxy to determine grass and wood contributions, where C_{27} and C_{29} n-alkanes are derived mainly from woody OM while C_{31} *n*-alkanes are derived from grasses. CPI values of greater than 1 also suggest a dominance of terrestrial over marine OM, but can be lowered by thermal degradation of odd-chain n-alkanes. Both proxies have also been used as paleoclimatic indicators, because land-plants tend to produce longer chained n-alkanes in leaf waxes to prevent water loss during cold and arid periods. ACL values stay within the range of 28 to 29.3, showing a dominance of woody rather than grassy OM. CPI also shows a narrow range with no trend. At values between 1.10 and 1.91, a dominance of terrestrial OM is suggested, but the range is lower than that usually seen in fresh vegetation. The reasons for low CPI could be the contribution of old petrogenic carbon that may have lowered the CPI of the study, as similarly seen in core samples taken from the southern South China Sea and the presence of Mesozoic pollens in Pliocene sediments of Brunei (Li et al., 2013; Wilf et al., 2022). Furthermore, in this study, P_{aq} and CPI shows a good negative correlation (R^2 = -0.74). Since high P_{aq} can indicate higher precipitation (Seki et al., 2009), increased

erosion could have increased the amount of petrogenic carbon to the sea. Based on $\delta^{18}O$ data of northern South China Sea, the sediments of this study (12 to 10 Ma) were deposited during a period of stable sea-surface temperature. As such, the lack of variations of the ACL and CPI values seen in this study may also be due to constant climates.

Triterpenoids with ursane, lupane and oleanane skeletons are the diagenetic products of β-amyrin, which is abundantly found in resins of angiosperms(Stout, 1992). Cadalene, a sesquiterpenoid, is also derived from angiosperms(Ficken et al., 2000; Seki et al., 2009). Similar to long-chain n-alkanes and perylene concentration, triterpenoid concentrations are generally lower in the offshore zone. This suggests that terrigenous OM accumulation in the marine environment of ancient north Borneo is largely controlled by facies changes and distance from the river mouth. However, in the younger offshore sediments, cadalene concentrations are around 20 times higher than that of older shoreface sediments, suggesting that changes in facies were not a major control. In modern day Borneo, most of lowland vegetation consists of the family *dipterocarpacaea,* which is abundant in cadalene (Widodo et al., 2009). Hence, it is possible that low-land area expansion of due to progradation caused more accommodation space for the growth of cadalene-rich vegetation.

In this study, aliphatic diterpenoids were not detected. However, aromatic diterpenoids such as dehydroabiatane and simonellite were detected. Similar to cadalene, we interpret that the higher amounts of diterpenoids in younger offshore zones than shoreface zones is not related to facies change. It is commonly interpreted that gymnosperm expansion is a result of global or regional cooling events (eg. (S. Chen et al., 2015)). However, $\delta^{18}O$ data taken from the South China Sea does not show any large fluctuations in sea-surface temperatures from 12 Ma to 10 Ma, which could rule out global climatic cooling as the cause. However, due to the continuous uplifting of the Bornean hinterland since the Oligocene-Eocene which created the Crocker-Rajang mountain range, the gradual increase in elevation could have promoted the growth of coniferous or alpine mountains. A study done by Kitayama (1992) has shown increasing montane forest coverage as elevations increase. Thus, we propose that uplifting of the Bornean Hinterland in the Miocene increased montane forest coverage as mountains grew (Fig 2.9).

2.5.2. Primary production variations

Higher branch isoprenoids (HBI) *n*-alkanes and thiophenes are produced by certain species of diatoms. They have been used to reconstruct past primary productivity. Dinosteranes are biomarkers derived from dinoflagellates. In upper shoreface environments, dinoflagellates tend to have a higher relative abundance than diatoms. However, in lower shoreface settings, diatoms tend to be more abundant than dinoflagellates. In offshore settings, diatom concentrations are around 10 to 20 times higher than that of shoreface settings, with large fluctuations. The difference in diatom concentration within seaward facies changes is interpreted to be controlled by the different physico-chemical properties of each facies. Using the nearby active Baram delta as an analogue, sediment concentration decreases seawards while salinity increases. In this study, Pr/Ph values shows higher oxicity in shoreface than offshore zones, suggesting a reduction in freshwater abundance sea-wards. Furthermore, the lower concentrations of long-chain *n*-alkane concentrations as well as perylene in the offshore zone suggests lower concentrations of terrigenous material in the offshore zones. Thus, it is possible that the lack of terrigenous material or sediments in the offshore zone enhanced light-penetration in the photic zone. As for salinity, bacteriovorous ciliates that live on the interface between stratified water layers produce a biomarker called tetrahymanol, which is the precursor for gammacerane. As such, the gammacerane index has been used as an indicator for water column stratification. Offshore zones appear more stratified that shoreface zones due to the higher gammacerane index. In addition, the high amounts of agglutinated foraminiferas also suggest a deep environmental setting. Thus, the higher salinity of the offshore zone is also considered to be a factor contributing to higher diatom abundances. As for the large fluctuations seen in offshore zone diatom-derived primary productivity, a study on the modern day South China Sea revealed that plankton communities change with the monsoons. Off the coast of North Borneo, during southwest (summer) monsoons, phototrophic cyanobacteria are the dominant primary producers. However, during northeast (winter) monsoons, upwelling is enhanced and diatoms become the main primary producers (Ning et al., 2004). Such fluctuations may have contributed to the large fluctuations seen in offshore zones's diatom abundances.

Apart from primary producer compositions, food-web dynamics were also elucidated. As previously mentioned, gammacerane is derived from bacteriovorous ciliates. Hopanes, which are produced by bacteria, show a good correlation with gammacerane compositions (R = 0.7). These results are similar to trends between bacteria and ciliates reported by Rassoulzadeggan, in which the predator and prey relationship were interpreted as the cause for the correlation.

2.5.4. Implication

Lipid biomarker compositions in marine sediments are often used for marine and terrestrial paleoenvironment and terrestrial paleovegetation reconstruction, especially in the context of global or regional climatic changes. However, such studies often do not consider tectono-sedimentary processes and usually only consider changing sea-surface temperatures. In this study, we can see that tectono-sedimentary processes in periods of stable climates can affect lipid biomarker compositions in a way that can be mistaken as climate-change induced changes. For example, increasing gymnosperm-derived pollens or diterpenoid concentrations are often interpreted as a result of climatic cooling (add eg.). However, in this study, an increase in gymnosperm cover determined by increasing diterpenoid concentrations occurred during stable climates and increasing mountain-elevation. Furthermore, cadalene is often used in paleoclimatic reconstruction. Specifically, it forms the Higher Plant Parameter proxy [HPP = retene/(cadalene+retene)] which is widely used as a paleoclimatic indicator that determines arid or humid climates, as based on Van Aarsen. Retene is considered to be derived from diagenetic degradation of abietane-type bioditerpenoids present in conifers but can also be formed from wildfires (Hautevelle et al., 2006). Lower values of HPP, where cadalenes are low in abundance with respect to retene, indicate arid climates. Oppositely, higher values of HPP often indicate warmer climates with a higher abundance of retene (eg. van Aarsen et al., 2000). Cesar and Grice (2019) have noted similar trends where cadalene increased during arid-climatic episodes whereas retene increased during during humid episodes. In this study, retene was not detected, but cadalene was detected and provides an alternative interpretation to the simple "cadalene = arid or retene = warm climate" model. Using Mg/Ca of planktonic foraminiferas from IODP 1501 drill cores taken from the northern South China Sea, Yang et al. (2021) shows stable sea-surface temperatures from around 12.5 Ma to 9.5 Ma in the northern South China Sea were stable, concurrent with the depositional ages of the Meragang and Batong outcrops of this study. Wang et al., (2003) also reports similar results from ODP 1146 also taken from the South China Sea. Furthermore, analysis by Friederich et al. (2016) on Bornean and Southeast Asian coals shows that ever-wet climates persisted in the Borneo Island since the Eocene, and remained ever-wet despite concurrent global aridification. Thus, the increase in cadalene during stable sea-surface temperatures and high precipitation levels is contrary to the concept that cadalene-rich vegetation expands in arid climates. Since progradation of shallow water sedimentary systems create more land through the seawards building of shorelines, it is possible that an increase in accommodation space for their

growth contributed to their expansion rather than climatic changes. Thus, local tectono-sedimentary systems should be considered when interpreting cadalene or retene variations.

Secondly, reconstruction of marine environmental conditions in Borneo has been limited primarily due to the poor preservation of microfossils (except foraminifera). In this study, diatom-derived HBI was used to reconstruct past primary productivity within different facies and possibly monsoonal variations also. Thus, this proves that diatoms have existed in shallow-water environments of North Borneo and can allow us to further our understanding ancient marginal-marine environments in tropical south South China Sea throughout geological time. Furthermore, the usage of organism-specific lipid biomarkers such as HBI, dinosterane and hopanes can also help reconstruct marine ecosystem changes throughout geological time. Thus, the usage of biomarkers as an alternative to microfossils may be a promising research method for future research.

2.6. Summary

Shoreface (~12 Ma) and offshore (~10 Ma) sediments deposited during a period of tectonic uplifting and stable SSTs were analysed to study the effects of facies and climatic changes, tectonics and hinterland land-mass expansion on terrestrial OM delivery to the ocean, paleovegetation change and primary productivity. Terrestrial OM transport to the ocean is concordant with modern day trends where OM_{terr} decreases in seawards direction and is interpreted to be controlled by facies changes. However, over geological time, angiosperm-derived triterpenoids and gymnosperm-derived diterpenoids contributions to the ocean appear to be dependents on hinterland and local tectonics also. Cadalene increased in younger sediments and is interpreted to have been caused by increased accommodation space for *Dipterocarpacaea* growth due to low-land expansion caused by increased erosion and sediment supply to the margins of ancient North Borneo during tectonic uplifting of the Bornean hinterland. Simonellite and dehydroabieatane, which are gymnosperm-derived biomarkers, increased in younger sediments and is interpreted to be due to increased elevation that would have cooler mountain-top temperatures, as also seen in modern-day trends where low-land vegetation of Borneo is mostly dipterocarp forests while montane-forests are common in high altitudes. Diatom concentrations appear to be controlled by facies and is also concordant with modern-day trends where an increase is seen in the seawards direction. Large fluctuations within diatoms could be due to monsoonal activity that changes upwelling strength.

2.7. Figures

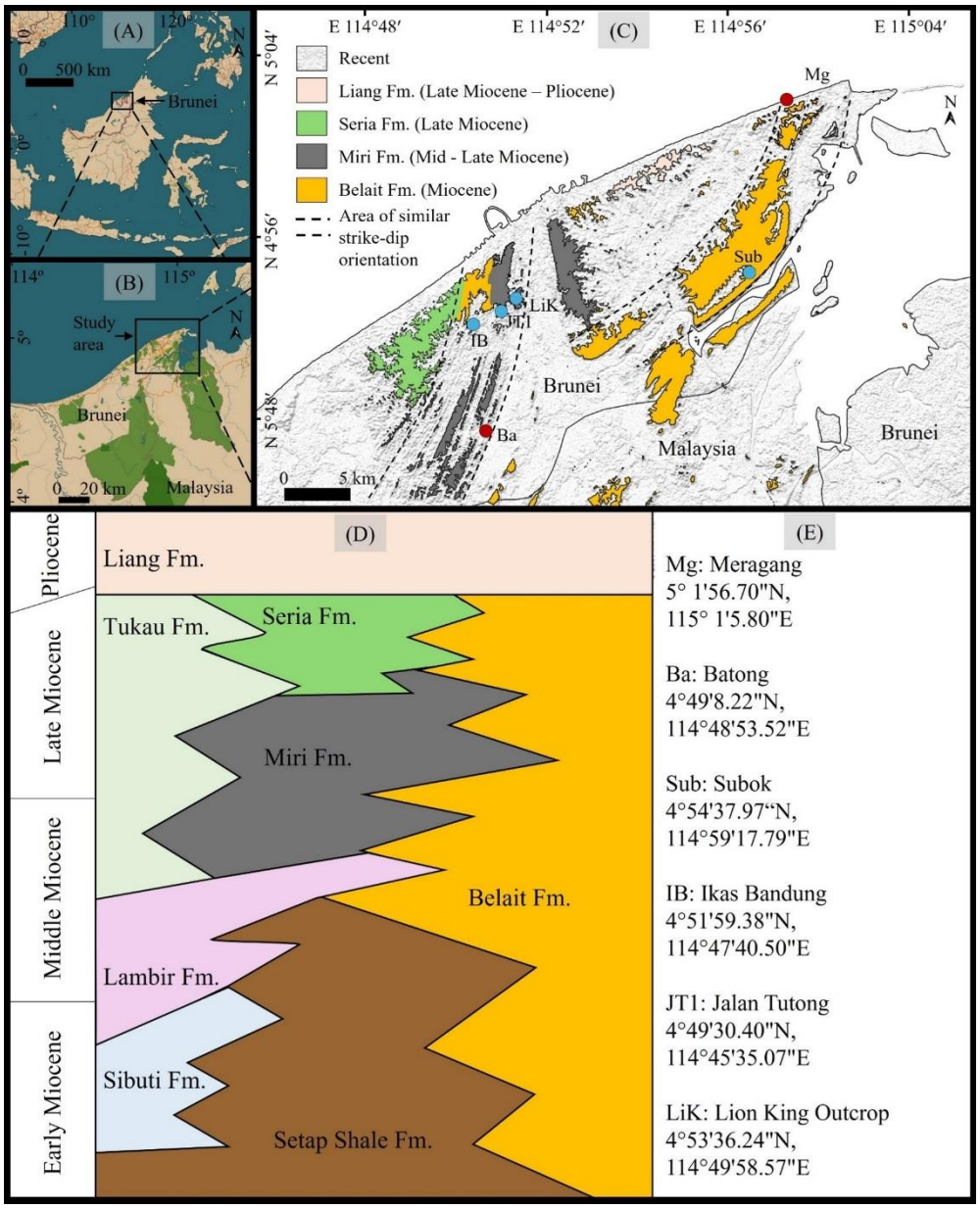

Figure 2.1. (A) Location of Brunei on North Borneo of Southeast Asia. (B) Map of Brunei with study area in black box. (C) Lithostratigraphic map of the study area showing key outcrops in blue dots and outcrops of this study in red dots. (D) Lithostratigraphy of Brunei. Tukau, Lambir and Sibuti Formations are not exposed in figure C, but are exposed to the west of Brunei. (E) Important outcrops of this study and their coordinates. Meragang and Batong are outcrops of this study and cannot be dated, while other outcrops (blue dots) were dated by Laszlo et al.

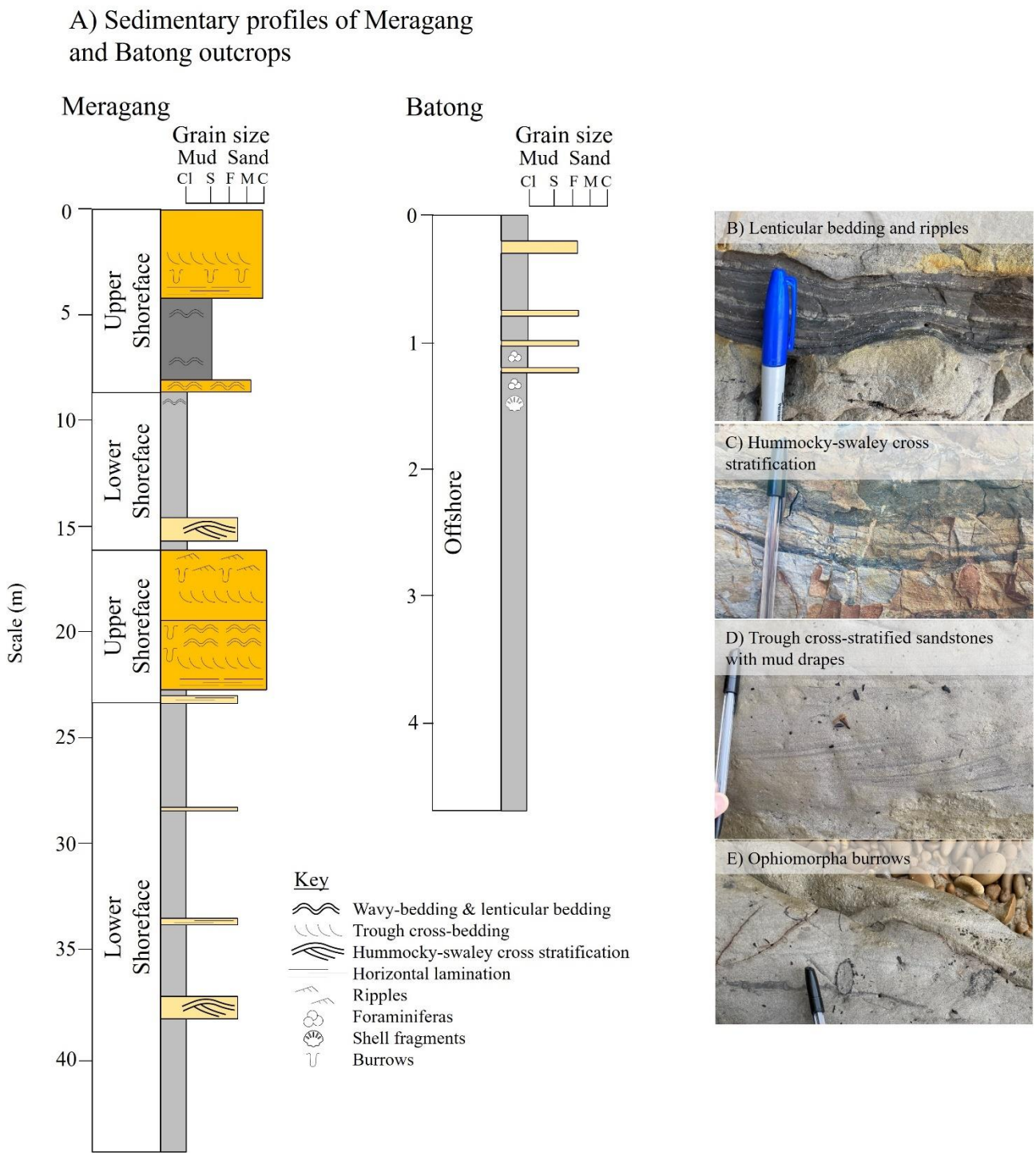

Figure 2.2. (A) Sedimentary profiles of Meragang Beach outcrop and Batong outcrop. (B – E) Sedimentary structures and bioturbation found in Meragang Beach outcrop.

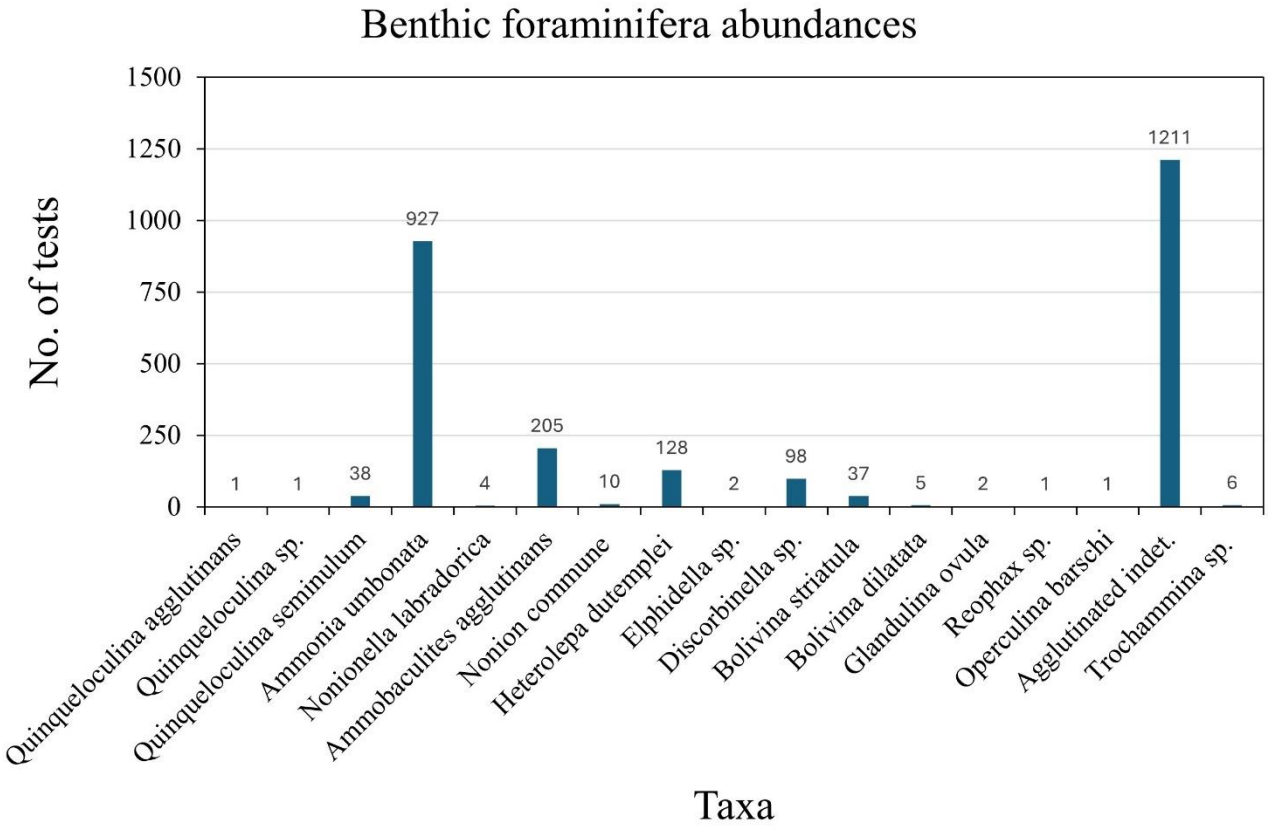

Figure 2.3. Total foraminifera assemblage of the two calcareous layers of the Batong outcrop

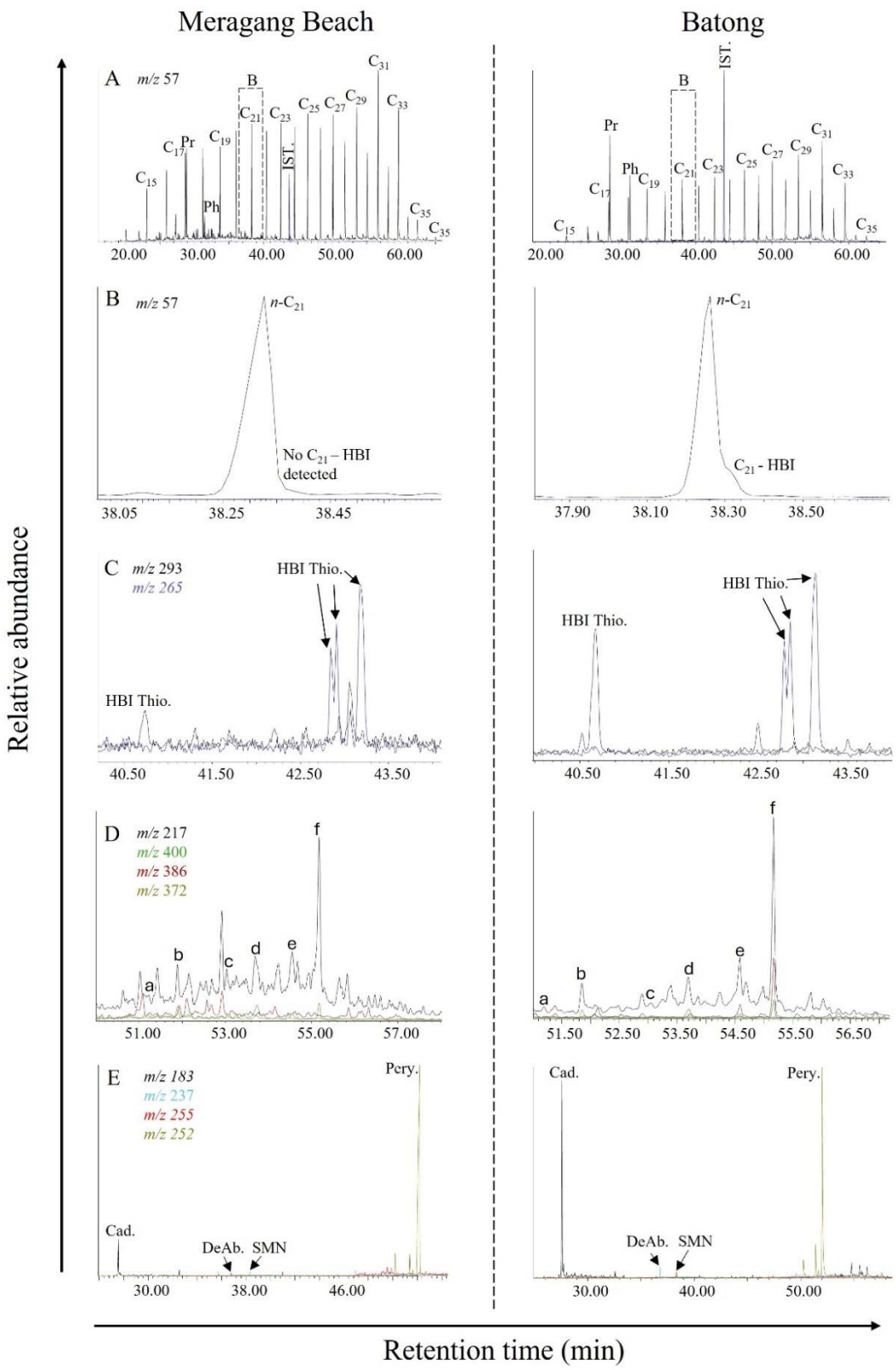

Figure 2.4. Gas chromatogram of selected biomarkers. Ph: prystane, Ph: phytane, IST.: internal standard, HBI Thio.: HBI thiophene, a: C_{27} 5β(H),20R, b: C_{27} 5α(H),20R, c: C_{28} 5β(H),20R, d: C_{28} 5α(H),20R, e: C_{29} 5β(H),20R, f: C_{29} C_{27} 5α(H),20R, Cad: Cadalene, DeAb.: Dehydroabieatane, SMN: Simonellite, Pery.: Perylene.

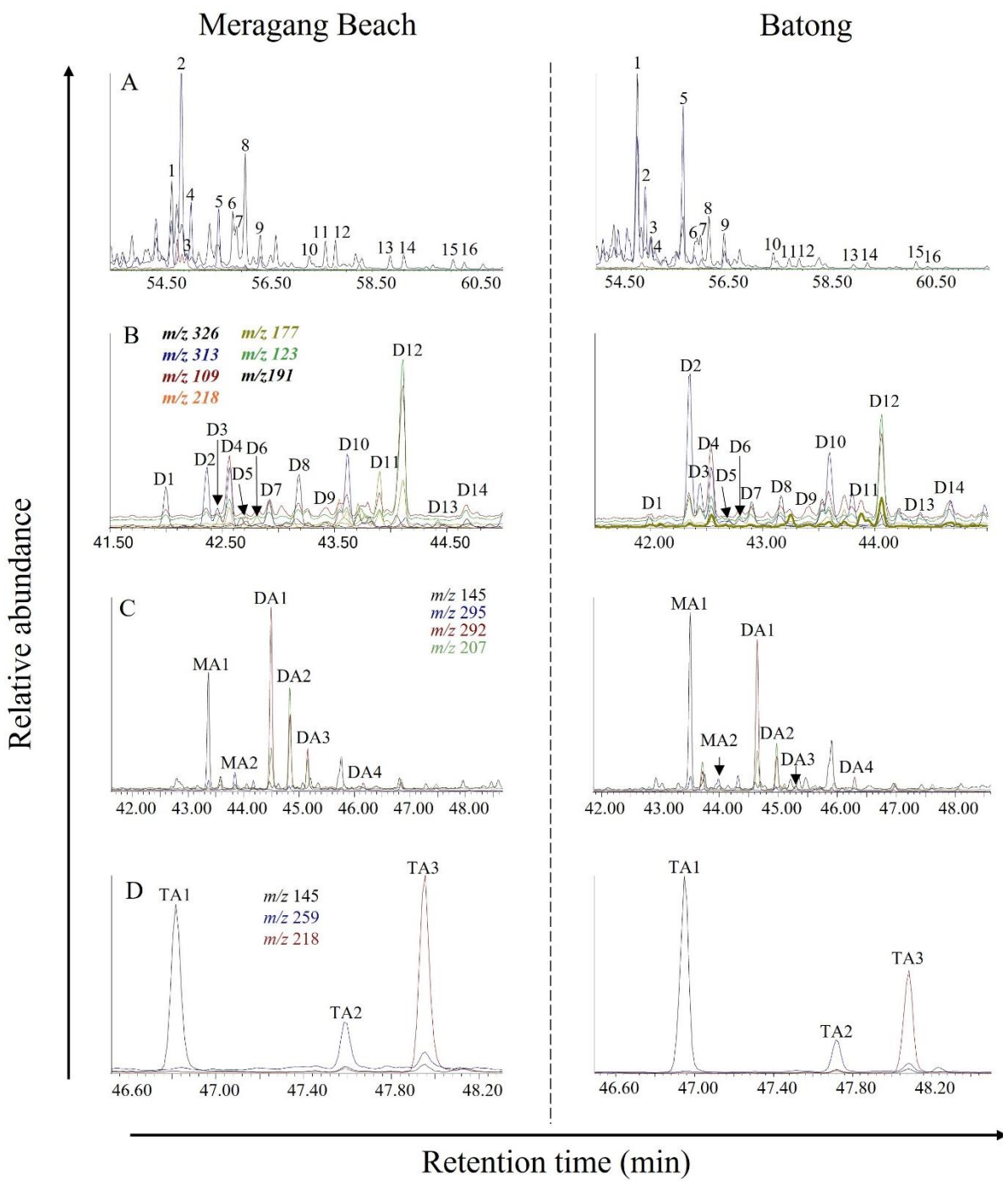

Figure 2.5. (A) Aliphatic triterpenoid and hopanoid biomarkers. (B) Aliphatic degraded (des-A) triterpenoids. (C) Mono- and diaromatic des-A-triterpenoids. (D) Triaromatic des-A-triterpenoids. See tables 2.2 and 2.3 for identification.

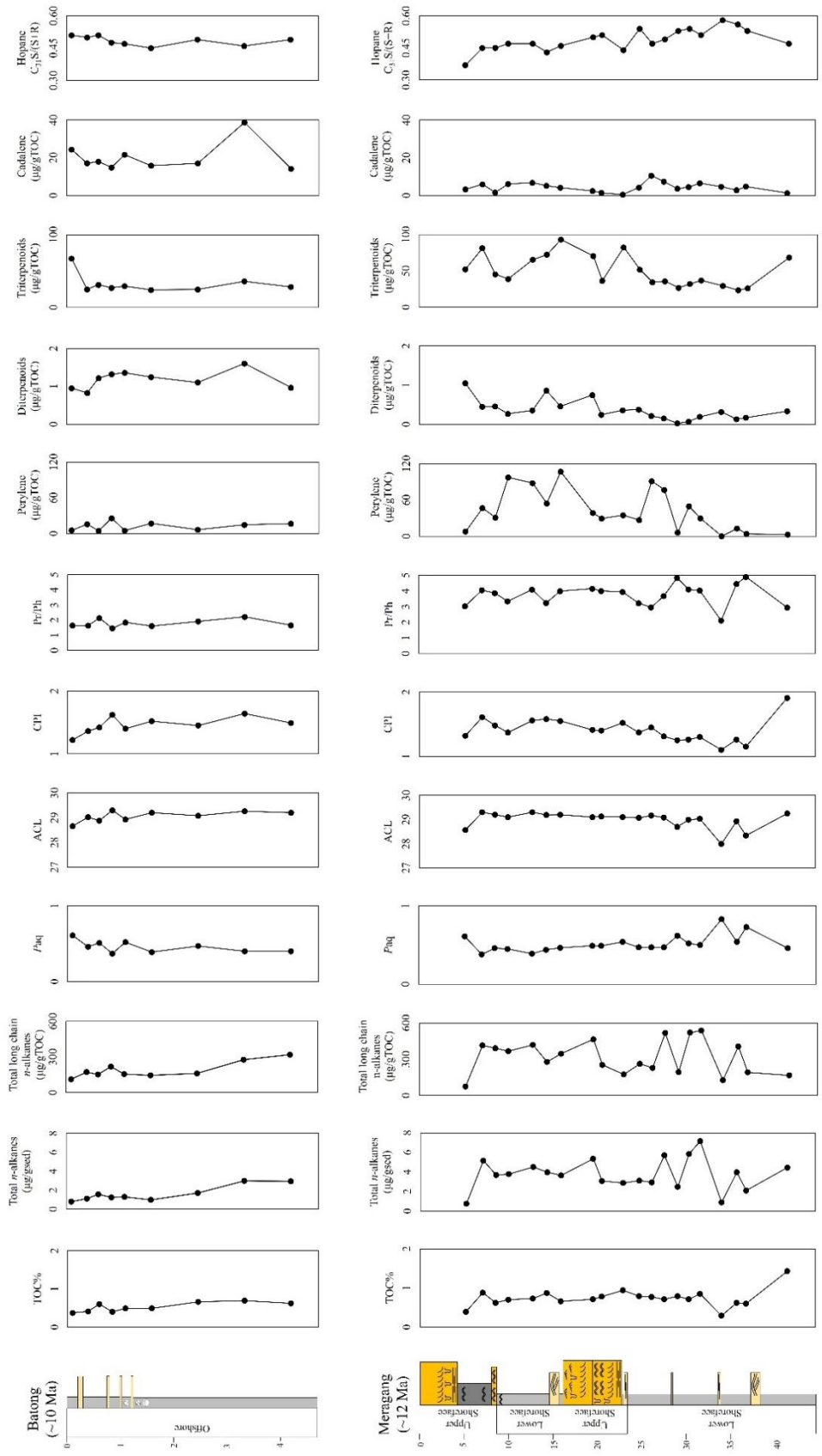

Figure 2.6. TOC% and terrigenous biomarker data of Meragang Beach and Batong outcrops.

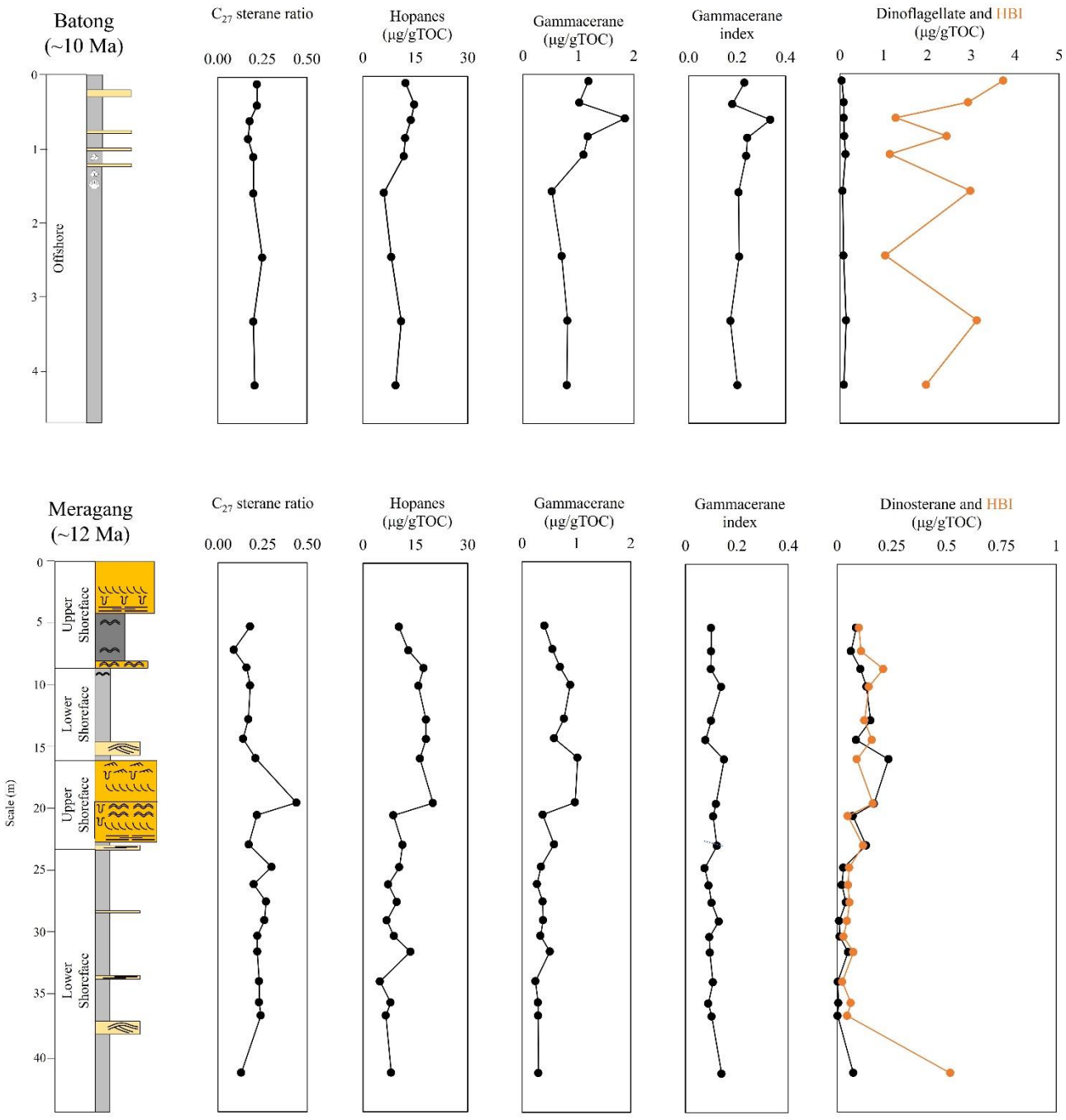

Figure 2.7. TOC% and marine biomarker data of Meragang and Batong outcrops.

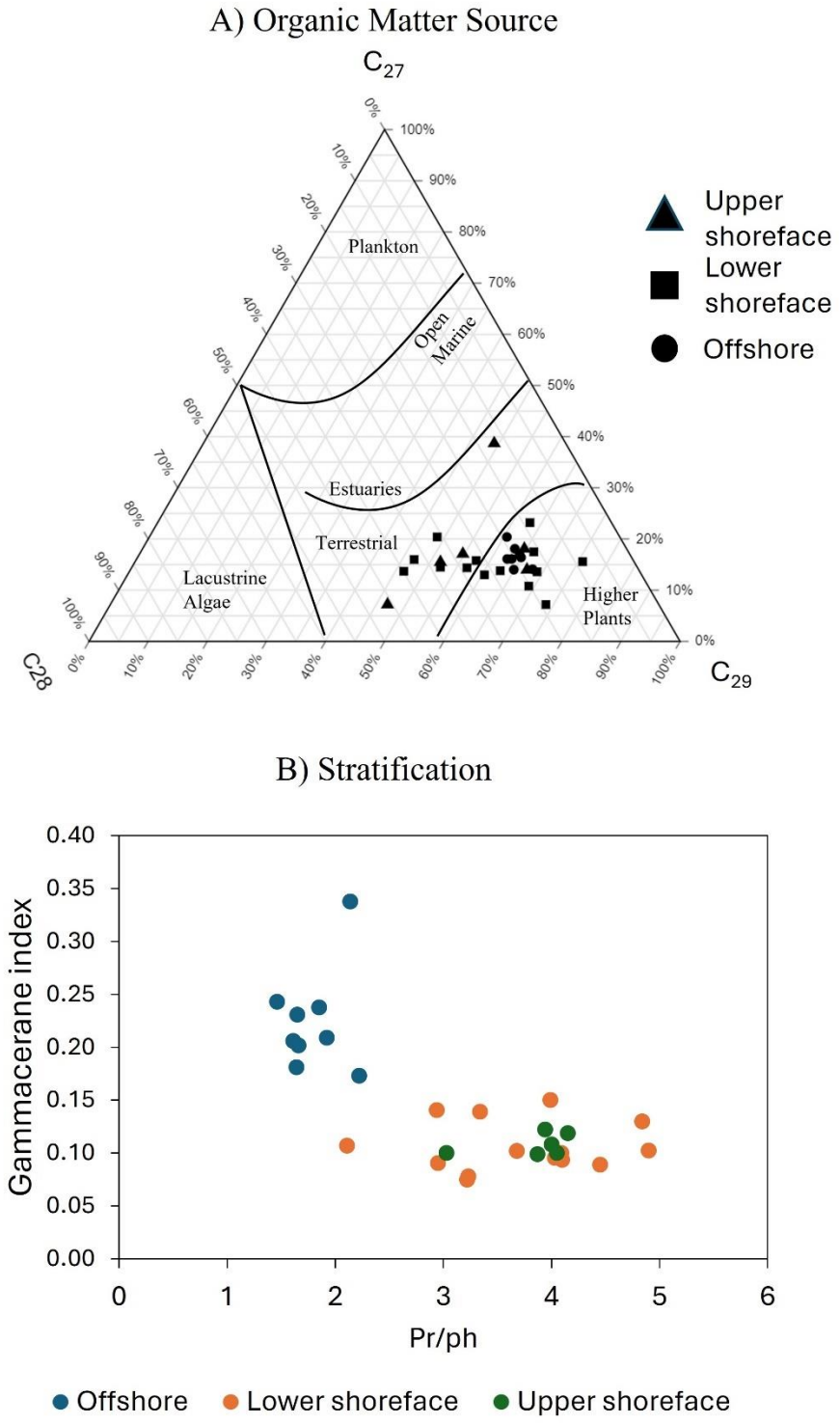

Figure 2.8. (A) Ternary diagram showing the OM source based on regular sterane compositions. (B) Stratification shown by a plot of the Gammacerane Index and Pr/Ph ratios.

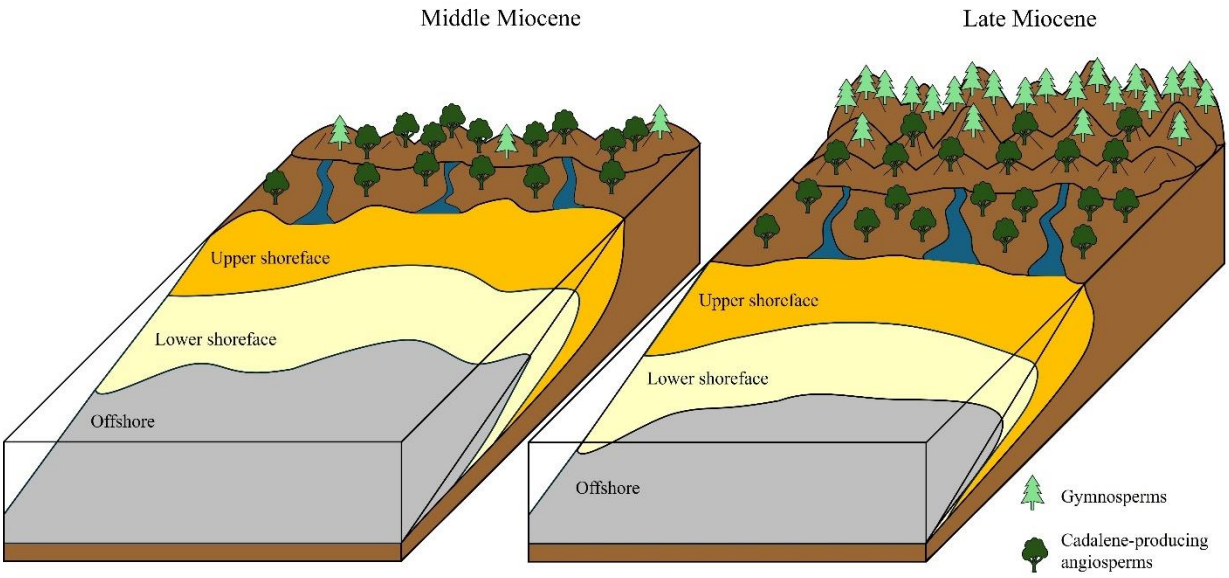

Figure 2.9. Depositional environment of Middle Miocene to Late Miocene Northern Borneo.

2.8. Tables

Table 2.1. Sedimentary facies and description of sediments found in Meragang Beach and Batong outcrops.

Facies	Description	Biogenic structures	Interpretation
Structureless coarse sandstones	Unstratified, large coarse-grained sandstones Poorly sorted but mainly consists of coarse-grained sands Occasionally contains visible plant fragments Sharp upper and lower boundaries	None	Rapid deposition of high-density flows that prevented efficeint sorting sorting (Magalhaes et al., 2015)
Trough cross-stratified sandstones	Found in amalgamated sandstones that are 4.9 m thick Well sorted medium-coarse grained sands Curved, unidirectional lee-side with abundant plant-material and mud-drapes and occasionally mud-clasts Sharp upper and lower boundaries	Skolithos Ophiomorpha Conichnus Paleophycus	Migration of S-shape dunes at relatively high-speeds (Miall, 1996). Deposition by tidal currents above fairweather wave-base and/or storm flows (Collins et al., 2018)
Planar cross-stratification sandstones	Well sorted medium-coarse grained sands Single-sets of planar, unidirectional lee-side foresets dipping at appr. 40 degrees Organic material and mud-drapes absent Sharp upper and lower boundaries		Straight-crested dune migration in a channel influenced by tides (Reineck and Wunderlich, 1968)
Horizontal laminated sandstones	Found in 4.8 m thick sandstone Well sorted fine or medium-coarse grained sands Laminations are parallel to bedding plane May contain organic material also orientated parallel to bedding plane Sharp upper and lower boundaries		Deposition of plane bed around the upper flow regime in a shallow environment (Alexander and Fielding, 1997)
Ripple-cross laminated sandstones and occasional siltstones	Well sorted coarse sands or silts Ripples are either symmetrical or asymmetrical Ripples may have thin muddy layers deposited on surface - forming wavy lamination May have thick muddly layers deposited on surface - forming lenticular beds When exposed on the bedding plane, they are often sinuos		Assymetric ripples show a tidally influenced environment in lower flow regimes (Collinson et al., 2006). Also indicatos flow reversal and oscillatory periodic flow (Reineck and Wunderlich, 1968). Wavy and lenticular beds suggests mud-deposition on top of ripples during slack tides (Martin, 2000).
Hummocky-swaley cross-stratified sandstones	Well sorted fine-grained sandstones Concave-shaped hummocks and convex-shaped swales present Sharp upper and lower boundaries	Skolithos Ophiomorpha	Deposition by infilling of scours created by storms below the fair-weather wave base (Myrow and Southard, 1991). Reworking of sediments in a distal to proximal delta front (Collins et al., 2018).
Structureless very fine to fine sandstones	Unstratified, very-fine to fine sandstones Sharp upper and lower boundaries	None	Settling of fine material during low energy periods (Bridge, 2006)
Mudstones	No sedimentary structures May have small or thin amounts of sands, but mostly mud-sized grains May have fragmented calcareous shells or bivalve moulds May have abundant foraminiferas	Fossilized bivalve burrows occassionally	Settling of muds during low-energy periods (Bridge, 2006). Prodelta or offshore shelf (Collins et al., 2018).

Table 2.2. Biomarker identification for aliphatic triterpenoids and hopanoids of figure 2.4.

ID	Compound name	Formula	*m/z*	M+
1	17α(H),21β(H)-30-norhopane	$C_{29}H_{50}$	191	412
2	Olean-13(18)-ene	$C_{30}H_{50}$	218	410
3	Olean-12-ene	$C_{30}H_{50}$	218	410
4	Olean-18-ene	$C_{30}H_{50}$	218	410
5	Urs-12-ene	$C_{30}H_{50}$	218	410
6	Oleanane	$C_{30}H_{52}$	191	412
7	Lupane	$C_{30}H_{52}$	191	412
8	17α(H),21β(H)-hopane	$C_{30}H_{52}$	191	412
9	17β(H),21α(H)-hopane (moretane)	$C_{30}H_{52}$	191	412
10	Rearranged gammacerane?	$C_{30}H_{52}$	191	412
11	22S-17α(H),21β(H)-30-homohopane	$C_{31}H_{54}$	191	426
12	22R-17α(H),21β(H)-30-homohopane	$C_{31}H_{54}$	191	426
13	22S-17α(H),21β(H)-30,31-bishomohopane	$C_{32}H_{56}$	191	440
14	22R-17α(H),21β(H)-30,31-bishomohopane	$C_{32}H_{56}$	191	440

Identification based on Wang et al. (2016)

Table 2.3. Identification for biomarkers found in figure 2.5.

Label	Name	Formula	Molecular weight	Base peak (m/z)	M+	M+ -15	Second peak	Retention Index #	Identification Level	References
	Aliphatic fraction									
D1	*Des* -A-oleanadiene	$C_{24}H_{38}$	326	326	326	311	173	2273	1	1
D2	*Des* -E-D:C-friedohop-22(29)-ene	$C_{24}H_{40}$	328	313	328	313	231	2291	2	2
D3	*Des* -E-D:C-friedohop-22(29)-ene	$C_{24}H_{40}$	328	313	328	313	231	2295	2	2
D4	*Des* -A-olean-13(18)ene	$C_{24}H_{40}$	328	109	328	313	313	2300	2	3, 4
D5	*Des* -A-olean-12-ene	$C_{24}H_{40}$	328	218	328	313	205	2307	2	3, 4
D6	Des-A-nortriterpane	$C_{23}H_{40}$	316	177	316	301	109	2312	1	
D7	Des-A-urs-13(18)-ene	$C_{24}H_{40}$	328	313	328	313	177	2331	2	4, 5
D8	Des-A-norlupane	$C_{23}H_{40}$	316	109	316	301	135	2325	1	
D9	Des-A-oleanadiene	$C_{24}H_{38}$	326	313	326	311	326	2318	1	1
D10	Des-A-norlupane	$C_{23}H_{48}$	316	109	316	301	122	2344	1	
D11	Des-A-urs-12-ene	$C_{24}H_{40}$	328	313	328	313	95	2354	2	4
D12	Des-A-oleanane	$C_{24}H_{42}$	330	191	330	315	109	2369	2	4, 6
D13	Des-A-lupane	$C_{24}H_{42}$	330	123	330	315	109	2381	2	4, 5
D14	Des-A-ursane	$C_{24}H_{42}$	330	109	330	315	191	2410	2	4, 6
D15	Des-A-lupane	$C_{24}H_{42}$	330	123	330	315	109	2423	1	
	Aromatic fraction									
MA1	Monoaromatic *des* -A-ursane / oleanane	$C_{23}H_{34}$	310	145	310	295	157	2354	1	
MA2	Monoaromatic des-A-lupane	$C_{23}H_{34}$	310	295	310	295	157	2374	2	7
DA1	Diaromatic des-A-oleanane	$C_{22}H_{28}$	292	292	292	277	207	2410	2	2
DA2	Diaromatic des-A-ursane	$C_{22}H_{28}$	292	207	292	277	292	2424	2	7, 9
DA3	Diaromatic des-A-lupane	$C_{22}H_{28}$	292	292	292	277	207	2438	2	7, 9
DA4	Diaromatic des-A-triterpane	$C_{22}H_{28}$	292	292	292	277	181	2493	1	
TA1	Triaromatic des-A-lupane	$C_{21}H_{22}$	274	231	274	259	215	2528	2	7, 9
TA2	Triaromatic des-A-ursane	$C_{21}H_{22}$	274	259	274	259	274	2570	2	7, 9
TA3	Triaromatic des-A-oleanane	$C_{21}H_{22}$	274	218	274	259	274	2594	2	7, 9

References; 1: Huang et al. (2008), 2: Hauke et al. (1993), 3: Logan and Eglington (1994), 4: Jacob et al. (2007), 5: van Bree et al. (2016), 6: Woolhouse et al. (1992), 7: Freeman et al. (1994), 8: de las Heras (1991), 9: Huang et al. (2013), 10: ten Haven et al. (1992)

Table 2.4. TOC% and biomarkers found in Meragang Beach and Batong outcrops.

Sample depth (m)	Environment	TOC %	Pr/Ph	P_{aq}	ACL	CPI	Total *n*-alkane (µg/gsed)	Total long chain *n*-alkane (µg/gTOC)	Perylene (µg/gTOC)	Total triterpenoids (µg/gTOC)	Total diterpenoids (µg/gTOC)	Cadalene (µg/gTOC)	Hopane C_{31} ratio	Total Hopane (µg/gTOC)	Gammacerane (µg/gTOC)	Gammacerane Index	C_{27} sterane ratio	Dinosterane (µg/gTOC)	Total HBI (µg/gTOC)	Sterane ratios		
																				C_{27} %	C_{28}%	C_{29}%
Batong																						
0.10	Offs	0.37	1.65	0.61	28.66	1.22	0.80	111.6	5.4	80.5	0.95	24.4	0.51	12.2	1.18	0.231	0.22	0.047	3.73	17.4	21.0	61.6
0.41	Offs	0.41	1.64	0.46	29.02	1.36	1.11	172.5	15.7	71.1	0.83	17.1	0.5	14.7	1.02	0.181	0.22	0.090	2.93	18.1	18.9	63.0
0.63	Offs	0.60	2.14	0.51	28.88	1.42	1.58	152.3	4.5	88.6	1.22	18.0	0.51	13.7	1.84	0.338	0.18	0.088	1.28	14.0	21.1	64.8
0.89	Offs	0.40	1.46	0.37	29.3	1.62	1.24	218.6	25.9	76.8	1.32	14.9	0.476	12.1	1.17	0.243	0.17	0.100	2.44	14.1	17.9	68.0
1.15	Offs	0.45	1.85	0.52	28.93	1.4	1.30	169.5	5.5	80.7	1.48	23.5	0.47	11.7	1.19	0.238	0.20	0.144	1.24	16.4	18.7	64.9
1.68	Offs	0.49	1.61	0.39	29.2	1.52	0.99	145.8	16.9	51.6	1.25	15.8	0.45	6.0	0.52	0.206	0.20	0.063	2.98	16.1	21.2	62.7
2.60	Offs	0.66	1.92	0.47	29.08	1.45	1.71	160.8	6.4	59.8	1.10	17.0	0.49	8.1	0.70	0.209	0.25	0.083	1.04	20.4	19.1	60.5
3.53	Offs	0.69	2.22	0.4	29.26	1.64	2.99	276.6	14.7	74.7	1.60	38.7	0.46	11.0	0.80	0.173	0.20	0.143	3.13	16.1	20.4	63.4
4.45	Offs	0.62	1.66	0.4	29.2	1.49	2.95	319.0	16.6	63.0	0.97	14.2	0.49	9.4	0.79	0.202	0.21	0.095	1.97	16.9	18.7	64.4
Meragang																						
5.18	UShF	0.39	3.03	0.61	28.57	1.32	0.75	74.1	7.9	50.3	1.05	3.3	0.35	10.3	0.41	1.020	0.18	0.087	0.10	7.2	45.9	46.9
7.09	UShF	0.88	4.05	0.38	29.3	1.61	5.16	414.1	46.7	91.4	0.45	5.9	0.47	13.0	0.56	0.100	0.09	0.064	0.11	17.1	28.2	54.7
8.53	UShF	0.62	3.87	0.46	29.2	1.48	3.69	390.3	31.0	54.6	0.46	1.6	0.45	17.4	0.70	0.099	0.16	0.107	0.21	15.5	32.8	51.7
9.97	LShF	0.70	3.34	0.45	29.1	1.37	3.78	365.9	97.4	46.8	0.27	6.1	0.49	15.9	0.89	0.139	0.18	0.134	0.15	13.7	39.9	46.4
12.72	LShF	0.73	4.09	0.39	29.3	1.558	4.51	418.4	87.9	75.5	0.36	6.8	0.45	18.1	0.77	0.100	0.17	0.153	0.13	15.8	26.6	57.6
14.31	LShF	0.87	3.23	0.44	29.19	1.58	3.97	277.2	54.3	84.4	0.86	5.2	0.42	18.1	0.59	0.078	0.14	0.087	0.16	14.5	33.3	52.2
15.88	LShF	0.66	3.99	0.464	29.2	1.55	3.65	345.6	106.8	107.2	0.46	4.2	0.45	16.3	1.02	0.150	0.21	0.235	0.09	16.0	37.0	47.0
19.50	UShF	0.71	4.15	0.49	29.1	1.41	5.35	463.8	38.8	84.1	0.75	2.4	0.47	20.0	0.98	0.119	0.44	0.169	0.16	23.2	13.8	63.0
20.50	UShF	0.78	4.00	0.49	29.13	1.4	3.08	252.9	29.4	41.9	0.25	1.4	0.49	8.7	0.38	0.108	0.22	0.073	0.05	14.4	28.9	56.8
22.90	UShF	0.94	3.94	0.54	29.1	1.52	2.88	174.2	34.9	94.5	0.36	0.5	0.40	11.3	0.59	0.122	0.17	0.133	0.12	20.4	30.9	48.7
24.72	LShF	0.79	3.22	0.47	29.07	1.37	3.12	261.9	27.0	58.1	0.38	4.3	0.52	10.4	0.35	0.075	0.30	0.029	0.06	14.0	18.9	67.1
26.13	LShF	0.77	2.95	0.47	29.17	1.45	2.94	227.7	91.1	38.6	0.21	10.6	0.45	7.3	0.28	0.090	0.20	0.022	0.05	18.1	17.3	64.6
27.54	LShF	0.71	3.68	0.47	29.08	1.31	5.70	516.7	76.9	39.9	0.15	7.4	0.48	9.7	0.38	0.102	0.27	0.041	0.06	38.7	12.1	49.2
29.05	LShF	0.79	4.84	0.62	28.7	1.25	2.49	194.0	6.2	30.6	0.03	3.7	0.51	6.8	0.39	0.130	0.26	0.010	0.05	17.5	16.0	66.5
30.32	LShF	0.71	4.10	0.52	28.99	1.26	5.85	520.0	49.7	35.8	0.07	4.5	0.54	8.9	0.34	0.094	0.22	0.013	0.03	10.8	20.2	69.0
31.59	LShF	0.85	4.03	0.5	29.03	1.3	7.15	535.7	29.8	50.7	0.19	6.5	0.49	13.6	0.51	0.095	0.22	0.051	0.08	15.6	8.7	75.8
34.00	LShF	0.29	2.11	0.83	27.99	1.1	0.89	126.6	0.2	31.7	0.32	4.7	0.53	4.9	0.25	0.107	0.23	0.003	0.02	13.8	23.5	62.6
35.72	LShF	0.62	4.45	0.54	28.93	1.26	3.97	405.6	13.1	26.7	0.13	2.9	0.52	7.9	0.30	0.089	0.23	0.006	0.06	13.6	17.4	69.0
36.78	LShF	0.60	4.90	0.73	28.34	1.15	2.10	191.5	4.0	29.8	0.17	4.7	0.52	6.6	0.30	0.102	0.24	0.003	0.05	7.2	19.1	73.7
41.43	LShF	1.43	2.94	0.46	29.25	1.91	4.45	166.7	3.1	198.7	0.33	1.3	0.43	8.1	0.30	0.141	0.13	0.075	0.52	13.0	26.6	60.4

Chapter 3

Investigation of primary productivity changes and terrigenous OM input of the Japan Sea due to global cooling and strengthening East Asian Winter Monsoon

3.1. Introduction

General Cenozoic cooling

The uplifting of the Himalayan Tibetan Plateau (HTP) is considered to be one of the most dominant factors that caused the Cenozoic Cooling. Seawater Sr records suggest uplifting and weathering of the HTP from 40 Ma, which eventually lead to the drawdown of CO_2 as the weathering of silicate material and increased organic carbon burial lowered atmospheric CO_2 levels. This is believed to have caused the Antarctic Glaciation at around 35 Ma, the Miocene Cooling Trend since around 15 Ma, and the Northern Hemisphere Glaciation at around 2.5 Ma (Raymo & Ruddiman, 1992). The combined effects of the uplifting of the HTP and cooling has also been considered a major factor in global aridification and the development of the East Asian Monsoon system (EAM). Since the Miocene, many tectonic, climatic and oceanographic changes have been occurring simultaneously in the Northern Hemisphere such as Global Cooling, intensifying EAM, uplifting of the HTP, shifting bottom water conditions of the Japan Sea, and a shift from carbonate rich to silicate rich oceans in the North Pacific (Cortese et al., 2004; Lübbers et al., 2019; Tada, 1994; Tada et al., 2016). These changes have been shown to affect terrigenous and marine primary productivity both negatively and positively.

Monsoons such as the EAM are important climatic processes as they redistribute heat and moisture around the globe (Beck et al., 2018). The EAM is divided into two: The East Asian Summer Monsoon (EASM) and the East Asian Winter Monsoon (EAWM). The EASM brings in warm air moisture from the Pacific Ocean to the East Asian region via southeasterly winds, increasing rainfall across the region. The EAWM brings eolian dust as well as dry and cold air from Siberia via westerlies to the East Asian and Northwestern Pacific. Due to continued uplift of the HTP and Cenozoic Cooling, the relative strengths of the EASM and EAWM has been changing throughout time, with a general consensus that the EAWM has been strengthening while the EASM has been weakening since the Miocene, which has resulted in increased aridification in the East Asian region. On shorter time-scales, the EAM system is even more complex and poorly understood, with research showing that EAW intensities can be linked to glacial-interglacial as well as Pacific Decadal Oscillation shifts (Kim et al., 2014; Tamburini et al., 2003).

The intensifying EAWM since the Miocene has changed terrestrial carbon production in Central Asia as well as biogeochemical properties of the Japan Sea. Research done by (Peng et al., 2016) on Loess sediments from Central Asia shows an increase in long-chain *n*-alkane biomarker proxies

between 14.5 to 12.5 Ma and from 10 to 4 Ma, indicating a drying regime and shift from woodlands to grasslands. Research done on black carbon compositions taken IODP 1430 core samples (exp. 346, collected from the Japan Sea) shows that all black carbon since 15 Ma came from wildfires in the Central Asian region rather than Japanese Islands, with a decrease in black carbon in younger sediments being indicative of desertification-related vegetation loss rather than reduced wildfire activity (Shen et al., 2018). Evidently, aridification caused by global cooling and intensifying EAWM causes terrestrial OM production to cease.

Mineral analysis done on IODP 1430 (exp. 346, collected from the Japan Sea) core samples shows an increase in Central Asia-derived illite and chlorite from 15 Ma onwards, while Japanese Island-derived smectite decreased. Isotope data also shows an increase in Central Asia-derived sediments relative to Japanese Island-derived sediments in a step-wise manner and was attributed to intensifying EAWM and Global Cooling (Shen et al., 2017).

From the Miocene, the Japan Sea has also been responding to climatic and tectonic changes. Initially, before 15.5 Ma, Japan Sea surface waters were warm with suboxic bottom waters associated with inflow of oxygen-poor and saline Oxygen Minimum Zone waters (OMZ). Primary producers were also mainly calcareous planktons during this time. However, from 15.5 Ma onwards, surface waters gradually cooled, with OMZ waters only flowing in during high sea-levels, creating bottom waters that fluctuated between oxic and dysoxic or euxenic. During this period, the southern channel was closed from 10 to 3.5 Ma, making the Japan Sea a restricted basin only open to the north. From 2.5 Ma onwards, the Japan Sea surface and bottom waters fluctuated between warm and cold and hyperoxic to euxenic respectively, as glacial lowstands caused isolation of the sea and euxenic bottom water conditions, while interglacials allowed the inflow of the Tsushima Warm Current and the formation of deep waters in the Japan Sea (Tada, 1994).

As seen from the above, the effects of tectonics, global cooling and intensifying EAWM on aridification of Central Asia and the Japan Sea's physico-chemical properties are relatively well studied. However, the effects of global cooling and intensifying EAWM on terrestrial carbon production and delivery to the Japan Sea has not been well studied. Thus, the objective of this research is to study the effects of such climatic phenomenons and the Japanese Islands' paleovegetation, terrestrial OM production and transport to the Japan Sea and their effects on the Japan Sea's biogeochemical properties by utilizing lipid biomarkers preserved in Miocene sediments.

3.2. Geological setting and study area

The Kawabata Formation, distributed in south-central Hokkaido, Japan (Fig. 3.1), consists of sandy and muddy gravity flow deposits formed in the Ishikari-Teshio Belt deposited along the western side of the Hidaka collision zone during the middle to late Miocene (Kawakami et al., 2004). This unit has been subdivided by Kawakami et al. (2002) into two members: the Amagiri Sandstone and Mudstone Lower Member and the Higashiyama Sandstone and Conglomerate Upper Member. The Amagiri Sandstone and Mudstone Member is characterized as a basinal turbidite system consisting of mudstone dominated mudstone-sandstone interbeds, and the Higashiyama Sandstone and Conglomerate Member is characterized by sandstone dominated alternations and thick conglomerate layers deposited by slope-apron turbidite system (Kawakami et al., 2002). There are five key beds of acidic tuff (K1 - K5 tuffs), and the age of the K5 tuff in the Higashiyama Member shows an age of 13.2 ± 0.9 Ma by fission-track dating (Kawakami et al., 2002). It was estimated that the Kawabata Formation was deposited below 1000 m water depth by the presence of the benthic foraminifera *Uvigerina proboscidea* that is associated with the lower middle bathyal marine zone (Tsubakihara, 1990). Due to burying and isostatic uplift of the hinterland orogen, the basin shallowed, and this shallowing caused the change in sedimentary systems from the basinal environment of the Amagiri Member to the slope-apron environment of the Higashiyama Member (Kawakami et al., 2004; Kawakami, 2013).

The 2 intervals of interest that belong to the Miocene Kawabata Formation are the Soumokumaisawa-River section and the Higashiyama-River section that are both deposited along the Soumokumaisawa and Higashiyama rivers of Yubari, central Hokkaido, respectively. In general, the Soumokumaisawa-River interval is older and belongs to the Amagiri Sandstone-Mudstone member, whereas the Higashiyama-River section is mostly younger and belongs to the Higashiyama Sandstone-Conglomerate Member. The 13.2 Ma K5 tuff layer mentioned above can be found in the upper part of the Soumokumaisawa-River section and is connected to the lower part of the Higashiyama-River section (Fig. 3.1). The base of the soumokumaisawa-river section is located above the base of the Takinoe Formation, giving it an age of ~15 Ma at the base. The youngest of the two intervals is at the top of the Higashiyama River section, which lies directly below the Oiwake/Iwamizawa Formation. Thus, the Soumokumaisawa River and Higashiyama River sections were deposited between 15 Ma and 9 Ma.

3.3. Methodology

3.3.1. Fieldwork and sampling

Fieldwork was done based on Kawakami et al., (2002). In summary, coarser sedimentary layers consists of conglomerates, sandstones and pebbly sands. Mud-containing layers were either pure mudstones, sand-rich mud and sand alternations, even mud and sand alterations, mud-rich mud and sand alternations. A tuff layer was also found in both sections. A total of 49 mudstones were collected from both successions for total organic carbon (TOC%) and lipid biomarker analysis (n = 49).

3.3.2 Total Organic Carbon% (TOC%)

A portion of each powdered sediment sample was acidified with 1 M HCl and allowed to stand for half a day to remove carbonates. Carbonate-free samples were then vacuum-dried and analyzed for TOC content using a J-Science Micro Corder JM10 instrument at the Center for Instrumental Analysis of Hokkaido University.

3.3.3. Biomarker extraction and analysis

Extraction and separation of lipids were performed as reported in Sawada (2006). Briefly, the sediment samples were extracted with methanol (MeOH) and dichloromethane (DCM). Afterwards, an internal standard, tetracosane-d_{50} was added, and the extract was dried in a rotary evaporator and redissolved in hexane. The hexane extract was then separated into 4 fractions such as the aliphatic hydrocarbon (F1), aromatic hydrocarbon (F2), ketone-ester (F3) and polar lipid (F4) fractions.

For F1 and F2, reduced copper was added to the solution to remove any sulfur. Afterwards, the above fractions were then evaporated in a rotary evaporator and then redissolved in hexane before being passed through a gas chromatograph coupled with a mass spectrometer (GC/MS). In this study, the Agilent Technologies 7890B GC System (with DB-5HT fused silica column) coupled to an Agilent Technologies 5977A Mass Spectrometer (electron voltage of 70 eV, initial temperature of 50°C held a 4 mins, then ramped up to 310°C at 4°C/min and held at 20 min, scan range: *m/z* 50 – *m/z* 650 in 1.3s).

3.4. Results

TOC% and biomarkers were measured and are shown in figures 3.2, 3.3, 3.4 and in table 3.1. TOC% generally ranges between 0.31 and 0.99 throughout both successions and does not show any trends, with one anomalously high reading of 1.77.

Pr/Ph is used as a redox indicator as well as a non-specific terrigenous OM indicator. Phytol, derived from the epicuticular leaf waxes of land plants and phytoplankton, degrades to produce more pristane (Pr) than phytane (Ph) under oxic conditions, while under anoxic conditions it produces more phytane than pristane (Didyk et al., 1978). It has been interpreted that Pr/Ph ratios greater than 1.5 indicate oxic environments. In addition, the Pr/Ph values > 3 indicates high input of terrigenous OM (Powell, 1988). In this study, Pr/Ph ratios are used to measure bottom water oxicity. Pr/Ph values generally decrease from a highest value of 3.12 in older horizons to as low as 0.51 in younger horizons.

The aquatic macrophyte *n*-alkane proxy, P_{aq}, is deduced by the relative amounts of C_{23} and C_{25} *n*-alkanes compared to C_{29} and C_{31} *n*-alkanes (Ficken et al., 2000). The carbon preference index (CPI) is used to determine the ratio of odd-chain, epicuticular leaf wax derived *n*-alkanes from land plants to even-chain *n*-alkanes from marine sources but should be used with caution as degradation or thermal alteration can convert odd-numbered *n*-alkanes to even-numbered *n*-alkanes (Bray and Evans, 1961; Eglinton and Hamilton, 1963; Chen et al., 2021). The average chain length (ACL) is used to estimate the proportion of woody OM to grassy OM, with the former producing high amounts of C_{27} and C_{29} *n*-alkanes and the latter producing C_{31} *n*-alkanes. CPI, P_{aq} and ACL all show little variation, with values ranging from 0.27 to 0.78, 0.23 to 2.87 and 28.14 to 29.2 respectively.

Long chain *n*-alkanes with odd carbon numbers (C_{25} to C_{33}) are derived from epicuticular leaf waxes and are quite stable in the fossil record for tens of millions of years due to being straight-chain hydrocarbons with no functional groups (Eglinton and Logan, 1991). Hence, they are used to determine leaf wax concentrations in the sediments (Peters et al., 1991). Total *n*-alkane concentrations (μg/gsed) and total long-chain *n*-alkane concentrations (μg/gTOC) both decrease in younger sediments, with values ranging from a high of 10.90 and 1369.12 in Soumokumaizawa's older sediments and generally falls to a minimum of 1.93 and 134.9 in younger sediments of the Higashiyama section respectively. *N*-alkane C_{31}/C_{27} and *n*-alkane $(C_{31}+C_{33})/(C_{27}+C_{29})$ ratios have been used to estimate aridity throughout time. Both show similar trends with no variations throughout both successions, with values ranging from 0.16 to 1.41 and 0.11 to 0.89 respectively.

Triterpenoids with oleanane-, lupane-, and ursane-skeletons are derived from angiosperm leaves and bark and their concentrations can be used to infer angiosperm input (Stout, 1992). They include aliphatic triterpenoids as well as aromatic triterpenoids. Triterpenoid concentrations (μg/gTOC) remain within the range of 24.3 to 803.04 throughout both areas, with an anomalously high value of 1581.6 at the youngest layer of the Higashiyama section. Diterpenoids are derived from gymnosperm resins and can be used to infer gymnosperm input (Otto & Wilde, 2001). In this study, aliphatic diterpenoids were detected using their respective base peaks and M+ ions shown in figure 3.5 and table 3.2. The aromatic diterpenoids simonellite and dehydroabieatane were detected using m/z 237 and 255 respectively. The sum of aliphatic and aromatic diterpenoid concentrations (μg/gTOC) generally increase from a value of 2.53 in older soumokumaisawa sediments to a high value of 56.81 in the youngest Higashiyama horizon.

Using *m/z* 217 and the molecular ions M+ 372, 386, and 400 for C_{27}, C_{28} and C_{29} regular steranes respectively, steranes were identified and quantified. The C_{27} and C_{28} regular steranes are steroids derived from phytoplankton and zooplankton while C_{29} steroids are generally derived from higher plants (Volkman, 1986). $C_{27}/(C_{27}+C_{29})$ sterane ratios are at low levels in the older Soumokumaisawa section, with values less than 0.34 at depth of 0 to 913 m , but increase to 0.47 at 918 m depth. In younger sediments deposited onwards upwards, ratios remain higher, fluctuating between 0.24 and 0.49.

Highly branched isoprenoid (HBI) alkane with a C_{25} carbon number is an isoprenoid derived from certain species of diatoms and is identified with base peak m/z 57 and M+238 (Sinninghe Damsté et al., 2004). The HBI thiophenes were identified using the base peak *m/z* 293 and *m/z* 265 with an M+ ion of 378. HBI/n-C21 ratios are low in older Soumokumaisawa sediments, with values close to 0.00 but increases after xx depth to 0.59. In younger sediments afterwards and throughout the Higashiyama section, values fluctuate but show an increasing trend towards a high value of 2.21 in Higashiyama. Total HBI concentrations (μg/gTOC) also show a general increasing trend in younger horizons, with values as low as 2.67 in older Soumokumaisawa horizons and increasing rapidly at xx depth. Afterwards, eventhough large fluctuations are seen, total HBI concentrations generally increase to a maximum value of 223.6 in younger Hishayama horizons. Total HBI concentrations also show a good negative correlation with Pr/Ph values, at R= -0.66, but a less reliable negative correlation with long-chain *n*-alkanes, at R= -0.13.

Dinosteranes are identified using m/z 231 and M+ 414 and are derived from dinoflagellates. Dinosterane concentrations (μg/gTOC) generally remain at low levels between 0.00 and 36.8 in both sections, but an anomalously high amount is found in the youngest horizon of Higashiyama at a value of 153.68.

Gammacerane is derived from tetrahymanol, which is produced by bacteriocvorous ciliates living in stratified water columns (Harvey & Mcmanus, 1991; Sinninghe Damste et al., 1995). Thus, they can be used as a stratification index. Gammacerane concentrations (μg/gTOC) are generally lower in older Soumokumaisawa horizons, with values ranging from 0.01 to 2.67. In younger Higashiyama horizons, gammacerane concentrations are higher but fluctuates, with values between 0.39 to 4.22. Gammacerane concentrations also show a good correlation with total HBI concentrations, at R2= 0.55. The gammacerane index show similar trends, with lower values in older Soumokumaisawa sediments ranging between 0.0009 and 0.07 but increases in range to being between 0.015 to 0.23 in younger Higashiyama sediments. A plot of the Gammacerane Index against Pr/Ph ratios shows that most younger sediments, especially those deposited after 13.2 Ma, were deposited in a more saline environment than older sediments.

Methylchromans are salinity-sensitive biomarkers that can be used to infer paleosalinity of the marine environment (Sinninghe Damsté et al., 1987). In both the Soumokumaisawa and Higashiyama sections. MTTCs fluctuate between 0.86 and 0.92. However, a plot of MTTCI and Pr/Ph shows some level of discrimination which is explained in the discussion.

Hopane C_{31}S/(S+R) ratios decrease in younger sediments, from a high of 0.43 in older soumokumaisawa sediments to a low of 0.19 in Higashiyama's younger horizons.

3.5. Discussion

3.5.1. Variations of terrigenous OM transport to ancient North Japan Sea and paleo-precipitation reconstruction

C_{25} to C_{35} long chain *n*-alkanes are primarily produced by the leaf waxes of epicuticular plants (Eglinton & Hamilton, 1963b). As such, long-chain *n*-alkanes can be used to determine the relative delivery of terrigenous OM into the Japan Sea via riverine discharge. In this study, both total *n*-alkanes concentrations (μg/g-sed) and long-chain *n*-alkanes normalized to TOC (μg/g-TOC) show a

slightly decreasing trend in younger sediments, suggesting a reduced input of terrigenous OM transported from the Japanese Islands.

C_{27} sterane ratios, $C_{27}/(C_{27}+C_{29})$, can also be used to determine the relative input of marine and terrestrial OM into the system. The C_{27} sterane ratios are low in older soumokumaisawa-gawa river sediments, suggesting that terrestrial OM input is high. However, C_{27} sterane ratios increase in younger sediments, also suggesting a reduction in terrigenous organic matter input relative to marine OM input. This could be due to a reduction in precipitation received by the Japanese Islands from increasing aridification caused by global cooling and/or a strengthening East Asian Winter Monsoon – which would reduce river discharge. These results are also concordant with mineral analysis done from IODP core 1430 which was taken from the southern part of the Japan Sea. Basically, a reduction of Japanese Island derived smectite rich sediments is seen from 15 Ma to Recent in comparison to Central Asia-derived eolian dust, which is rich in illite and chlorite (Shen et al., 2017).

Analysis of *n*-alkane derived proxies such as Carbon Preference Index (CPI), Average Chain Length (ACL), Aquatic Macrophyte Index (P_{aq}) and two long-chain *n*-alkane ratios which are C_{31}/C_{27} and $(C_{31}+C_{33})/(C_{27}+C_{29})$ can be used to measure the relative precipitation received by the Japanese Islands. While CPI and ACL can be used to determine the source of OM, they can also be used to measure aridity. In the case of CPI, ACL and the two long-chain *n*-alkane ratios, intensifying aridity or reduced precipitation will increase the value of these indices as plants produce leaf-waxes with longer carbon chains during arid or drought periods to prevent water loss from evapotranspiration (Andersson et al., 2011; Zhou et al., 2010). P_{aq}, which is used to measure the relative abundance of submerged aquatic macrophytes, can also be used to measure lake levels (Sun et al., 2023). In this study, all the above proxies do not show notable variation from 15 Ma to 9 Ma, showing that even though global cooling was progressing, changes in precipitation in the Japanese Island were minimal or negligible. This could also mean that the effects of aridity were not yet intense in the Japanese Islands compared to Central Asia. The study by Shen et al (2017) mentioned above saw an increase in eolian dust in the Japan Sea from 15 Ma to Recent and is attributed to increased drying of Central Asia. However, a biomarker study done by (Peng et al., 2016) used the same biomarker indices shown here and suggested that aridification of Central Asia only intensified after ~10 Ma. Thus, it is possible that different latitudes experienced the effects of global cooling and strengthening East Asian Winter Monsoon at different times.

3.5.2. Paleovegetation change of the Japanese Islands

Pentacyclic triterpenoids generally come from the leaf and bark of angiosperm plants. Increasing maturity, diagenesis in anoxic environments and also microbial degradation can cause progressive aromatization of aliphatic triterpenoids to degraded-aliphatic triterpenoids (des-A-triterpenoids) and degraded aromatic triterpenoids (mono-, di-, triaromatic des-A-triterpenoids). Thus, the total of angiosperm-derived triterpenoids was used as an indicator for angiosperm input and angiosperm growth in the Japanese Islands. In this study, angiosperm concentrations appear to fluctuate but show no apparent trend, suggesting no large net changes in angiosperm cover.

Diterpenoids are derived from the resins of gymnospermous plants. Similar to triterpenoids, increased maturity can also cause aromatization of aliphatic diterpenoids. Thus, the total of aliphatic and aromatic diterpenoids were used to measure diterpenoid input and gymnosperm forest cover. In the older sediments of Soumokumaisawa, diterpenoid concentrations are lower. However, they gently increase in concentration in the younger sediments of Higashiyama. The diterpenoid/triterpenoid ratio also shows an increasing trend in gymnosperm coverage in younger sediments This shows an increase of gymnosperm growth in the Northern Japan from 15 to 9 Ma and may be attributed to global cooling as gymnosperm forests tend to expand in cooler climates (Wang et al., 2001). However, these results are different than those seen in southern Japan, which are recorded from pollens found in the Himi area of Toyama, Japan (Wang et al., 2001). In southern Japan, an increase of angiosperms and a decrease in gymnosperms was seen from 15 to 9 Ma, which is the opposite of our results. Thus, we propose that cooling in the Japanese Islands and its effects occurred earlier in the higher latitudes of the Japanese Islands.

3.5.3. Primary productivity in the ancient Japan Sea

Dinoflagellates produce dinosteranes while diatoms produce Highly Branched Isoprenoids (HBI) *n*-alkanes and thiophenes. In older Soumokumaisawa-River sediments dinosterane concentrations are low but sometimes show dominance over diatoms, suggesting that this is a low-nutrient environment. However, at 918m depth of the Soumokumaisawa section (before 13.2 Ma) there is a sharp increase in C_{27} ratios that also coincides with a large increase in HBI biomarkers over dinosteranes, which suggests that diatoms had become the dominant primary producer at this time. Afterwards, C_{27} sterane ratios and diatoms remain high and more abundant than dinosteranes throughout both

successions but show large fluctuations. Tada (1994) has noted two events that could enhance diatom primary productivity. First is upwelling of the Oxygen Minimum Zone, which is an anoxic and nutrient rich deep-water body flowing from the Pacific Ocean. During this period, the OMZ was flowing into the Japan Sea via a shallow north or northeastern channel. Based on Tada (1994), weak upwelling is enough to maintain diatom productivity on the sea surface as seen from biogenic silica abundances. The second event is related to global cooling. Tada (1994) noted that inflow of cool waters from the Pacific Ocean and the southward migration of the subpolar front from 15.5 to 14 Ma resulted in cooling of surface waters in the Japan Sea. Thirdly, 10.5 to 6 Ma was a period of falling sea level according to Haq et al. (1987). Thus, eustatic sea-level fluctuations has been proposed as a mechanism responsible for the amount of inflow of OMZ waters into the Japan Sea. During high-sea levels, OMZ waters can flow over the shallow northern channel, whereas during low-sealevels, OMZ inflow is restricted (Tada, 1994). In this study, the MTTCI ratio vs pr/ph plots shows a tendency towards saline conditions after the environmental change event (Fig 3.6A). Gammacerane concentrations, deep-water oxicity, and HBI show some correlation. Gammaceranes are produced by bacterivorous ciliates that dwell in saline waters and are used as a salinity and stratification index. In this study, gammacerane concentrations and HBI correlations show a correlation of R = 0.55, showing that increasing salinity may influence increases in diatom abundances. HBI also shows a correlation of R = - 0.66 with pr/ph ratios, showing that diatom abundances increase when bottom waters are dysoxic or anoxic. Increasing stratification is also seen in gammacerane index vs pr/ph plots, where most sediments after the possible intrusion event show greater stratification (Fig 3.6 B, C, D). Thus, the inflow of saline and oxygen-poor OMZ waters coupled with upwelling could have promoted diatom growth. Large fluctuations in diatom abundances could also be linked to the presence of shallow sills allowing and restricting inflow of OMZ waters during high and low-eustatic sea levels respectively. Diatom abundances show very poor correlation with long-chain, leaf-wax derived *n*-alkanes, at R = - 0.2, showing that diatom abundances may not have been controlled by terrigenous nutrient input from the Japanese Islands.

Furthermore, another factor that could contribute to diatom growth is nutrient derived from the central Asian region during intensifying East Asian Winter Monsoon. Although different localities will give different results on the timing of aridification, it is generally accepted that the East Asian Winter Monsoon intensified during the Miocene (Tada et al., 2016). Studies have shown that chlorophyll-a concentrations in the South China Sea increases in during heavy dust years as Central Asian sediments supply iron (Fe) necessary for diatom growth (Wang et al., 2019). However, pre-

existing studies on long-time scale variations in Fe supply cannot be found, and so the input of Iron to the Japan Sea since the Miocene is not known.

3.6. Summary

The Kawabata Formation, deposited between 15.7 and 9 Ma, is exposed at the Soumokumaisawa and Higashiyama Rivers. These sediments were deposited during the Miocene Cooling Trends, increasing East Asian Winter Monsoon, and an increase of nutrient delivery to the Pacific Ocean. The long-chain n-alkane concentrations decreased throughout time while the diterpenoids increased relative to triterpenoids. These suggest a cooling climate where precipitation weakened and encouraged the growth of gymnosperms, which occurred earlier than Southern Japan. P_{aq}, ACL, CPI and two long chain n-alkane ratios did not show any changes, suggesting that aridification in the Japanese Island was weak between 15.7 and 9 Ma. Diatom contents, measured by HBI, increased in younger sediments, with good correlation with pr/ph and/or gammacerane concentrations, suggesting a relationship between diatom growth and bottom water anoxicity and more saline conditions. Such conditions could be due to the intrusion of the OMZ waters that provided nutrients that were upwelled to the surface, encouraging diatom growth. This study shows that strengthening EAWM in the Japanese Islands was weaker than in Central Asia, while in the Japan Sea the main source of nutrients came from upwelling of nutrient rich deep waters rather than terrestrial input.

3.7. Figures

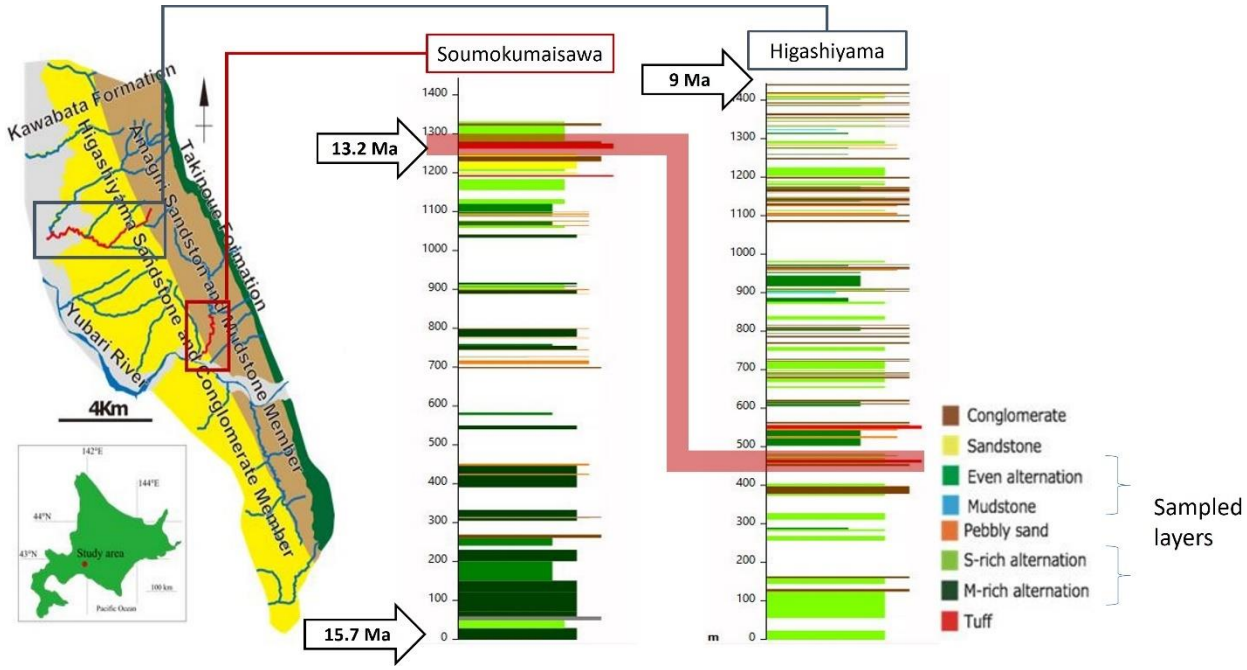

Figure 3.1. Study area and sample locations of the Soumokumaisawa and Higashiyama River sections.

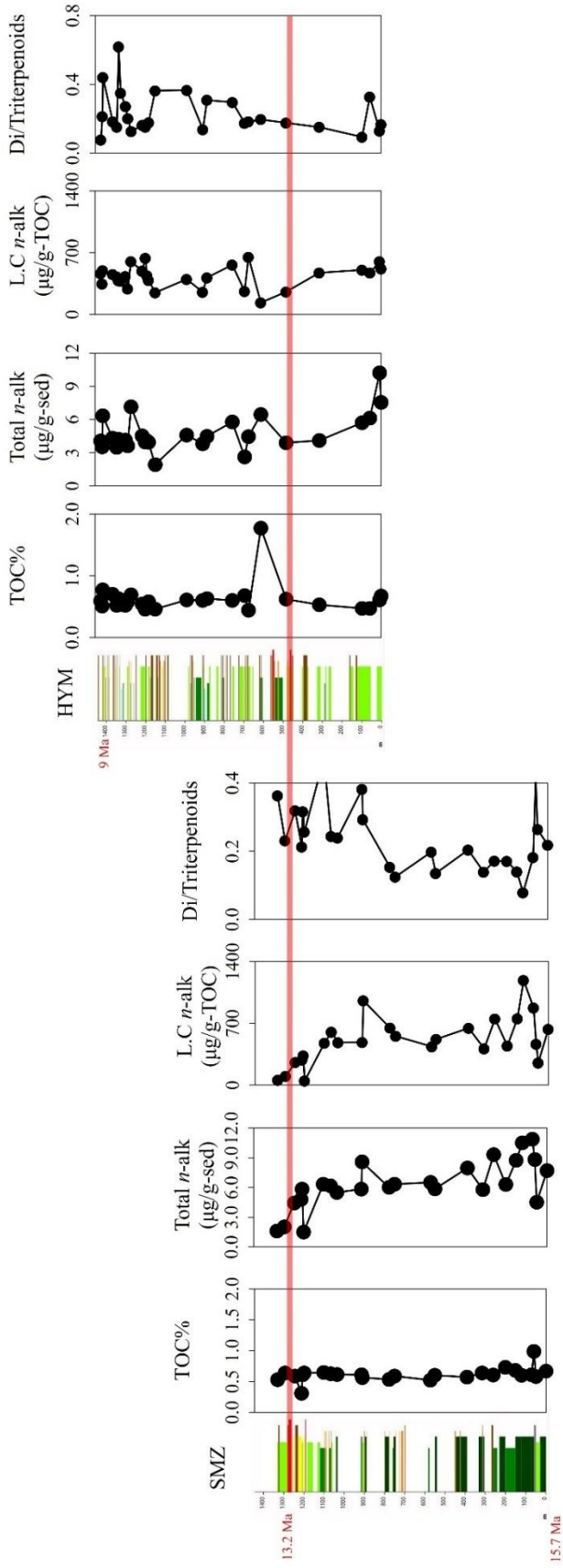

Figure 3.2. TOC% and terrigenous biomarkers of the Soumokumaisawa and Higashiyama River sections.

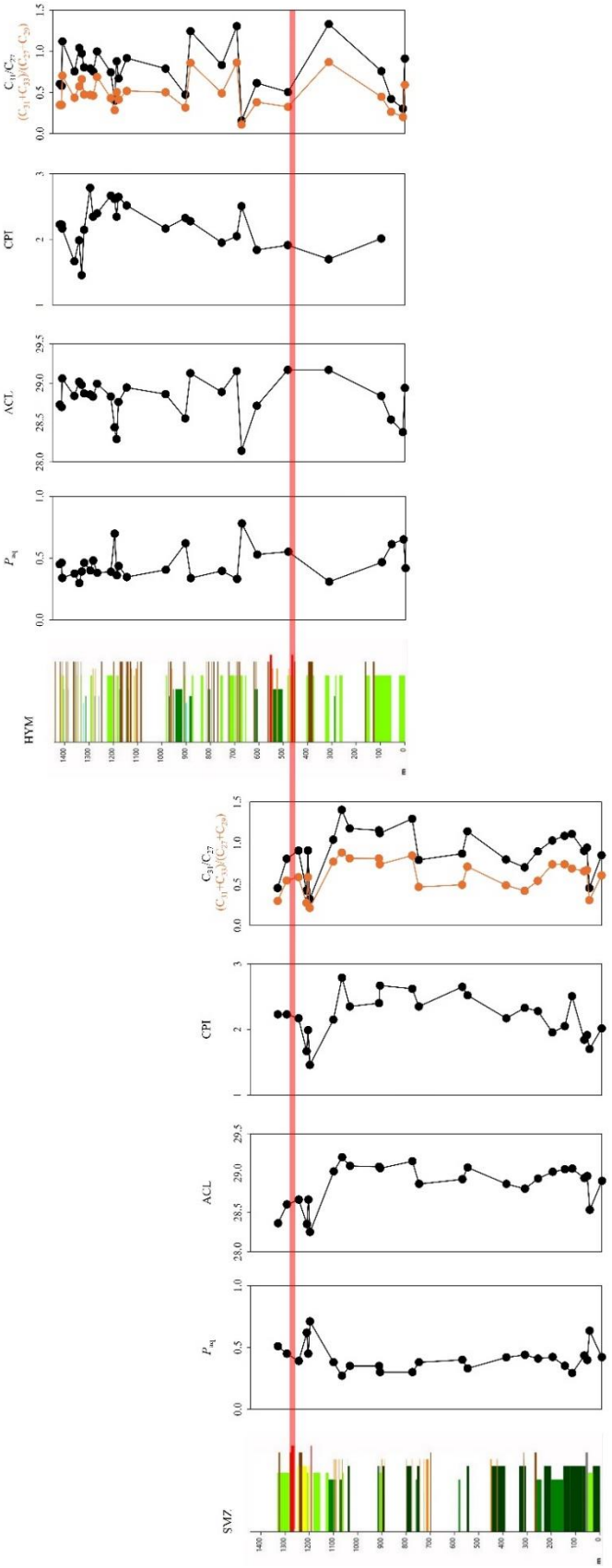

Figure 3.3. P_{aq}, ACL, CPI and long-chain n-alkane ratios of the Soumokumaisawa and Higashiyama River sections.

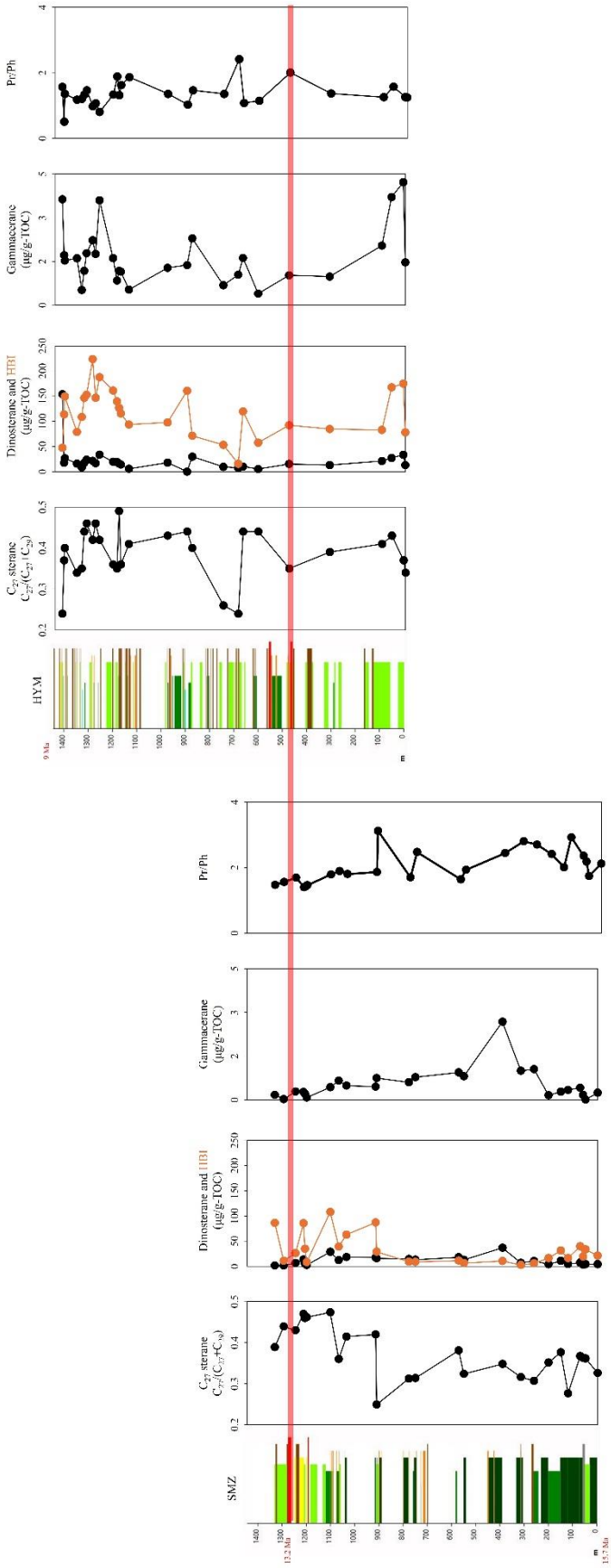

Figure 3.4. Marine biomarkers of the Soumokumaisawa and Higashiyama River sections.

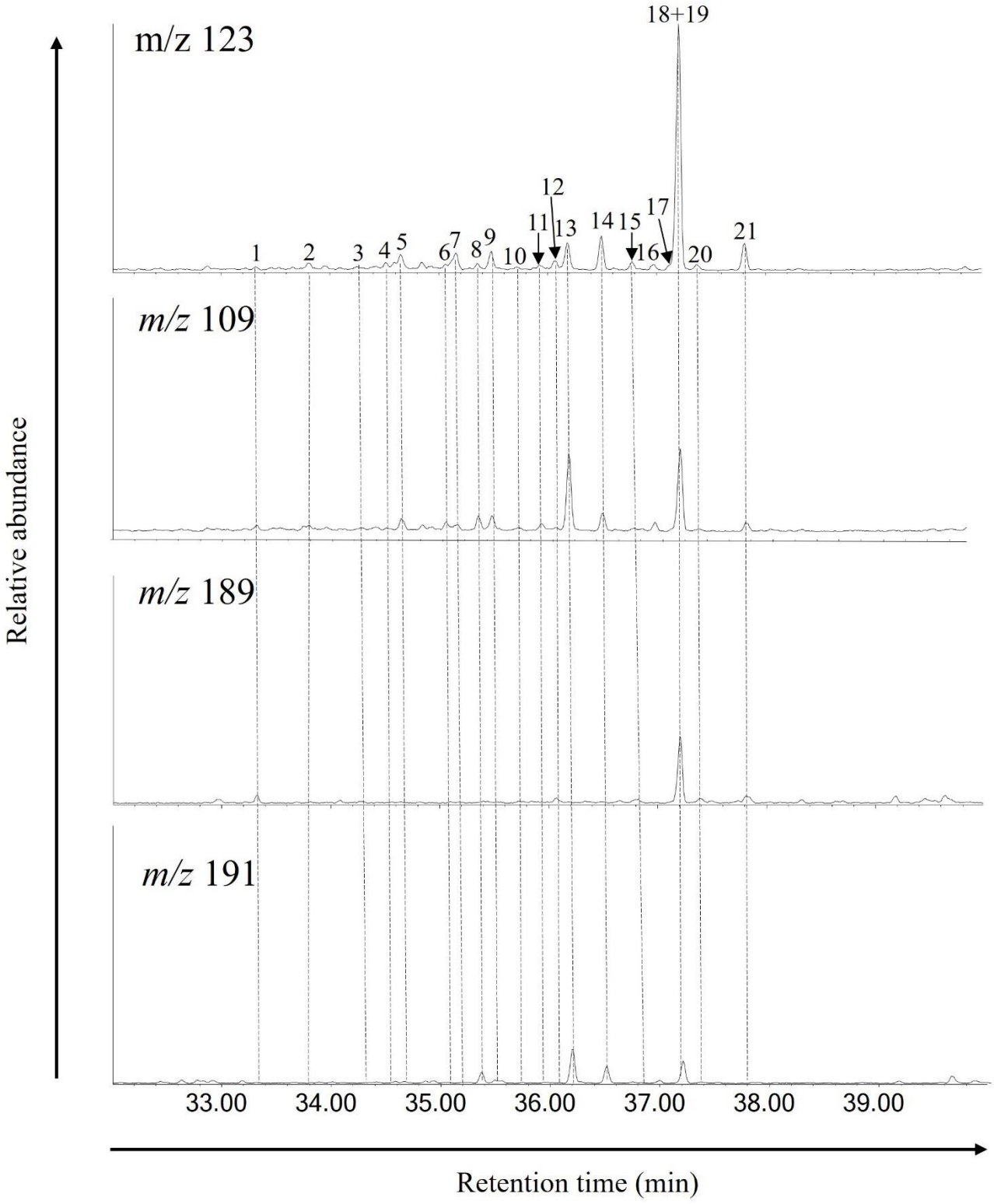

Figure 3.5. Aliphatic diterpenoids identified using base peak m/z 123. Further identification was done using m/z109, 189 and 191. See table 3.2 for identification.

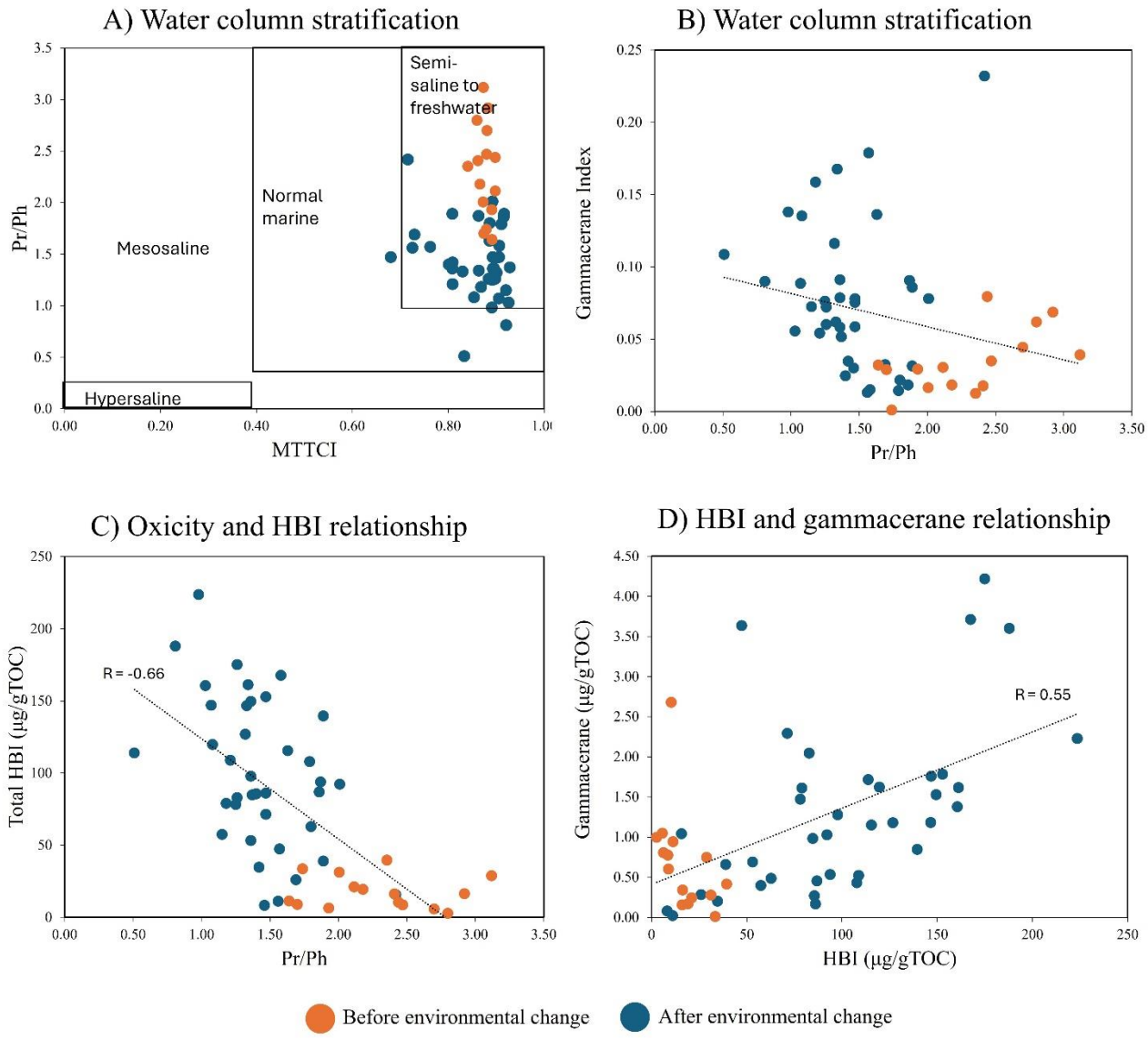

Figure 3.6. Correlations between HBI and other proxies.

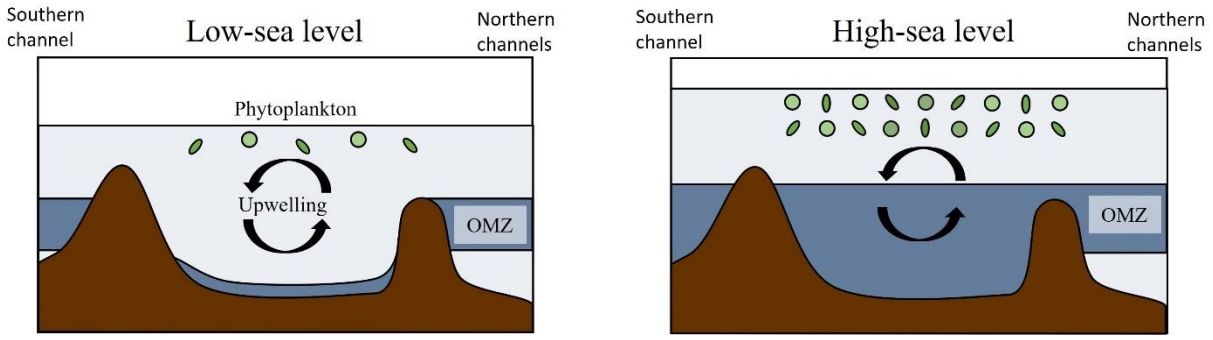

Figure 3.7. Mechanism for intrusion of OMZ and its effects on upwelling. Based on Tada (1994).

3. 8. Tables

Table 3.1. Biomarker data of Higashiyama and Soumokumaisawa River sections.

Thickness	TOC %	Pr/Ph	P_{aq}	ACL	CPI	HPP	Total *n*-alkane (μg/gsed)	Total long chain *n*-alkane (μg/gTOC)	HBI/*n*-C_{21}	C_{27} sterane ratio $C_{29}/(C_{27}+C_{29})$	Diasterane (μg/gTOC)	Total HBI (μg/gTOC)	Hopane/C_{31} $C_{31}S/(C_{31}S+C_{31}R)$	HBI/(C_{27}+C_{28} sterane)	*n*-alkane C31/C27	*n*-alkane $(C_{31}+C_{33})/(C_{27}+C_{29})$	Gammacerane (μg/gTOC)	Total triterpenoids (μg/gTOC)	Total diterpenoids (μg/gTOC)	Di/Triterpenoids	Gammacerane Index	MTTCI
Soumokumaisawa																						
1332.1	0.53	1.47	0.51	28.36	2.23	0.22	1.63	58.49	0.45	0.39	1.57	86.13	0.26	0.40	0.46	0.30	0.17	65.68	23.9	0.4	0.08	0.68
1293.6	0.64	1.56	0.45	28.60	2.23	0.33	2.03	101.51	0.32	0.44	1.37	11.11	0.33	1.63	0.81	0.55	0.02	49.60	11.5	0.2	0.01	0.73
1248.16	0.59	1.69	0.39	28.66	2.17	0.35	4.44	257.46	0.40	0.43	6.38	26.06	0.32	0.32	0.91	0.59	0.28	123.38	39.4	0.3	0.03	0.73
1216.9	0.31	1.40	0.62	28.35	1.67	0.40	4.82	287.05	0.37	0.47	13.30	85.59	0.35	0.62	0.42	0.28	0.27	134.02	28.6	0.2	0.02	0.80
1209.3	0.61	1.42	0.45	28.66	1.99	0.36	5.84	333.66	0.30	0.46	5.20	34.67	0.30	0.49	0.91	0.59	0.20	49.06	15.5	0.3	0.03	0.81
1201.2	0.64	1.46	0.71	28.25	1.46	0.27	1.50	47.87	0.30	0.46	2.39	8.28	0.39	0.35	0.32	0.22	0.08	24.32	6.2	0.3	0.03	0.90
1104.5	0.65	1.79	0.38	29.02	2.15	0.55	6.35	477.90	0.60	0.47	28.70	107.81	0.39	0.44	1.04	0.78	0.43	165.32	78.2	0.5	0.01	0.91
1073.2	0.63	1.89	0.27	29.20	2.79	0.90	6.20	601.18	0.29	0.36	12.18	38.97	0.37	0.43	1.41	0.89	0.66	114.89	28.0	0.2	0.03	0.92
1040.3	0.61	1.80	0.35	29.09	2.35	0.52	5.51	482.58	0.34	0.41	18.18	62.87	0.35	0.54	1.18	0.82	0.49	230.87	55.3	0.2	0.02	0.89
918.3	0.61	1.86	0.35	29.08	2.40	0.47	5.86	487.05	0.38	0.42	17.70	86.89	0.35	0.77	1.16	0.82	0.45	165.84	63.4	0.4	0.02	0.92
913.8	0.57	3.12	0.30	29.06	2.67	0.47	8.59	959.09	0.16	0.25	15.89	28.89	0.37	0.50	1.12	0.75	0.75	286.39	84.0	0.3	0.04	0.87
860.06	0.54	1.70	0.30	29.15	2.62	0.70	6.04	647.88	0.00	0.31	14.63	8.98	0.37	0.15	1.30	0.85	0.60	167.40	25.7	0.2	0.03	0.87
758.9	0.59	2.47	0.38	28.86	2.35	0.56	6.34	556.71	0.00	0.31	13.13	8.61	0.37	0.14	0.80	0.47	0.78	434.63	54.3	0.1	0.03	0.88
582.7	0.52	1.64	0.40	28.92	2.65	0.49	6.52	435.46	0.00	0.38	17.98	11.31	0.37	0.10	0.87	0.49	0.94	184.98	36.6	0.2	0.03	0.89
547.1	0.60	1.93	0.33	29.07	2.52	0.63	5.88	521.60	0.00	0.32	12.63	6.30	0.40	0.10	1.14	0.72	0.61	236.28	32.0	0.1	0.03	0.89
468.5	0.57	2.44	0.42	28.86	2.17	0.87	7.99	646.62	0.00	0.35	36.89	10.37	0.43	0.07	0.90	0.49	2.68	597.20	121.8	0.2	0.08	0.90
425.5	0.64	2.70	0.44	28.90	2.33	0.50	9.74	774.91	0.00	0.32	6.84	5.68	0.42	0.05	0.71	0.42	1.00	457.98	78.8	0.1	0.06	0.86
232	0.79	2.41	0.42	29.01	1.95	0.53	6.31	443.96	0.15	0.35	4.07	16.17	0.42	0.45	0.90	0.75	0.16	76.53	13.1	0.2	0.02	0.86
202	0.68	2.01	0.35	29.05	2.05	0.31	8.77	753.48	0.19	0.38	10.60	31.19	0.44	0.36	1.09	0.74	0.28	192.34	26.9	0.1	0.02	0.87
152	0.60	2.92	0.29	29.06	2.51	0.43	10.52	1187.50	0.11	0.28	4.45	16.38	0.46	0.62	1.11	0.69	0.34	178.06	14.0	0.1	0.07	0.88
122	0.61	2.35	0.43	28.94	1.84	0.39	10.90	876.08	0.16	0.37	7.27	39.52	0.46	0.76	0.91	0.66	0.41	139.18	25.4	0.2	0.01	0.84
72	0.99	2.18	0.40	28.96	1.92	0.45	8.84	466.62	0.18	0.36	3.27	19.27	0.44	0.83	0.95	0.68	0.17	45.72	18.9	0.4	0.02	0.87
60	0.58	1.74	0.63	28.53	1.70	0.54	4.53	251.89	0.24	0.36	4.01	33.55	0.43	0.98	0.46	0.31	0.01	122.63	32.4	0.3	0.00	0.88
30	0.67	2.12	0.42	28.90	2.02	0.47	7.71	634.55	0.13	0.33	4.20	21.14	0.46	0.70	0.85	0.61	0.24	124.50	27.2	0.2	0.03	0.90
Higashiyama																						
1474.3	0.59	1.57	0.45	28.73	2.87	0.49	4.05	464.92	0.61	0.24	153.68	47.41	0.28	0.67	0.60	0.35	3.63	1581.63	122.3	0.1	0.18	0.76
1466.7	0.51	0.51	0.46	28.70	1.66	0.40	3.52	346.70	1.26	0.37	17.63	113.88	0.22	0.40	0.58	0.35	1.72	348.28	74.6	0.2	0.11	0.83
1443.5	0.77	1.36	0.34	29.06	2.55	0.29	6.33	498.78	1.18	0.40	26.76	149.56	0.21	0.35	1.12	0.71	1.53	305.29	134.6	0.4	0.09	0.90
1412.7	0.70	1.18	0.38	28.84	2.41	0.50	4.31	457.03	1.14	0.34	15.91	79.01	0.20	0.49	0.76	0.44	1.61	300.61	55.5	0.2	0.16	0.87
1393.4	0.52	1.21	0.30	29.02	2.40	0.51	3.47	430.86	1.11	0.35	8.38	108.77	0.28	1.45	1.04	0.57	0.52	251.42	38.5	0.2	0.05	0.81
1381.8	0.63	1.33	0.39	28.98	2.02	0.52	4.23	385.14	0.95	0.44	17.68	146.62	0.29	0.53	0.97	0.66	1.18	122.40	75.8	0.6	0.06	0.83
1374.1	0.53	1.47	0.46	28.87	1.70	0.50	4.14	378.94	1.22	0.46	23.68	152.85	0.41	0.29	0.81	0.48	1.79	213.90	74.7	0.3	0.08	0.89
1345.2	0.52	0.98	0.40	28.86	1.89	0.56	4.13	433.22	1.75	0.42	21.39	223.60	0.29	0.61	0.79	0.47	2.23	303.30	82.3	0.3	0.14	0.89
1337.4	0.58	1.07	0.48	28.83	1.61	0.52	3.62	291.49	1.11	0.46	16.72	146.92	0.35	0.36	0.76	0.46	1.76	219.00	44.1	0.2	0.09	0.91
1320.1	0.69	0.81	0.38	28.99	1.86	0.61	7.14	692.95	0.83	0.42	33.86	187.92	0.29	0.26	1.00	0.69	3.60	326.91	41.5	0.1	0.09	0.92
1273.9	0.54	1.34	0.39	28.83	2.22	0.49	4.52	494.67	0.86	0.36	19.63	161.18	0.19	0.85	0.75	0.43	1.62	370.22	60.4	0.2	0.17	0.86
1248.8	0.46	1.89	0.70	28.44	2.23	0.55	4.45	640.75	2.21	0.35	19.08	139.55	0.22	1.08	0.40	0.29	0.65	377.24	57.5	0.2	0.09	0.81
1241.1	0.56	1.52	0.44	28.76	2.33	0.47	3.97	447.39	1.12	0.49	15.02	126.79	0.31	0.40	0.88	0.51	1.18	353.39	69.4	0.2	0.13	0.90
1231.5	0.58	1.63	0.44	28.76	2.21	0.37	3.94	390.26	0.95	0.36	14.26	115.54	0.38	0.66	0.67	0.41	1.15	340.97	60.6	0.2	0.14	0.89
1198.7	0.46	1.87	0.35	28.94	2.03	0.44	1.93	248.25	1.08	0.41	5.70	93.79	0.32	1.36	0.92	0.52	0.54	169.89	61.8	0.4	0.09	0.86
1067.7	0.61	1.36	0.41	28.86	1.94	0.59	4.59	400.31	0.88	0.43	17.86	97.76	0.32	0.30	0.79	0.50	1.28	155.43	57.0	0.4	0.06	0.89
901.8	0.60	1.03	0.62	28.55	1.49	0.42	3.81	254.82	1.32	0.44	0.00	160.61	0.34	0.50	0.47	0.32	1.38	226.64	31.3	0.1	0.06	0.93
886.4	0.63	1.47	0.34	29.13	2.05	0.49	4.47	418.21	0.49	0.40	29.79	71.29	0.37	0.20	1.25	0.86	2.29	534.63	165.0	0.3	0.06	0.91
755.3	0.60	1.36	0.40	28.89	2.03	0.85	5.77	564.81	0.36	0.26	9.64	53.12	0.28	0.78	0.84	0.49	0.69	253.51	75.0	0.3	0.08	0.81
689.8	0.68	2.42	0.33	29.15	1.87	0.49	2.61	263.04	0.38	0.24	7.28	15.75	0.25	0.80	1.31	0.86	1.04	803.04	140.3	0.2	0.23	0.72
673.7	0.44	1.08	0.78	28.14	0.31	0.50	4.45	650.54	0.45	0.44	10.17	119.71	0.33	0.41	0.16	0.11	1.62	436.45	79.9	0.2	0.14	0.85
608.1	1.77	1.15	0.53	28.71	1.69	0.42	6.45	134.91	0.49	0.44	5.31	57.47	0.38	0.56	0.62	0.38	0.40	143.35	28.2	0.2	0.07	0.92
482.9	0.62	2.01	0.55	29.17	1.67	0.48	3.90	257.29	0.87	0.35	15.25	92.16	0.32	0.57	0.51	0.33	1.03	294.21	52.1	0.2	0.08	0.89
320.9	0.53	1.37	0.31	29.17	1.55	0.59	4.11	472.67	0.59	0.39	13.09	84.73	0.30	0.60	1.33	0.87	0.98	218.88	33.2	0.2	0.05	0.93
108.8	0.47	1.26	0.47	28.84	1.43	0.60	5.71	506.45	0.50	0.41	21.25	82.85	0.32	0.29	0.76	0.45	2.05	368.63	35.0	0.1	0.06	0.88
66.5	0.47	1.58	0.61	28.54	1.41	0.83	6.13	472.77	0.63	0.43	27.35	167.62	0.39	0.35	0.42	0.27	3.71	289.70	94.7	0.3	0.02	0.91
19.6	0.61	1.26	0.65	28.38	1.74	0.89	10.21	690.39	0.37	0.37	33.70	175.02	0.33	0.48	0.31	0.20	4.22	537.46	70.1	0.1	0.07	0.90
4.1	0.67	1.25	0.42	28.94	1.74	0.89	7.53	519.18	0.32	0.34	12.92	78.10	0.28	0.48	0.91	0.59	1.47	234.17	39.2	0.2	0.08	0.89

Table 3.2. Identification of aliphatic triterpenoids.

Label	Name	Formula	M+	References
1	Norpimarane isomer?	$C_{19}H_{34}$	262	1
2	Tricylic triterpenoid?	$C_{19}H_{34}$	262	
3	?	$C_{19}H_{34}$	262	
4	8β-labdane	$C_{20}H_{38}$	278	2, 3, 4
5	19-Norisopimarane	$C_{19}H_{34}$	262	2, 3, 4
6	Nortricyclic diterpenoid	$C_{19}H_{34}$	262	
7	Tricyclic diterpenoid?	$C_{20}H_{26}$	276	
8	Norabietane (Fichtelite) isomer	$C_{19}H_{34}$	262	4
9	18-Norisopimarane	$C_{19}H_{34}$	262	3
10	Rimuane	$C_{20}H_{36}$	276	2, 3, 4
11	Pimarane	$C_{20}H_{36}$	276	4
12	Beyerane	$C_{20}H_{34}$	274	2, 3, 4
13	Norabietane (Fichtelite) isomer	$C_{19}H_{34}$	262	4
14	Isopimarane	$C_{20}H_{36}$	276	2, 3, 4
15	16β-phyllocladane	$C_{20}H_{34}$	274	2, 3, 4
16	Totarane	$C_{20}H_{36}$	276	
17	16β-Kaurane	$C_{20}H_{34}$	274	2, 3, 4
18	Atisane isomer ?	$C_{20}H_{34}$	274	4
19	Abieatane	$C_{20}H_{36}$	276	4
20	16α-phyllocladane	$C_{20}H_{34}$	274	2, 3, 4
21	Atisane isomer?	$C_{20}H_{34}$	274	4
22	16α-kaurane	$C_{20}H_{34}$	274	2, 3, 4

References: 1: Philip (1985), 2: Noble et al. (1986), 3: (Killops et al. 1995), 4: Peters et al. (2005)

4. Overall conclusion

Lipid biomarkers were used to reconstruct the linkage between climate, sedimentary processes and the Earth's biosphere. We can see that sedimentary processes such as tides and floods can create sandstones that are rich in OM and can have TOC% greater than mudstones. These findings are significant in a way that carbon influx and preservation is possible even in sandy depocenters, opposing the view that only muddy depocenters can preserve organic carbon. We can also see that vegetational changes in the hinterland is not simply a result of climatic changes. Expansion of low-land areas due to increased sediment delivery and increased elevation both caused by an uplifting hinterland can create accommodation space for the growth of certain vegetations even during stable and unchanging climates. Hence, these should be factored in when interpreting vegetation changes over geological time. Lastly, we can also see that the effects of global cooling and a strengthening East Asian Monsoon system may not be uniform. While the effects of aridification was strong in Central Asia in the Middle Miocene, we can see that it was not strong enough in the Japanese Islands. The use of biomarkers in reconstructing bottom water conditions and phytoplankton growth was also used to interpret that in the Japan Sea, oceanographic events were more responsible for diatom growth rather than terrigenous input. However, increased iron delivery by eolian dust and an enrichment of silica to the North Pacific Ocean could have also played a role in diatom growths.

5. References

Andersson, R. A., Kuhry, P., Meyers, P., Zebühr, Y., Crill, P., & Mörth, M. (2011). Impacts of paleohydrological changes on *n*-alkane biomarker compositions of a Holocene peat sequence in the eastern European Russian Arctic. *Organic Geochemistry*, *42*(9), 1065–1075. https://doi.org/10.1016/j.orggeochem.2011.06.020

Armstrong, H. A., & Allen, M. B. (2011). Shifts in the Intertropical Convergence Zone, Himalayan exhumation, and late Cenozoic climate. *Geology*, *39*(1), 11–14. https://doi.org/10.1130/G31005.1

Bastow, T. P., Alexander, R., & Kagi, R. I. (1997). Identification and analysis of dihydro-*ar*-curcumene enantiomers and related compounds in petroleum. *Organic Geochemistry*, *26*(1), 79–83. https://doi.org/10.1016/S0146-6380(96)00155-6

Berner, R. (1989). Biogeochemical cycles of carbon and sulfur and their effect on atmospheric oxygen over phanerozoic time. *Global and Planetary Change*, *1*, 97–122.

Blair, N. E., & Aller, R. C. (2012). The Fate of Terrestrial Organic Carbon in the Marine Environment. *Annual Review of Marine Science*, *4*(Volume 4, 2012), 401–423. https://doi.org/10.1146/annurev-marine-120709-142717

Bouma, A. (1964). Turbidites. *Developments in Sedimentology*, *3*, 247–256.

Bray, E., & Evans, E. (1961). Distribution of n-paraffins as a clue to recognition of source beds. *Geochimica et Cosmochimica Acta*, *22*, 2–15.

Breckenridge, J., Maravelis, A. G., Catuneanu, O., Ruming, K., Holmes, E., & Collins, W. J. (2019). Outcrop analysis and facies model of an Upper Permian tidally influenced fluvio-deltaic system: Northern Sydney Basin, SE Australia. *Geological Magazine*, *156*(10), 1715–1741. https://doi.org/10.1017/S0016756818000973

Burdige, D. J. (2005). Burial of terrestrial organic matter in marine sediments: A re-assessment. *Global Biogeochemical Cycles*, *19*(4). https://doi.org/10.1029/2004GB002368

Chen, S., Steel, R. J., & Olariu, C. (2015). Chapter 7—Palaeo-Orinoco (Pliocene) channels on the tide-dominated Morne L'Enfer delta lobes and estuaries, SW Trinidad. In P. J. Ashworth, J. L. Best, & D. R. Parsons (Eds.), *Developments in Sedimentology* (Vol. 68, pp. 227–281). Elsevier. https://doi.org/10.1016/B978-0-444-63529-7.00010-9

Chen, X., Liu, X., Lin, D.-C., Wang, J., Chen, L., Yu, P.-S., Wang, L., Xiong, Z., & Chen, M.-T. (2021). A potential suite of climate markers of long-chain n-alkanes and alkenones preservd in the top sediments from the Pacific sector of the Southern Ocean. *Progress in Earth and Planetary Science*, *8*, 23. https://doi.org/10.1186/s40645-021-00416-9

Clift, P., & Jonell, T. (2021). Monsoon controls on sediment generation and transport: Mass budget and provenance constraints from the Indus River catchment, delta and submarine fan over tectonics and multimillenial timescales. *Earth-Science Reviews*, *220*, 103682. https://doi.org/10.1016/j.earscirev.2021.103682

Collins, D. S., Johnson, H. D., Allison, P. A., & Damit, A. R. (2018). Mixed Process, Humid-tropical, Shoreline–shelf Deposition and Preservation: Middle Miocene–modern Baram Delta Province, Northwest Borneo. *Journal of Sedimentary Research*, *88*(4), 399–430. https://doi.org/10.2110/jsr.2018.19

Cortese, G., Gersonde, R., Hillenbrand, C.-D., & Kuhn, G. (2004). Opal sedimentation shifts in the World Ocean over the last 15 Myr. *Earth and Planetary Science Letters*, *224*(3–4), 509–527. https://doi.org/10.1016/j.epsl.2004.05.035

Cui, X., Bianchi, T. S., Hutchings, J. A., Savage, C., & Curtis, J. H. (2016). Partitioning of organic carbon among density fractions in surface sediments of Fiordland, New Zealand. *Journal of*

Geophysical Research: Biogeosciences, *121*(3), 1016–1031. https://doi.org/10.1002/2015JG003225

Dadson, S., Hovius, N., Pegg, S., Dade, W., Horng, M., & Chen, H. (2005). Hyperpycnal river flows from an active mountain belt. *Journal of Geophysical Research*, *110*, 04016. https://doi.org/10.1029/2004JF000244

Daidu, F., Yuan, W., & Min, L. (2013). Classifications, sedimentary features and facies associations of tidal flats. *Journal of Palaeogeography*, *2*(1), 66–80. https://doi.org/10.3724/SP.J.1261.2013.00018

Damsté, J., Muyzer, G., Abbas, B., Rampen, S., Massé, G., Allard, W., Belt, S., Robert, J.-M., Rowland, S., Maldowan, J., Barbanti, S., Fago, F., Denisevich, P., Dahl, J., Trindade, L., & Schouten, S. (2004). The rise of Rhizosolenid Diatoms. *Science*, *304*, 584–586.

Damsté, J. S. S., Kock-Van Dalen, A. C., De Leeuw, J. W., Schenck, P. A., Guoying, S., & Brassell, S. C. (1987). The identification of mono-, di- and trimethyl 2-methyl-2-(4,8,12-trimethyltridecyl)chromans and their occurrence in the geosphere. *Geochimica et Cosmochimica Acta*, *51*(9), 2393–2400. https://doi.org/10.1016/0016-7037(87)90292-4

Demaison, G. J., & Moore, G. T. (1980). Anoxic environments and oil source bed genesis. *Organic Geochemistry*, *2*(1), 9–31. https://doi.org/10.1016/0146-6380(80)90017-0

Didyk, B., Simoneit, B., Brassell, S., & Eglinton, G. (1978a). Organic geochemical indicators of paleoenvironmental conditions of sedimentation. *Nature*, *272*, 216–222.

Didyk, B., Simoneit, B., Brassell, S., & Eglinton, G. (1978b). Organic geochemical indicators of paleoenvironmental conditions of sedimentation. *Nature*, *272*, 216–222.

Eglinton, G., & Hamilton, R. (1963a). The distribution of n-alkanes. In *T. Swain, Chemical Plant Taxonomy* (pp. 187–240). Academic Press.

Eglinton, G., & Hamilton, R. (1963b). *The distribution of n-alkanes* (T. Swain, Ed.). Academic Press.

Eglinton, G., & Logan, G. (1991). Molecular preservation. *Philosophical Transactions of the Royal Society of London B, 333*, 315–328.

Esterle, J. S., & Ferm, J. C. (1994). Spatial variability in modern tropical peat deposits from Sarawak, Malaysia and Sumatra, Indonesia: Analogues for coal. *International Journal of Coal Geology*, *26*(1), 1–41. https://doi.org/10.1016/0166-5162(94)90030-2

Ficken, K., Li, B., Swain, D., & Eglinton, G. (2000). An n-alkane proxy for the sedimentary input of submerged/floating freshwater aquatic macrophytes. *Organic Geochemistry*, *31*, 745–749.

Fikri, H. N., Sachsenhofer, R. F., Bechtel, A., & Gross, D. (2022). Coal deposition in the Barito Basin (Southeast Borneo): The Eocene Tanjung Formation compared to the Miocene Warukin Formation. *International Journal of Coal Geology*, *263*, 104117. https://doi.org/10.1016/j.coal.2022.104117

Fleck, S., Michels, R., Ferry, S., Malartre, F., Elion, P., & Landais, P. (2002). Organic geochemistry in a sequence stratigraphic framework. The siliciclastic shelf environment of Cretaceous series, SE France. *Organic Geochemistry*, *33*(12), 1533–1557. https://doi.org/10.1016/S0146-6380(02)00174-2

Furota, S., Sawada, K., & Kawakami, G. (2021). Deposition processes of plant fragment-concentrated sandstones in turbiditic sequences recorded by plant biomarkers (Miocene Kawabata Formation, Japan. *International Journal of Coal Geology*, *233*, 103642. https://doi.org/10.1016/j.coal.2020.103643

Gong, C., Wang, Y., Zheng, R., Hernández-Molina, F. J., Li, Y., Stow, D., Xu, Q., & Brackenridge, R. E. (2016). Middle Miocene reworked turbidites in the Baiyun Sag of the Pearl River

Mouth Basin, northern South China Sea margin: Processes, genesis, and implications. *Journal of Asian Earth Sciences*, *128*, 116–129. https://doi.org/10.1016/j.jseaes.2016.06.025

Hage, S., Galy, V. V., Cartigny, M. J. B., Acikalin, S., Clare, M. A., Gröcke, D. R., Hilton, R. G., Hunt, J. E., Lintern, D. G., McGhee, C. A., Parsons, D. R., Stacey, C. D., Sumner, E. J., & Talling, P. J. (2020). Efficient preservation of young terrestrial organic carbon in sandy turbidity-current deposits. *Geology*, *48*, 882–887.

Hartnett, H., R.G, K., Hedges, J., & Devo, A. (1998). Influence of oxygen exposure time on organic carbon preservation in continental margin sediments. *Nature*, *391*, 572–575.

Harvey, H. R., & Mcmanus, G. B. (1991). Marine ciliates as a widespread source of tetrahymanol and hopan-3β-ol in sediments. *Geochimica et Cosmochimica Acta*, *55*(11), 3387–3390. https://doi.org/10.1016/0016-7037(91)90496-R

Hedges, J., Keil, R., & Benner, R. (1997). What happens to terrestrial organic matter in the ocean? *Organic Geochemistry*, *27*, 195–212.

Hedges, J., & Keil, R. G. (1995). Sedimentary organic matter preservation: An assessment and speculative synthesis. *Marine Chemistry*, *49*, 81–115.

HUTCHISON, C. S., BERGMAN, S. C., SWAUGER, D. A., & GRAVES, J. E. (2000). A Miocene collisional belt in north Borneo: Uplift mechanism and isostatic adjustment quantified by thermochronology. *Journal of the Geological Society*, *157*(4), 783–793. https://doi.org/10.1144/jgs.157.4.783

Ibach, L. E. (1982). Relationship between sedimentation rate and total organic carbon content in ancient marine sediments. *The American Association of Petroleum Geologists Bulletin*, *66*(2), 170–188.

Jiang, C., Alexander, R., Kagi, R. I., & Murray, A. P. (2000). Origin of perylene in ancient sediments and its geological significance. *Organic Geochemistry*, *31*(12), 1545–1559. https://doi.org/10.1016/S0146-6380(00)00074-7

Kao, S. J., Dai, M., Selvaraj, K., Zhai, W., Cai, P., Chen, S. N., Yang, J. Y. T., Liu, J. Y., Liu, C. C., & Syvitski, J. P. M. (2010). Cyclone-driven deep sea injection of freshwater and heat by hyperpycnal flow in the subtropics. *Geophysical Research Letters*, *37*, 21702. https://doi.org/10.1029/2010GL044893

Kawakami, G., Arita, K., Okada, T., & Itaya, T. (2004). Early exhumation of the collisional orogen and concurrent infill of foredeep basins in the Miocene Eurasian –Okhotsk Plate boundary, central Hokkaido, Japan: Inferences from K-Ar dating of granitoid clasts. *Island Arc, 13*, 359–369.

Kim, J.-W., Yeh, S.-W., & Chang, E.-C. (2014). Combined effect of El Niño-Southern Oscillation and Pacific Decadal Oscillation on the East Asian winter monsoon. *Climate Dynamics*, *42*(3), 957–971. https://doi.org/10.1007/s00382-013-1730-z

Kitayama, K. (1992). An altitudinal transect study of the vegetation on Mount Kinabalu, Borneo. *Vegetatio*, *102*(2), 149–171. https://doi.org/10.1007/BF00044731

Kocsis, L., Briguglio, A., Cipriani, A., Frijia, G., Vennemann, T., Baumgartner, C., & Roslim, A. (2022). Strontium isotope stratigraphy of late Cenozoic fossiliferous marine deposits in North Borneo (Brunei, and Sarawak, Malaysia). *Journal of Asian Earth Sciences*, *231*, 105213. https://doi.org/10.1016/j.jseaes.2022.105213

Li, L., Li, Q., Tian, J., Wang, H., & Wang, P. (2013). Low latitude hydro-climatic changes during the Plio-Pleistocene: Evidence from high resolution alkane records in the southern South China Sea. *Quaternary Science Reviews*, *78*, 209–224. https://doi.org/10.1016/j.quascirev.2013.08.007

Liechti, P., Roe, F. W., & Haile, N. S. (1960). *The Geology of Sarawak, Brunei and the Western Part of North Borneo*. U.S. Government Printing Office.

Lihong, Z., Zhihua, S., Ge, T., Dunqing, X., Zheng, C., Haiqing, W., Junqing, S., Shuangjun, H., Wei, G. E., & Changwei, C. (2020). Pliocene hyperpycnal flow and its sedimentary pattern in D block of Rakhine Basin in Bay of Bengal. *Petroleum Exploration and Development*, *47*(2), 318–330.

Lübbers, J., Kuhnt, W., Holbourn, A. E., Bolton, C. T., Gray, E., Usui, Y., Kochhann, K. G. D., Beil, S., & Andersen, N. (2019). The middle to late Miocene 'Carbonate Crash' in the equatorial Indian Ocean [dataset]. In *Supplement to: Lübbers, J et al. (2019): The Middle to Late Miocene 'Carbonate Crash' in the Equatorial Indian Ocean. Paleoceanography and Paleoclimatology, 34(5), 813-832, https://doi.org/10.1029/2018PA003482*. PANGAEA. https://doi.org/10.1594/PANGAEA.900847

Manh, N., Dung, N., Hung, N., Merz, B., & Apel, H. (2014). Large-scale suspended sediment transport and sediment deposition in the Mekong Delta. *Hydrology and Earth System Sciences*, *18*, 3033–3053.

Mayer, L. (1994). Relationships between mineral surfaces and organic carbon concentrations in soils and sediments. *Chemical Geology*, *114*, 347–363.

McKee, B., Aller, R., Allison, M., Bianchi, T., & Kineke, G. (2004). Transport and transformation of dissolved and particulate materials on continental margins influenced by major rivers: Benthic boundary layer and seabed processes. *Continental Shelf Research*, *24*, 899–926.

Meade, R. (1996). River-sediment inputs to major deltas. In J. Milliman & B. Haq (Eds.), *Sea-level rise and coastal subsidence* (pp. 63–85). Kluwer Academic Publishing.

MORLEY, C. K., & BACK, S. (2008). Estimating hinterland exhumation from late orogenic basin volume, NW Borneo. *Journal of the Geological Society*, *165*(1), 353–366. https://doi.org/10.1144/0016-76492007-067

Morley, R. J. (1998). Palynological evidence for Tertiary plant dispersals in the SE Asian region in relation to plate tectonics and climate. *Biogeography and Geological Evolution of SE Asia*, 211–234.

Mulder, T., Syvitski, J. P., Migeon, S., Faugeres, J.-C., & Savoye, B. (2003). Marine hyperpycnal flows: Initiation, behavior and related deposits. A review. *Marine and Petroleum Geology*, *20*, 861–882.

Ning, X., Chai, F., Xue, H., Cai, Y., Liu, C., & Shi, J. (2004). Physical-biological oceanographic coupling influencing phytoplankton and primary production in the South China Sea. *Journal of Geophysical Research: Oceans*, *109*(C10). https://doi.org/10.1029/2004JC002365

Otto, A., & Wilde, V. (2001). Sesqui-, di-, and triterpenoids as chemosystematic markers in extant conifers—A review. *The Botanical Review*, *67*(2), 141–238. https://doi.org/10.1007/BF02858076

Page, S., Wüst, R., & Banks, C. (2010). Past and present carbon accumulation and loss in Southeast Asian peatlands. *PAGES News*, *18*(1), 25–27. https://doi.org/10.22498/pages.18.1.25

Peng, T., Li, J., Song, C., Guo, B., Liu, J., Zhao, Z., & Zhang, J. (2016). An integrated biomarker perspective on Neogene–Quaternary climatic evolution in NE Tibetan Plateau: Implications for the Asian aridification. *Quaternary International*, *399*, 174–182. https://doi.org/10.1016/j.quaint.2015.04.020

Peters, K., Walters, C., & Moldowan, J. (2005). *The Biomarker Guide Vol. 1: Biomarkers and Isotopes in the Environment and Human History* (2nd ed.). Cambridge University Press.

Pierdomenico, M., Casalbore, D., & Chiocci, F. (2019). Massive benthic litter funnelled to deep sea by flash-flood generated hyperpycnal flows. *Scientific Reports*, *9*, 5330. https://doi.org/10.1038/s41598-019-41816-8

Quattrocchio, M., Olivera, D., Martinez, M., Ponce, J., & Carmona, N. (2018). Palynofacies associated to hyperpycnite deposits of the Miocene, Cabo Viamonte Beds, Austral Basin, Argentina. *Facies*, *64*, 22. https://doi.org/10.1007/s10347-018-0535-2

Raymo, M. E., & Ruddiman, W. F. (1992). Tectonic forcing of late Cenozoic climate. *Nature*, *359*(6391), 117–122. https://doi.org/10.1038/359117a0

Sandal, S. T. (1996). *The geology and hydrocarbon resources of Negara Brunei Darussalam* (2nd [rev.] ed). Syabas.

Seki, O., Meyers, P. A., Kawamura, K., Zheng, Y., & Zhou, W. (2009). Hydrogen isotopic ratios of plant wax *n*-alkanes in a peat bog deposited in northeast China during the last 16 kyr. *Organic Geochemistry*, *40*(6), 671–677. https://doi.org/10.1016/j.orggeochem.2009.03.007

Selvaraj, K., Lee, T., Yang, J., Canuel, E., Huang, J., Dai, M., Liu, J. T., & Kao, S. (2015). Stable isotope and biomarker evidence of terrigenous OM export to the deep sea during tropical storms. *Marine Geology*, *364*, 32–42.

Shanley, K. W., McCABE, P. J., & Hettinger, R. D. (1992). Tidal influence in Cretaceous fluvial strata from Utah, USA: A key to sequence stratigraphic interpretation. *Sedimentology*, *39*(5), 905–930. https://doi.org/10.1111/j.1365-3091.1992.tb02159.x

Shen, X., Wan, S., Colin, C., Tada, R., Shi, X., Pei, W., Tan, Y., Jiang, X., & Li, A. (2018). Increased seasonality and aridity drove the C4 plant expansion in Central Asia since the Miocene–Pliocene boundary. *Earth and Planetary Science Letters*, *502*, 74–83. https://doi.org/10.1016/j.epsl.2018.08.056

Shen, X., Wan, S., France-Lanord, C., Clift, P. D., Tada, R., Révillon, S., Shi, X., Zhao, D., Liu, Y., Yin, X., Song, Z., & Li, A. (2017). History of Asian eolian input to the Sea of Japan since 15 Ma: Links to Tibetan uplift or global cooling? *Earth and Planetary Science Letters*, *474*, 296–308. https://doi.org/10.1016/j.epsl.2017.06.053

Simmons, M. D., Bidgood, M. D., Brenac, P., Crevello, P. D., Lambiase, J. J., & Morley, C. K. (1999). Microfossil assemblages as proxies for precise palaeoenvironmental determination—An example from Miocene sediments of northwest Borneo. *Geological Society, London, Special Publications*, *152*(1), 219–241. https://doi.org/10.1144/GSL.SP.1999.152.01.13

Sinninghe Damste, J. S., Kenig, F., Koopmans, M. P., Koster, J., Schouten, S., Hayes, J. M., & de Leeuw, J. W. (1995). Evidence for gammacerane as an indicator of water column stratification. *Geochimica Et Cosmochimica Acta*, *59*(9), 1895–1900. https://doi.org/10.1016/0016-7037(95)00073-9

Slater, S., McKie, T., Vieira, M., Wellman, C., & Vajda, V. (2017). Episodic river flooding events revealed by palynological assemblages in Jurassic deposits of the Brent Group, North Sea. *Paleogeography, Palaeoclimatology, Palaeoecology*, *485*, 389–400.

Staub, J., Among, H., & Gastaldo, R. (2000). Seasonal sediment transport and deposition in the Rajang River delta, Sarawak, East Malaysia. *Sedimentary Geology*, *133*, 249–264.

Stout, S. A. (1992). Aliphatic and aromatic triterpenoid hydrocarbons in a Tertiary angiospermous lignite. *Organic Geochemistry*, *18*, 51–66. https://doi.org/10.1016/0146-6380(92)90143-L

Sun, W., Zhang, E., Liu, E., You, Y., Li, J., Ni, Z., Meng, X., Zhang, W., & Chen, R. (2023). Hydroclimate changes since the last glacial maximum from sedimentary biomarkers in a crater lake in the Great Khingan Mountains, Northeast China. *Quaternary Science Reviews*, *312*, 108175. https://doi.org/10.1016/j.quascirev.2023.108175

Tada, R. (1994). Paleoceanographic evolution of the Japan Sea. *Palaeogeography, Palaeoclimatology, Palaeoecology*, *108*(3), 487–508. https://doi.org/10.1016/0031-0182(94)90248-8

Tada, R., Zheng, H., & Clift, P. D. (2016). Evolution and variability of the Asian monsoon and its potential linkage with uplift of the Himalaya and Tibetan Plateau. *Progress in Earth and Planetary Science*, *3*(1), 4. https://doi.org/10.1186/s40645-016-0080-y

Takano, O., & Waseda, A. (2003). Sequence stratigraphic architecture of a differentially subsiding bay to fluvial basin: The Eocene Ishikari Group, Ishikari Coal Field, Hokkaido, Japan. *Sedimentary Geology*, *160*(1), 131–158. https://doi.org/10.1016/S0037-0738(02)00370-6

Tamburini, F., Adatte, T., Föllmi, K., Bernasconi, S. M., & Steinmann, P. (2003). Investigating the history of East Asian monsoon and climate during the last glacial–interglacial period (0–140 000 years): Mineralogy and geochemistry of ODP Sites 1143 and 1144, South China Sea. *Marine Geology*, *201*(1), 147–168. https://doi.org/10.1016/S0025-3227(03)00214-7

T.G, P. (1988). Pristane / phytane ratio as environmental indicator. *Nature*, *333*, 604.

Tsubakihara, S. (1990). Stratigraphy and Depositional Environments of Upper Cenozoic sediments in Kuriyama and Kurisawa towns in the eastern marginal area of the Ishikari Lowland, Hokkaido, Japan. *Earth Science. (Chikyu Kagaku*, *44*, 263–278.

van Aarssen, B. G. K., Alexander, R., & Kagi, R. I. (2000). Higher plant biomarkers reflect palaeovegetation changes during Jurassic times. *Geochimica et Cosmochimica Acta*, *64*(8), 1417–1424. https://doi.org/10.1016/S0016-7037(99)00432-9

Volkman, J. (1986). A review of sterol markers for marine and terrigenous OM. *Organic Geochemistry*, *9*, 83–99.

Wakeham, S. G., Canuel, E. A., Lerberg, E. J., Mason, P., Sampere, T. P., & Bianchi, T. S. (2009). Partitioning of organic matter in continental margin sediments among density fractions. *Marine Chemistry*, *115*(3), 211–225. https://doi.org/10.1016/j.marchem.2009.08.005

Walters, C. C. (2006). The Origin of Petroleum. In C. S. Hsu & P. R. Robinson (Eds.), *Practical Advances in Petroleum Processing* (pp. 79–101). Springer New York. https://doi.org/10.1007/978-0-387-25789-1_2

Wang, H., Bi, N., Wang, Y., Saito, Y., & Yang, Z. (2010). Tide-modulated hyperpycnal flows off the Huanghe (Yellow River) mouth, China. *Earth Surface Processes and Landforms*, *35*, 1315–1329.

Wang, P., Zhao, Q., Jian, Z., Cheng, X., Huang, W., Tian, J., Wang, J., Li, Q., Li, B., & Su, X. (2003). Thirty million year deep sea records in the South China Sea. *Chinese Science Bulletin*, *48*(23), 2524–2535. https://doi.org/10.1007/BF03037016

Wang, W., Zhang, H., Chen, H., Zhuang, Y., Huang, Y., & Liu, G. (2019). Effects of Asian dust input on eukaryotic phytoplankton community structure in the open areas in the Northwestern Pacific Ocean. *Marine Biology Research*, *15*(1), 49–60. https://doi.org/10.1080/17451000.2019.1588981

Wang, W.-M., Saito, T., & Nakagawa, T. (2001). Palynostratigraphy and climatic implications of Neogene deposits in the Himi area of Toyama Prefecture, Central Japan. *Review of Palaeobotany and Palynology*, *117*(4), 281–295. https://doi.org/10.1016/S0034-6667(01)00097-5

Wang, Z., Yang, C., Yang, Z., Brown, C. E., Hollebone, B. P., & Stout, S. A. (2016). 4—Petroleum biomarker fingerprinting for oil spill characterization and source identification. In S. A. Stout & Z. Wang (Eds.), *Standard Handbook Oil Spill Environmental Forensics (Second Edition)* (pp. 131–254). Academic Press. https://doi.org/10.1016/B978-0-12-803832-1.00004-0

Widodo, S., Bechtel, A., Anggayana, K., & Püttmann, W. (2009). Reconstruction of floral changes during deposition of the Miocene Embalut coal from Kutai Basin, Mahakam Delta, East Kalimantan, Indonesia by use of aromatic hydrocarbon composition and stable carbon isotope ratios of organic matter. *Organic Geochemistry*, *40*(2), 206–218. https://doi.org/10.1016/j.orggeochem.2008.10.008

Wilf, P., Zou, X., Donovan, M. P., Kocsis, L., Briguglio, A., Shaw, D., Slik, J. F., & Lambiase, J. J. (2022). First fossil-leaf floras from Brunei Darussalam show dipterocarp dominance in Borneo by the Pliocene. *PeerJ*, *10*, e12949. https://doi.org/10.7717/peerj.12949

Xing, L., Zhang, H., Yuan, Z., Sun, Y., & Zhao, M. (2011). Terrestrial and marine biomarker estimates of organic matter sources and distributions in surface sediments from East China Sea shelf. *Continantal Shelf Research*, *31*, 1106–1115.

Yang, C., Dang, H., Zhou, X., Zhang, H., Wang, X., Wang, Y., Qiao, P., Jiang, X., & Jian, Z. (2021). Upper ocean hydrographic changes in response to the evolution of the East Asian monsoon in the northern South China Sea during the middle to late Miocene. *Global and Planetary Change*, *201*, 103478. https://doi.org/10.1016/j.gloplacha.2021.103478

Yang, Z., Ji, Y., Bi, N., Lei, K., & Wang, H. (2011). Sediment transport off the Huanghe (Yellow River) delta and in the adjacent Bohai Sea in winter and seasonal comparison. *Estuarine, Coastal and Shelf Science*, *93*, 173–181.

Yoshida, M., Yoshiuchi, Y., & Hoyanagi, K. (2009). Occurence conditions of hyperpycnal flows, and their significance for organic-matter sedimentation in a Holocene estuary, Niigata Plain, Central Japan. *Island Arc*, *18*, 320–332.

Zakrzewski, A., & Kosakowski, P. (2021). Impact of palaeo-wildfires on higher plant parameter revealed by new biomarker indicator. *Palaeogeography, Palaeoclimatology, Palaeoecology*, *579*, 110606. https://doi.org/10.1016/j.palaeo.2021.110606

Zavala, C., & Arcuri, M. (2016). Intrabasinal and extrabasinal turbidites: Origin and distinctive characteristics. *Sedimentary Geology*, *337*, 36–54.

Zavala, C., Arcuri, M., & Valiente, L. (2012). The importance of plant remains as diagnostic criteria for the recognition of ancient hyerpycnites. *Revue de Paleobiologie*, *Geneve*, *11*, 457–469.

Zhou, W., Zheng, Y., Meyers, P. A., Jull, A. J. T., & Xie, S. (2010). Postglacial climate-change record in biomarker lipid compositions of the Hani peat sequence, Northeastern China. *Earth and Planetary Science Letters*, *294*(1), 37–46. https://doi.org/10.1016/j.epsl.2010.02.035